DISSERTATION ZUR ERLANGUNG DES
DOKTORGRADES DER FAKULTÄT FÜR CHEMIE
UND PHARMAZIE DER
LUDWIG-MAXIMILIANS-UNIVERSITÄT MÜNCHEN

Comprehensive proteome and phosphoproteome analysis of human LRRK2 Drosophila model of Parkinson's disease

Md. Shariful Islam

Aus

Bhola, Bangladesh

2016

Erklaerung

Diese Dissertation wurde im Sinne von § 7 der Promotionsordnung vom 28. November 2011 von Herrn PD. Dr. Hermann Heumann betreut.

Eidesstattliche Versicherung

Diese Dissertation wurde eigenständig und ohne unerlaubte Hilfe erarbeitet.

Munich, 01.02.2016

_____

Md. Shariful Islam

Dissertation eingereicht am

1. Gutachter: PD. Dr. Hermann Heumann
2. Gutachter: Prof. Dr. Marcus Krueger

Tag der Einreichung: 18.3.2016

Muendliche Pruefung am 17.10.2016

"A journey of a thousand miles begins with a single step"

Laosi

Abstract

Gene mutations in the leucine-rich repeat kinase 2 (LRRK2) are the most common cause of autosomal dominant Parkinson's Disease (PD) and elevated levels of hLRRK2 mutant variants in *Drosophila* induces PD. Here, we introduced the human LRRK2 (R1441C) variant in dopaminergic neurons of flies and observed a reduced locomotor activity, an age dependent degeneration of dopaminergic neurons, and shorter lifetime. To better understand the hLRRK2 (R1441C) induced pathobiology, we performed stable isotope labeling in fly to accurately quantify the proteome and phosphoproteome dynamics. We quantified almost 3000 proteins and found several regulated cytoskeletal, mitochondrial, and synaptic vesicle (SV) proteins in our PD fly model. To explore the hLRRK2 (R1441C) function more precisely, we compared our model to three different α-Synuclein (αS) overexpressing fly strains (αS, αS-A30P, αS-A53T), which show a similar PD phenotype but distinct pathobiology mechanisms. For example, synaptotagmin, syntaxin and rab3 were only affected in hLRRK2 (R1441C) flies compared to all other tested fly strains. Moreover, our global phosphoproteome analysis revealed several synaptic vesicle proteins with enhanced phosphorylation, including synaptojanin (pT1131)and we show that the conserved phosphorylation site on human synaptojanin is modulated by the hLRRK2 (R1441C) mutant variant. Consistently, a protein-protein interaction screen confirmed that hLRRK2 is tightly associated with synaptic vesicle proteins. Thus, our results provide a systemic view on the pathobiology mechanism caused by hLRRK and αS overexpression and suggest that the increased kinase activity of the hLRRK2 (R1441C) mutant results in enhanced phosphorylation of synaptojanin. These findings may contribute to develop new therapeutic strategies to prevent hLRRK2-induced Parkinson disease.

Acknowledgements

There are so many people who have contributed in different ways to get me close to where I stand today- the completion of PhD thesis. I would like to begin by thanking my parents, MD Gias Uddin Ahmed and Rezia Begum for their biased love and support throughout my life. Without your continuous prayer, enthusiastic encouragement and inspiration, I would have never materialized the successful completion of the thesis.

I would like to offer my special thanks and gratitude to my PhD thesis supervisor PD. Dr. Hermann Heumann for his encouragement, detailed guidance, direction and active participation in discussions and comments throughout my thesis work.

I am really grateful to Prof. Marcus Krueger, for his sincere guidance, direction and advice throughout my PhD. I was always inspired by his love of rigorous science, great vision, and marvelous creativity. He tried his best in every aspect to assist my research and i am truly thankful for having his support and encouragement throughout my career.

I would extend my deep gratitude towards my Co-supervisor Prof. Rolf Heumann for his valuable feedback and suggestions which helped me to resolve burning questions and concerns. I am very grateful to my collaborator, Prof. Bernhard Hovemann and Dr. Anna Ziegler for their tremendous assistance in generating various genotypes flies for my research and has been offering insightful comments on the biological aspects of my findings.

I would also like to thank my peers, especially Hendrik Nolte, Sriram Aravamudhan for their offering of help, advice, and insightful scientific discussions. Suraya Hoelper and Sylvia Jeratsch deserve notable mentions for making my time enjoyable in the group!

Prof. Dr. Chris Turck, Prof. Dr. Thomas Carell and Prof. Dr. Foerstemann deserve hearty thanks for being part of my thesis committee.

Apart from the above, there are several individuals whose direct involvement deserves mighty thanks. I would like to share appreciation for Dr. Atikur Rahman Jewel and Zahed Zia for all the encouragements and motivations provided when I felt down spirited. Immense gratitude to Katja Schoder and Sebastian Schmidt for their administrative helps during my thesis. I also want to give thanks to my friend Abdullah Al Mamun, Sharif Mortoga Chowdhury, Arif Mortoga Chowdhury, Soyeb, S M Majedul Karim, Shafi Jamali, Murad Hossain, Sumit Anik, Munich Masti Group and Tabur Tal Matal Group for bringing lots of joy and fun. I have enjoyed very much spending time in such an interesting, fun, and Masti group!

Finally, I would like to thank the almighty Allah the most merciful and most beneficent for keeping me fit and committed in finishing the academic targets that I set for.

Md. Shariful Islam

Contents

List of Figures

List of Tables

Abbreviations

PD	**P**arkinson's **D**isease
DA	**D**opaminergic
SNpc	**S**ubstantial **N**igra **P**ars **C**ompacta
TH	**T**yrosine **H**ydroxylase
α**S**	**A**lpha **S**ynuclein
LRRK2	**L**eucine **R**ich **R**epeat **K**inase
ROC	**R**as **O**f **C**omplex
COR	**C** terminal **O**f **R**oc
MAPKKK	**M**itogen **A**ctivated **P**rotein **K**inase **K**inase **K**inase
GEFs	**G**uanine **N**ucleotide **E**xchange **F**actors
GAPs	**G**TPase **A**ctivating **P**roteins
SV	**S**ynaptic **V**esicle
MS	**M**ass **S**pectrometry
CID	**C**ollision **I**nduced **D**issociation
HCD	**H**igher energy **C**ollisional **D**issociation
ETD	**E**lectron **T**ransfer **D**issociation
SILAC	**S**table **I**sotope **L**abeling of **A**mino acid in **C**ell culture
LFQ	**L**abel **F**ree **Q**uantification
SCX	**S**trong **C**ation **X**change
ESI	**E**lectro **S**pray **I**onization
MALDI	**M**atrix **A**ssisted **L**aser **D**esorption **I**onization
LTQ	**L**inear **T**rap **Q**uadropole
FDR	**F**alse **D**iscovery **R**ate

Dedicated to my parents

Chapter 1

Introduction

1.1 Parkinson's disease (PD)

Parkinson's disease (PD) is the second most prevalent age-associated progressive, neurodegenerative movement disorder after Alzheimer's disease and affecting approximately 1 % of the population over 55 years of age [1]. PD was first described in 1817 by James Parkinson (1755-1824), the British physician, in his landmark publication called "An Essay on the Shaking Palsy" [2]. However, it was Jean Martin Charcot (1825-1893) who defined the syndrome and attributed the disorder as PD. Later on, Carlsson accelerated the pace of PD discoveries by identifying dopamine in the mammalian brain [3]. Although enormous advancement was made over the last 200 years to understand PD neurobiology, still there is no accurate diagnostic tool and remedy for this disorder. It is estimated that currently 6 million people around the world are affected by PD and interestingly, men suffer more frequently than women [4]. The PD prevalence was approximately 8334/100,000 in Germany [5] and the number is increasing due to the increased average age of the whole German population.

1.2 PD Features

Neuropathologically, nigrostriatal dopaminergic (DA) neurons loss in the substantia nigra and the presence of intracytoplasmic Lewy bodies in the remaining neurons are the two key hallmarks of the PD brain. Frederic Lewy (1885-1950) first discovered the presence of intraneuronal inclusions in the PD brain and termed it Lewy bodies in 1912 [6–8]. The cytoplasmic nigrostrital pathway is described as one of the most major dopamine pathways composed of DA neurons in substantial nigra pars compacta (SNpc) in the brain that is involved in controlling voluntary movement. Striatum and basal ganlia

gets the projection from SNpc through domapniergic neurons and PD causes significant dopamine reduction in the putamen and less significant dopamine reduction in the caudate nucleus, see 1.1. [9–11].

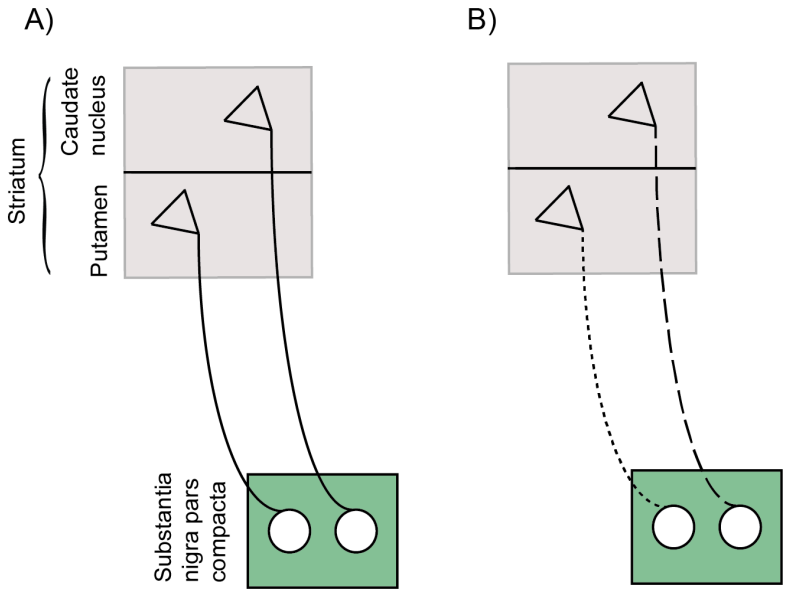

FIGURE 1.1: Schematic representation of the human nirgostiatal pathways. Sriatum is composed of putamen and caudate nucleus. A) putamen and caudate nucleus get normal projection from SNpc in a healthy brain. B) PD patients get less projection due to significant reduction of dopamine in putamen.

However, Braak and colleagues discovered progressive neurodegeneration also in the cerebral cortex and olfactory bulb at different stages of PD [12]. In addition to these pathological features of PD, there are some clinical features, namely, motor symptoms and non motor symptoms [13]. The motor symptoms of PD are resting tremor, rigidity, bradykinesia (slowness of movement) and postural rigidity and these are the result of DA degeneration in SNPc. Among the four motor symptoms, resting tremor is the most common symptom with 70 % of all PD patients. Nevertheless, PD patients may suffer from other motor symptoms such as gait and posture disturbance, decreased arm swing, masked face (hypomania), cramped handwriting (micrographia) and sustained muscle contractions (dystonia). Besides motor symptoms, individuals with PD also show varieties of non-motor symptoms which contribute significantly to PD morbidity. Mood disturbance is the most common non-motor symptom where 20-80 % patients suffer with depression [14]. Furthermore, patients may suffer with a range of cognitive disturbances, including impulse control, subjective awareness and difficulties in allocation of attention [15]. Dementia also occurs in PD patients, which cause slowing of thought, memory and behavioral regulation [16, 17]. Taken together, broad-based management is required for PD and there is no satisfactory cure for this chronic disorder.

1.3 Risk factors and Genes Association of PD

Although the exact cause of PD is still unknown in most of the cases, there is still a wide range of factors in PD contributing to nigrostriatal dysfunction. These are increasing age, environmental factors and genetic mutations in selected genes. Among all risk factors, age is the most common and 1-5 % of people of in 65-85 years age suffer from this complex disease [9]. Environmental factors are also considered as a prominent cause of PD in 1980 by discovering the fact that methyl-4-phenyl-1,2,3,6- tetrahydropyridine (MPTP) can also induce levodopa-responsive parkinsonism [18].
However, approximately 5-10 % of PD cases are termed familial PD and thought to be caused by genetic variation in selected genes. The percentage of these familial PD cases can be even higher for specific groups of patients selected for age of onset, positive family history and ethnic origin [19–21]. Recent ground breaking discoveries indicate that mutations in at least six genes positively induce familial PD including two autosomal dominant genes (αS and leucime rich repeat kinase 2) and three autosomal recessive genes such as parkin, Dj-1 and PINK1 [22]. Though mutation in the genes only represents the case in small groups of PD patients, studies of these genes highlight several pathways involved in sporadic PD pathogenesis, including protein aggregation, mitochondrial dysfunction, oxidative stress and ubiquitin-proteasome system defects [23–25]. Therefore, investigating the molecular mechanism of these PD genes may shed light on the underlying causes of both familial and sporadic PD.

1.3.1 Alpha-synuclein

The mutation in the αS gene (PARK1 and PARK2) was first discovered in 1997 as a causative factor for PD [26]. It was the first locus for autosomal dominantly inherited parkinsonism and was identified at the chromosomal location 4q21 [27, 28]. αS is known as the primary component of Lewy bodies (LBs) in PD patients [29]. Furthermore, three mutations such as A30P, E46K and A53T have been found as contributors to PD development [27, 28, 30, 31].

1.3.2 Parkin, PINK1, DJ-1, UCH-L1

Parkin (PARK2) is another known PD-linked gene causing a loss-of-function. Parkin contributes to autosomal recessive juvenile parkinsonism (AR-JP) [32]. In total, 25 point mutations have been found in the parkin gene which were reported to be linked with AR-JP. In contrast to both sporadic and familial PD, the brains of most AR-JP patients lack LB pathology [32]. Therefore, DA degeneration due to the AR-JP linked parkinsonism

might reflects different cellular pathways for degeneration compared with other PD cases.

PINK1 is a mitochondrial serine/threonine kinase [33–36]. Mutations in PINK1 were found in Europe, North America and Asian families.Though little is known about this protein, PINK1 is reported to be linked with the maintenance of mitochondrial membrane potential [37]. Mutation in DJ-1 is rare in PD and was first discovered in 2003 to cause early-onset autosomal-recessive PD [38]. It is localized in both glial and neuronal cells in the brain [39] and appears to function as an antioxidant [40]. UCH-L1 was first identified in a sibling pair with autosomal-dominant PD in 1998 [41], however, this is an extremely rare PD scenario to date [42, 43]. It is a neuronal specific protein that hydrolyzes polymeric ubiquitin chains into monomers [44, 45].

1.3.3 Leucine-rich repeat kinase 2 (LRRK2; PARK8)

PARK8 was first identified in 2004 in autosomal dominant PD linked to the PARK8 locus. The locus located within the chromosomal position 12q12 was first mapped in a large Japanese family [46]. However, PARK8 linked parkinsonism was also found in several European family, which shows its relative significance. The gene linked with this PARK8 locus is called LRRK2 [47–49]. LRRK2 was reported as the cause of both late-onset autosomal dominant familial PD, one of the most common forms of familial PD and sporadic PD . The LRRK2 gene is a big gene with 2527 amino acids and spans 144-kB genomic region with 51 exons. It conserves multiple independent domains, see 1.2, suggesting its complex cellular function and regulation [47, 49]. Since the molecular role of hLRRK2 in PD progression is the aim of this study, the study of LRRK2 domain structures will be of particular importance to understand the complex and multi cellular function.

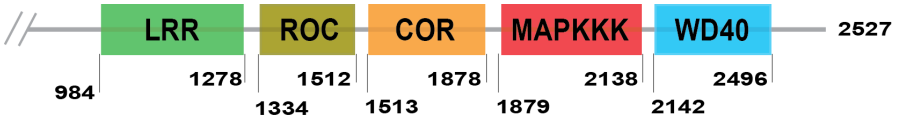

FIGURE 1.2: Schematic view of LRRK2 domain structure. It cotains four domains, namely, LRR, ROC, COR, MAPKKK and WD40 domain.

1.4 LRRK2 Domain Structure

LRRK2 is classified as a member of the ROCO protein family by the presence of 200-250 amino acids Ras complex (Roc) followed by a 300-400 amino acid domain called

COR (C terminal of Roc) [50]. Sequence analysis has showed few independent domains such as leucine rich repeat (LRR) domain, Roc domain followed by Cor domain, a mitogen activated protein kinase kinase kinase (MAPKKK) domain and C terminal WD40 domain in LRRK2 [51]. LRRK2 protein may serve as a scaffold for the assembly of a multi-protein signaling complex since it has both protein interaction domains (LRR and WD40) and enzymatic domains (Roc and MAPKKK).

1.4.1 Leucine rich repeat (LRR) domain

LRRK2 has 13 LRRs that are generally 20-29 residue long and contain sequence motif (LxxLxLxxN/CxL). The primary function of this motif might be to provide a versatile structural framework for protein protein interactions. However, this domain is also associated with several biological mechanisms including cell adhesion, cellular trafficking, neuronal development, cell polarization, apoptosis, gene regulation and cytoskeletal dynamics [51].

1.4.2 Ras of complex protein (Roc) domain and C-terminal of Roc (COR) domain

The Roc domain is classified as a member of ROCO family which conserves a separate monophyletic group of the Ras superfamily of small GTPases [52]. Ras-related GTPases are known as a molecular switch to regulate a variety of cellular functions by controlling the GTPase cycle. This cycle consist of two different conformation; active (GTP-bound) and inactive (GDP-bound).

The conversion between GDP to the GTP-bound is catalyzed by guanine nucleotide exchange factors (GEFs) and controls the downstream signaling. However, GTP to GDP-bound state is facilitated by intrinsic GTP hydrolysis. This process is accelerated by GTPase-activating proteins (GAPs) in order to terminate the signaling [53]. The diverse cellular functions are regulated by the interaction between the GTP-bound form and effector molecules. However, GDP-bound form interacts with GDP dissociation inhibitors (GDIs). The COR domain is a common feature of all ROCO proteins which always link with the Roc domain. It contains 300-400 amino acids. This (Roc-COR) domain pair has been conserved throughout evolution which reflects a functional interdependence on each other.

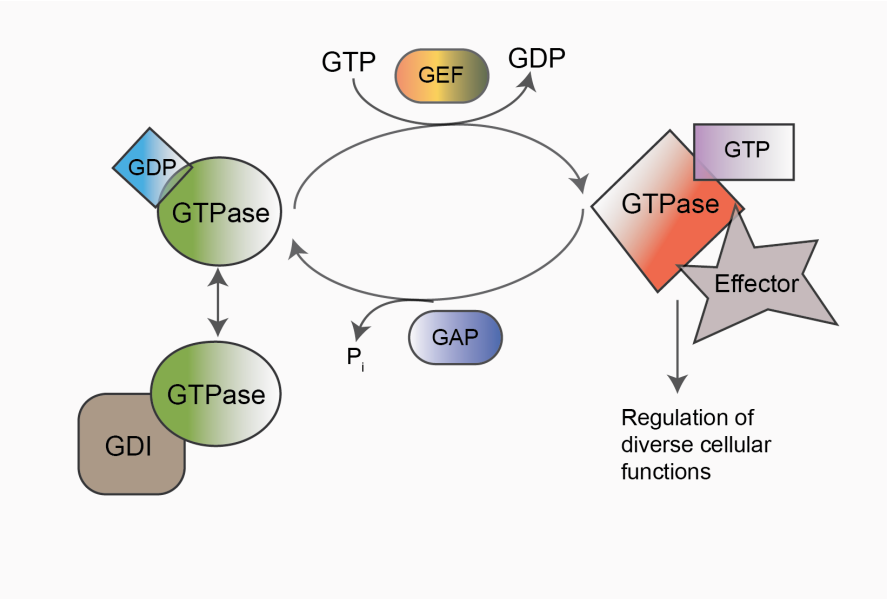

FIGURE 1.3: The GTPase cycle.

1.4.3 Mitogen-activated protein kinase kinase kinase (MAPKKK) domain

The kinase domain (MAPKKK domain) of LRRK2 has sequence similarity with the tyrosine kinase-like (TKL) subfamily of human protein kinases. Members of this family also conserve sequence similarity to both serine/threonine and tyrosine kinases (J144). The MAPKKK domain of LRRK2 resembles receptor interacting protein kinases (RIPKs) which are the key players to activate mitogen-activated protein kinase (MAPK) pathways and sensors for cellular stress. Extracellular signal-regulated kinase (ERK), c-Jun amino terminal kinase (JNK) and p38 MAPK are the three best characterized MAPKs [54]. MAPK pathways are activated through diverse extracellular stimuli and these pathways are three –tiered cascades comprising a MAPK kinase kinase, a MAPKK and a MAPK where each kinase of MAPK pathways activates the successive kinase through activation-loop phosphorylation. The majority of the active protein kinases need the phosphorylation of the activation segment which enables substrate access and catalysis to take place. The PD associated LRRK2 mutation G2019S lies at the N-terminal boundary of the activation segment and is known to augment LRRK2 kinase activity [55]. However, mutation (R1441C) in the ROC domain has been also reported to be associated with enhance kinase activity compared with wild type LRRK2 [56, 57]. Recent studies indicate that the LRRK2 has the capability to self-associate and autophosphorylate $in-vitro$, although the autophosphorylated sites and their interdependence are still unknown [58].

1.4.4 WD40 domain

LRRK2 has seven WD40 repeats where WD repeat generally contains a GH dipeptide 11-12 residues at N-terminus and a WD dipeptide at the C terminus [52]. A number of eurkaryotic proteins also has WD40 domain and these proteins are associated with a wide variety of functions such as signal transduction, RNA processing, transcriptional regulation, cytoskeletal assembly, regulation of vesicle formation and vesicular trafficking [59]. However, the WD40 domains most likely facilitate the protein-protein interactions in all these processes.

The development and pathogenesis of PD has been dynamically explored through the understanding of parkinsonism genetics, since genetics might play a significant role in the pathogenesis of PD. Studying LRRK2 will be of particular significance since mutations in this PD gene are the leading cause of both autosomal dominant forms of PD and sporadic.

1.5 Mutations associated with PD in LRRK2

Since familial PD cases have been reported to be linked with LRRK2 mutations, an extensive effort has been devoted to investigate the mutations of the LRRK2 gene in order to understand the potential mechanisms of PD. Up to now, p.G2019S, p.R1441C/G/H, p.Y1699C, p.I2020T and p.N143H are the established dominant inherited PD associated mutations in LRRK2 [61]. Among them, the G2019S and R1441C are the most common and were identified in several groups as a cause of both familial and sporadic PD [62]. For an example, G2019S contributes to 1-7 % of familial cases of parkinsonism of European and US origin and 1-3 % of sporadic PD [63]. However, R1441C mutations, located in Roc domain, were initially identified in several families and in some cases, R1441C mutation is more frequent than G2019S mutation in PD patients in some regions for example, in southern Italy. Another study reporting 60 European families with autosomal PD found a prevalence of 3.4 % for the R1441C mutation [64]. Some patients with the R1441C mutation had classic αS positive Lewy body and Lewy neurite pathology, some had tau pathology and others had asymmetric ubiquitin-positive inclusions [47]. In addition to these mutations, there are two missense variants (R1628P and G2385R) which are linked with susceptibility to PD in Han Chinese and East-Asians [61] and patients with the Y1699C mutation displayed dementia and amyotrophy [47, 65]. The DA degeneration of SNpc are not solely restricted to patients with both Y1699C and R1441C mutations, since PET scan analysis showed these two mutations are indistinguishable

from that of sporadic PD despite the pathological heterogenety [66]. These dynamic pathologies associated with LRRK2 mutations might reflect that this protein is involved in multiple cellular processes in neurons. Despite the known association between LRRK2 mutations and PD phenotypes, little is known about the molecular mechanisms of these mutated LRRK2 genes and their interaction in cells. Therefore, genetic analysis, based on animal models, might offer the promise to decipher underlying molecular bases of PD.

1.6 Animal models of LRRK2 Parkinsonism

Animal models have been widely used in the research of PD genes. For example, overexpression of LRRK2 leads to DA degeneration in *C.elegans*. These transgenic *C.elegans* showed longer lifespan compared with G2019S or nontransgenic age matched controls [67, 68].

Other models, such as transgenic mouse model are potentially not robust since they show only mild PD phenotypes. Transgenic mice, generated by using bacterial artificial chromosome (BAC), expressing LRRK2 or LRRK2 with R1441G or G2019S mutations showed minimal evidence of neurodegeneration [69]. Furthermore, making conditional expression of WT or transgenic G2019S LRRK2 mice through the calcium/calmodulin-dependent protein kinase II (CamK II) promotor also failed to induce DA neuronal degeneration [70]. However, the current LRRK2 transgenic mice showed nigrostriatal system impairment such as decreased dopamine release and behavioral deficits [61].

In contrast to vertebrate models, *Drosophila* PD models based on various form of PD-linked genes have been developed to understand their molecular function and how their dysfunction causes PD. For example, overexpression of both αS and LRRK2 mutated genes in *Drosophila* showed severe PD phenotypes including age dependent locomotor disability and DA degeneration [71–74]. Although there are physical differences between *Drosophila* and human, there is a remarkable degree of conservation in their fundamental biological pathways [75]. Thus, *Drosophila* offers a potential value of function analysis of human disease.

1.7 *D.melanogaster* as a PD model

D.melanogaster, commonly known as the fruit fly, is an excellent model organism for studying neurodegenerative diseases such as PD, Alzheimer's disease and Huntington's disease due to the following facts: it has short life span which is useful for scientist in

modeling neurodegenerative disease and secondly, it has DA system which partly resembles the human DA system. Furthermore, *Drosophila* culturing is cost effective and easy to handle in the laboratory. In addition, it has well characterized anatomy and a completely sequenced genome [76, 77]. There exists powerful genetic techniques developed by *Drosophila* researchers to make full use of the model [78]. For example, human neurodegenerative disease associated genes can be introduced into the *Drosophila* genome via the binary yeast transcriptional co-activator GAL4 and upstream activting sequence (UAS) system [79]. In addition, *Drosophila* contains 44% homologous sequences with humans [80] and approximately 77% of the genes are known to be associated with hereditary human disorders have *Drosophila* homologues including, parkin and DJ-1 [80]. Moreover, *Drosophila* has a complex central nervous system which makes it possible for PD researchers to explore large scale pharmaceutical screens [81]. In last decade, researchers generated various PD models in *Drosophila*, based on PD-associated genes, in order to understand the biological functions and how their dysfunction might lead to PD. In this study, we have chosen *Drosophila* PD models based on the two most intensively studied genes, LRRK2 and αS, in order to elucidate their fundamental molecular mechanism underlying PD.

1.8 Mass spectrometry based proteomics

The term proteomics defines the large-scale study of the whole complement of an organisms proteins. Mass spectrometry (MS) based proteomics is already a well-established powerful approach for studying biological process in health and diseases [84–86]. Several key features such as, unbiased identification of proteins and protein modifications from complex biological mixtures showed the robustness of this technique and the strength in understanding protein dynamics, protein-protein interactions and post translational modifications. In the discovery approach, proteomics is performed to identify the proteins in an assumption free manner. On the other hand, the targeted approach focuses only on some subsets proteome. Now a days, MS based proteomics has made it possible to identify several thousand proteins from complex mixtures and explore protein-protein interactions, mapping of post-translational modifications with confidence [87–90].MS based proteomics approaches might be classified into two major groups, namely top-down and bottom-up. In the top-down approach, ionized proteins are identified by the mass spectrometer by determining their intact and fragment mass-to-charge rations. This approach has some severe technical limitation of the complex protein mixture analysis since complex mixtures have a dynamic protein mass range, which might be challenging to solubilize and to separate from each other before measurement. However, the bottom-up approach, often referred to as shotgun proteomics, is performed with

proteins separation and digestion into peptides prior to MS analysis. Since ionization efficiency of peptides is better than proteins, it produces less complicated spectra which are easier to interpret. Therefore, this approach outlawed all the limitations of the top-down approach. Figure 1.4 represents the schematic workflow for the classical shotgun proteomics. Briefly, shotgun proteomics is performed with proteins mixtures derived from cells or tissue sample complexity is reduced by performing gel based methods, size exclusion or ion-exchange chromatography [91].

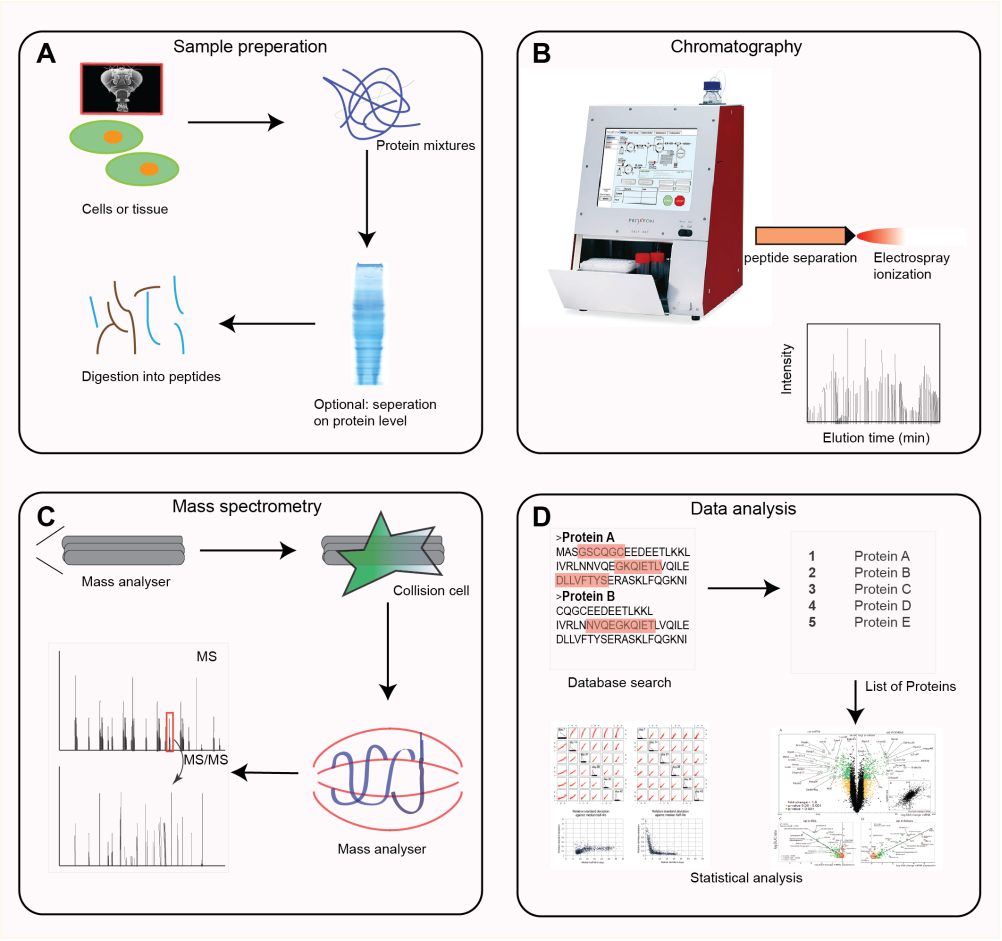

FIGURE 1.4: Proteins mixtures are separated (optional) and digested into peptides during the sample preparation and peptides are fractionated by nanoscale chromatography followed by transferring the peptides by electrospray ionization into the mass spectrometer. Masses of the intact and fragmented peptides are measured in mass spectrometer. Finally, proteins are identified through database search and significant candidates are determind by statistical analysis.

Certain biochemical procedures are performed to digest proteins into shorter peptides. Trypsin and lysC are the most frequently used enzyme due to their high specificity to ariginine / lysine [92]. However, some other enzymes, namely, GluC, AspN or LysN are also useful to increase deep protein sequence coverage depending on proteomics contexts

[89]. Currently, various protein digestion protocols such as, in solution, in gel and the filter-aided sample preparation (FASP) are being followed based on different samples [93]. Since, the digested peptide mixture is potentially complex, the peptide separation is executed by using liquid-chromatoraphy. The peptides binds with c18 material of a chromatography column at low pH by adding formic or acidic acid to samples. Furthermore, optimum gradient separation and column dimension are also important for shotgun proteomics to gain deep mass spectrometric analysis and less analytical problems respectively [94]. Separated peptides are directly sprayed in the mass spectrometer through electrospray ionization. The mass spectrometer measures the intact masses of peptides (MS1 scan, precursor mass) followed by fragmenting selected peptides for measurement (MS2 scan). Peptide fragmentation can be achieved by applying different methods such as collision induced dissociation (CID), higher energy collisional dissociation (HCD), electron transfer dissociation (ETD) and a ladder is created by the fragmentation to directly derive the amino acid sequence. Theoretical mass of a peptide is compared with intact and fragmented peptide mass by a search engine (Mascot or Andromeda) which performs a database search [95]. However, statistical algorithms are highly required for the best match in a database search, since most of the spectra hold only partial sequence information. Identified peptides are accumulated in order to provide protein information and significant proteins are highlighted by statistical analysis.

1.9 Quantitative approaches in MS based proteomics

In the last decade, MS-based proteomics have emerged as a robust and powerful technique for biological research to identify many proteins from complex mixtures in a relatively short time frame. Although the protein identification from various biological samples is important, it often requires the knowledge of protein amount, their changes and posttranslational modifications under different circumstances. Since the signal intensities from MS do not represent the peptide concentration solely due to the behavior of the peptides during ionization, quantitative information cannot be achieved by MS approach. Therefore, it was a prerequisite to develop the strategies in order to have the quantitative information by relative quantification (protein abundance difference between two samples) and absolute quantification (determine copy number per cell). The quantitative information can be achieved by applying two basic strategies, namely label free approach and stable isotope labeling approach, see 1.5.

1.9.1 Stable isotope labeling approach

The principle of stable isotope labeling is based on introducing a defined stable isotope in a sample which results in distinguishable spectra due to the mass difference with another sample. This approach allows to mix different labeled samples together to measure their relative abundance. Since labeled samples are introduced in the different stages and are measured together, the quantification accuracy is increased due to having less biological variability. The metabolic labeling approach introduces a non-radioactive isotope in the growth medium, food, or by replacing an essential amino acid in the medium or food with their heavy counterpart. The first approach, a global manner, replaces all the nitrogen atoms with heavy nitrogen and produces broad isotope distributions which are complicated to analyze [96]. Hence, it has some limited application in plants and bacterial biology. In contrast, the second approach is defined as Stable isotope labeling of amino acids in cell culture (SILAC). SILAC is a metabolic labeling approach used for quantitative proteomics where relative changes in protein abundance are most accurately measured by comparing the natural form of a peptide with its stable isotope labeled homolog [97]. The most frequently used essential amino acids for SILAC are arginine and lysine. Since trypsin or lysC protease cleaves the C–terminal to these amino acids, peptide digestion with tripsin or lysC results in peptides containing at least one labeled amino acid (ariginine or lysine). Therefore, every single peptide produces two isotope clusters, SILAC pair and the intensities of the SILAC pair gives a SILAC ratio (a reflection of an identified peptide). Although SILAC was introduced in cell culture at the beginning [98], recently it has been extended in living animals like mice, zebra fishes, *C.elegan* and flies [99–101].

1.9.2 Label-free approaches

Label free proteomics performs the quantification without applying the stable isotope labeling. It is a simple, economical method that can be applied to any samples including clinical samples. Although this approach is straight forward, it suffers with less accuracy, higher variability and requires complex statistical analysis due to sample preparation and separate measurement. However, label-free approaches are being improved by introducing an intensity-based label-free quantification (LFQ) with the MaxQuant software platform [103, 104] where the algorithm contains several normalization steps in order to reduce experimentally introduced variability. Hence, this method has been applied to relative quantification with increasing success [103].

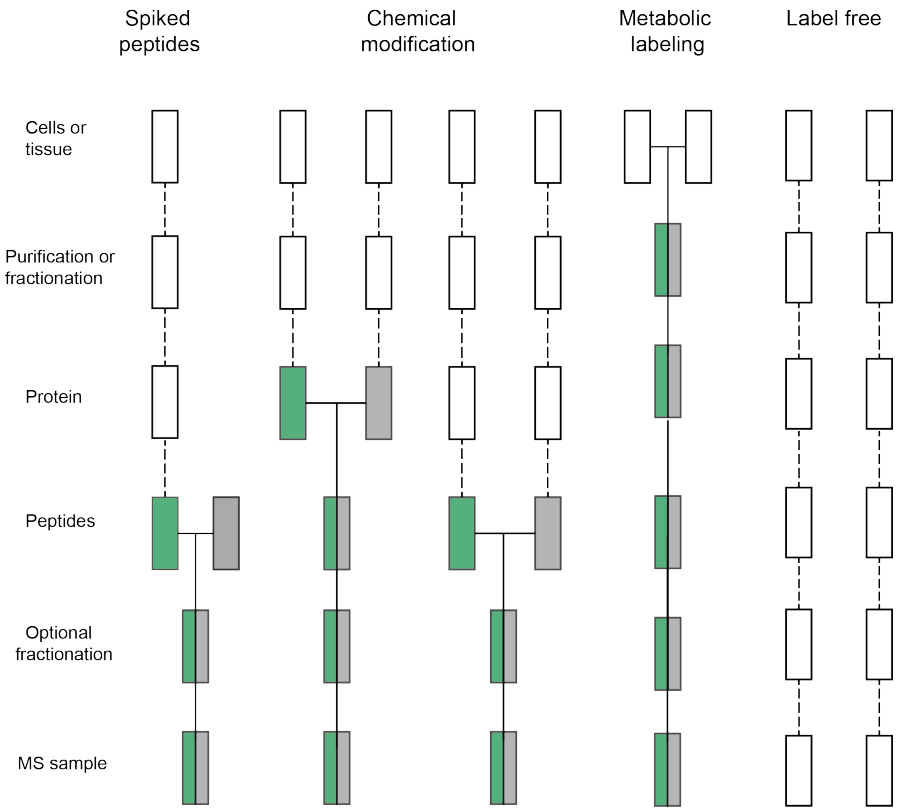

FIGURE 1.5: The labeling strategies and their impact on quantitative accuracy. The schematic depicts a typical label-based and label-free workflows. The labeled samples (colored boxes) can be distinguished in the mass spectrometer, however the unlabeled samples (empty boxes) are not. The experimental error can be reduced if the samples are pooled in the beginning [102].

1.10 Phosphoproteomics

Protein phosphorylation is one of the most significant post-translational modifications (PTMs) which has a significant importance, especially in signal transduction as an activating and deactivating switch for protein activity. During the later stages of signal progression, it plays a prominent role in both signal attenuation and termination. Disruption of these controlled systems often leads to different diseases like neurodegenerative disease, cancer [105–107] and hence, study of phosphoproteomics is of great importance. Phosphorylation is known to occur in one third of the proteome, meaning they are typically of low abundance [108]. There are various methods which have been developed to enrich the low abundant phosphorylated proteins or peptides and the chromatographic methods are the most commonly used due to their high enrichment efficiency and experimental simplicity [109–113].

1.10.1 Strong cation exchange (SCX)

SCX chromatography is a powerful approach for phosphorylated peptides enrichment, which works based on the difference in the solution charge states of phosphorylated and nonphosphorylated peptides. The typical tryptic peptides have a net charge of +2 at pH 2.7 due to an N-terminal amino group and protonated C-terminal arginine or lysine side chain and therefore, if a peptide is phosphorylated, the net positive charges will be reduced due to having additional negatively charged phosphate groups. Therefore, phosphopeptides can be enriched by SCX chromatography based on reduced positive charges on the phosphorylated peptides. Furthermore, SCX chromatography can be used to separate the peptides with different solution charge states on preparative or an analytical column by using a linear salt gradient. Gygi and coworkers showed that +1 SCX fractions containing less than 3 % of the total tryptic digests were highly enriched in phosphopeptides [114].

1.10.2 TiO2 enrichment

Titanium dioxide, TiO_2, particles are used as the column packing material like silica-based supports due to their chemical stability, rigidity and unique amphoteric ion-exchange properties [115]. It has been demonstrated that TiO_2 is capable to absorb organic phosphates effectively in acidic conditions and desorb in alkyline conditions. Therefore, TiO_2 has the potentiality to enrich phosphopeptides. Heck and coworkers reported the high enrichment efficiency (90%) of phosphopeptides in simple samples by TiO_2 chromatography [116]. However, this approach has some limitation for complex as because the non-specific binding of acidic amino residues such as glutamic acid and aspartic acid.

1.11 Mass spectrometric instrumentation

In general, any mass spectrometer requires three basic parts; an ion source, a mass analyzer and a detector. Furthermore, it also has an inlet system (for ion source), data system, vacuum system, and control electronics. The ion source ionizes the analytes and transfers them to a mass spectrometer, which will be further manipulated inside the instrument. The charged analytes flow to the mass analyzer due to pressure difference and a series of electric potential difference. Since all the charged analytes have their individual charge to mass ratio, they have different motion under an electromagnetic field which helps to separate and analyze the ions. The ion separation and analysis in the mass analyzer can be varied such as magnetic sector, time-of-flight, quadrupole, ion

trap and Fourier transform cyclotron resonance analyzer. The ion signal is measured in the detector and amplified to improve the signal and sensitivity for the instrument. The data is viewed as a spectrum in the detection system. In the proteomics context, mass to charge ratio represent the protein identity and the intensity signifies the abundance of a protein [117]. A short review of mass spectrometry is discussed in the following section.

1.11.1 Gentle ionization methods

Electron ionization, chemical and photo ionization used to be the common methods for mass spectrometers. However, they had certain limitations for large and fragile biomolecules because of their large biomolecule's decomposing capability during the ionization process which could lead to less informative spectra. Two groundbreaking gentle ionization methods are known to open the era of mass spectrometry based proteomics as these methods allowed for proteins to be brought into gas-phase without destroying them, see 1.6. In the electrospray ionization (ESI) method, a small needle is utilized to spray small droplets containing the charged sample molecules into a strong electric field [118]. The solvents are evaporated and enter the mass spectrometer as desolvated ions during the process. In contrast, matrix-assisted laser desorption ionization (MALDI) approach employs a laser that excavates and ionizes molecules from a solid matrix. Although both techniques are useful for the large biopolymer ionization, in principle they are very different in terms of coupling to mass spectrometers. ESI method performs in atmospheric pressure and produces ions in a continuous manner, in contrast, MALDI works in the vacuum of the mass spectrometer.

1.11.2 Mass analyzers

The core element of every mass spectrometer is its mass analyzer. There are various kinds of mass analyzers that exhibit unique characteristics, making them superior than others for different tasks. The key parameters of a mass spectrometer are the mass precision, mass accuracy, dynamic range, resolution, sensitivity, speed and fragmentation. The term mass precision defines the "repeatability" which means the variation in several measurements for the same mass and mass accuracy represent the deviation of the measured mass from the theoretical mass [119]. Dynamic range, the strongest signal to weak signal ratio, is a criterion for sampling deeply into a complex peptide mixture and resolution, a dimensionless number calculated by dividing the mass of the observed peak by its width, is important for proper quantification. Among various mass analyzers, two

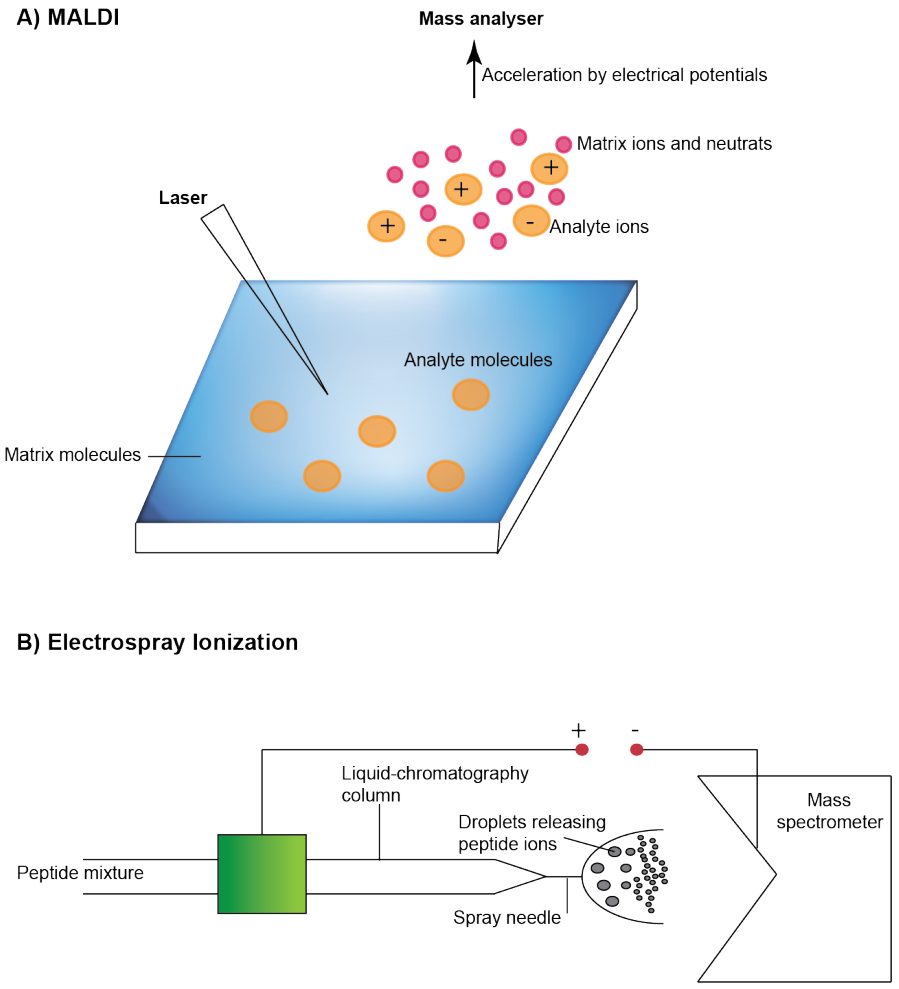

FIGURE 1.6: The schematic representation of soft ionization methods for biological mass spectrometry. ESI method produces ion in continuous manner where as MALDI generates singly charged ions. Adopted from [87].

most common mass analyzer such as, the linear ion trap and the orbitrap analyzers will be discussed below.

1.11.3 Ion trap

The quadrupole ion trap mass analyzer was first pioneered by Wolfgang Paul [120]. It is a very versatile mass analyzer in terms of mass selection, fragmentation and detection and this mass analyzer can be either a 3D or linear ion trap. Wolfgang Paul and Hans Georg Dehmelt shared the 1989 Nobel Prize in physics for their contributions to the development of quadrupole and magnetic ion traps. The ion trap is often called Paul traps, since the ion trap works based on Paul's principle. The trap consists of four precisely parallel metal hyperbolic rods and each has three axial sections. The discrete DC level of each section generates a potential well and traps ions in the axial direction [121].

The opposite rods are connected, paired and the radio frequency is applied to the pair. Therefore, one pair receives a positive and another pair a negative direct voltage (dc) that is superimposed by a time-dependent radio frequency (rf) potential. The oscillating electric field in the center of the quadrupole only allows a narrow mass-to-charge (m/z) range to pass on a stable trajectory when the ions are injected into the quadrupole in the direction of the rods and the leftover ions will be impinged on the rods. Hence, Only ions of specific mass to charge ratios are allowed to go through the narrow m/z range by ramping the rf and dc potential. In the ion trap instrument, ions can move in all directions due to three dimensional electric field effect and the x-z motion of the ions that go to the z direction can be described by the Mathieu equation, a second order differential equation.

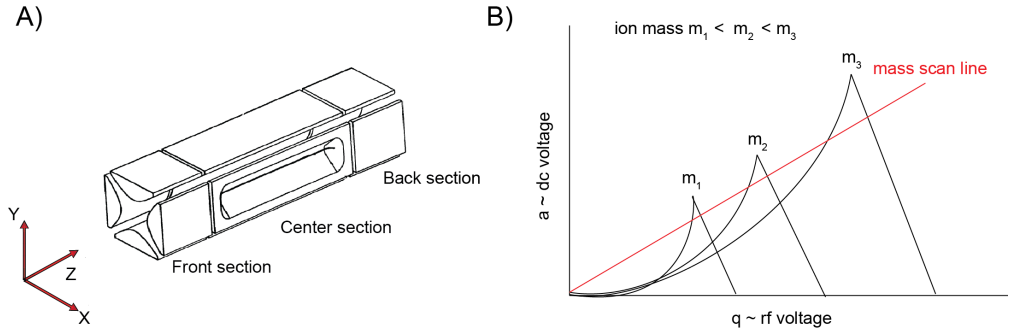

FIGURE 1.7: A) The schematic view of linear two dimensional ion trap mass analyzer. B) Plots of the dimensionless parameters a and q for different m / z values generate the stability diagram (adopted from [121]).

The solutions of this differential equation are two dimensionless parameters a and q which represent the amplitude of the dc and rf current. The intersecting mass-scan line (a/q constant) of the aq plot (stability diagram of quadrupole) provides the m/z ratios that can pass through the quadrupole without interruption. In general, though quadrupole mass analyzers are compact, it features a rather low mass resolution. In principle, the higher resolution can be achieved by narrowing down the rods diameter, increasing rf frequency and decreasing the acceleration potential of the ions. However, considering both resolution and mass range, the quadrupole characteristics improvement is challenging due to the substantial effort in manufacturing. For example, increasing the length of the rods will improve the mass resolution by increasing the number of oscillations of the ions, however increasing the length of the rods is restricted by practical limitations [95, 122–125]. Relatively high pressure in the range of 10^{-02} pa is required for ion trap operation compared with other mass spectrometers and this high pressure is achieved by the constant flow of inert gas (He) or nitrogen . The continuous flow of gas slows down the fast moving ions and act like a cushion. Hence, it helps to improve

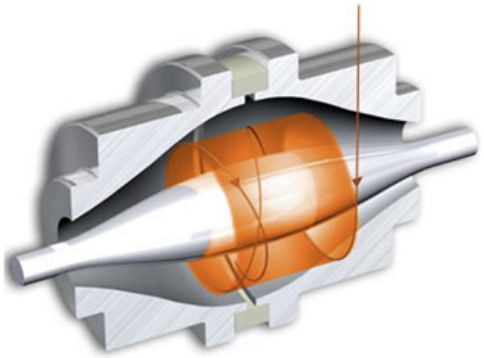

FIGURE 1.8: The cross-sectional view of the Orbitrap mass analyzer. The black arrows represent the radial (r) and axial (Z) directions. The orange arrow indicates the ion movement. The ions move along the axis and around the central electrode (Orange shade). The the image current is detected in outer barrel electrode which is splited into two electrically isolated halves (adopted from [129]).

the trapping efficiency and mass resolution. Taken together, ion trap has versatile capability including storing, isolating, fragmenting and detecting ions in combination with a multiplier .

1.11.4 The Orbitrap analyzer

The Orbitrap mass analyzer was first described by Alexander Makarov in 2000 although the basic design of the Orbitrap was based on Kingdon's trap from 1920 [126–128]. The Kindon trap was operated in an electrostatic field where an electric potential was applied between outer cylindrical electrode and an inner thin electrode (act as the central electrode). However, the Orbitrap consists of two parts, namely, the inner spindle-like central electrode and the outer barrel shaped electrode, see fig. 1.8. Since, the inner space between these two electrodes are not constant in the z direction due to analyzer configuration, the electric field also varies inside the analyzer. For example, the electric field is weakest in the equator plane (the largest space between two electrodes) and increases with the distance from the center. The ions are accumulated and stored in C-trap before entering the Orbitrap cell. The C-trap is an RF-only quadrupole with a shape of the letter "C". Once ions enter into Orbitrap from the C-trap, the two forces starts acting on the ions such as radial force and the axial force. The radial force is generated by the radial field (Er) which attracts the ions towards the central electrode. If the attraction force (centripetal force) and tangential velocity of the ions (centrifugal force) is equal, the ion will have a circular trajectory orbit motion around the central electrode an the initial energy of the ions determines the oscillation of the ions.

In contrast, the axial field has a heterogeneous form, first, the field intensity varies in the z direction in the opposite direction from the equator plane and second, the direction of the electric field vector at different points that are not parallel to each other along the z direction. The heterogeneous electric field generates a mass dependent ion oscillation towards the z direction simultaneously to the circular motion around the central electrode. Once ions are entered inside the analyzer, they are attracted towards the equator plane and traverse it. However, when the ions are in the other half of the Orbitrap cell, an opposite force pulls the ions back to the equator plane and these forces increase with distance from the equator plane until the kinetic energy becomes zero in the axial direction. Ions are then accelerated back to the equator plane and acquire an axial oscillation. These combinations of axial and radial movement lead to a stable spiral-like trajectory around the central electrode. The axial oscillation is independent of the initial energy of the ion and oscillating frequency can measure the mass of the ions directly (see equation). The equation below shows mass frequency correlation where ω is the frequency in rad/s and k is the instrumental constant.

$$\omega = \sqrt{\frac{k}{\frac{m}{z}}}$$

The Fourier transformation converts the frequency readout generated from the axial oscillation of all ions into m/z spectrum. Since the frequency of the ions can be measured with very high precision, the Orbitrap mass analyzer achieves a very high resolving power. The ion trapping capacity of the Orbitrap is significantly higher than the quadrupole ion trap and hence, posses much higher space charge tolerance. The Orbitrap mass accuracy requires very high vacuum in order to avoid the collisions with background molecules which can lead the dephasing of ions and thus deterioration of the mass accuracy and resolution. Therefore, ion activation through the collisions of neutral gas molecules is not possible in this analyzer. However, the mass accuracy can be further improved by doing a real time calibration with ions present in ambient air [130]. In general, Orbitrap is coupled to into an ion selection and fragmentation devices like ion trap or quadrupole or a dedicated collision cell, since it cannot perform the fragmentation.

1.12 Orbitrap in a hybrid instrument

Now a days, Orbitrap analyzer and linear ion trap are exclusively merged into mass spectrometers and commercially available by Thermo Fisher Scientific. These hybrid mass spectrometers such as linear trap quadropole (LTQ) Orbitrap, Orbitrap Velos, Orbittrap Elite, etc use the Orbitrap for high accuracy and precision recording of precursor masses and HCD fragment masses although the rapid peptide fragmentation is performed by a linear ion trap. However, the benchtop instrument like Q-Exactive has the Orbitrap as a sole mass analyzer, which performs precursor recording as well as ions fragmentation. The Orbitrap Velos and Q Exactive were used for all the measurements in this thesis and therefore, these instruments will be introduced in more details.

1.12.1 Orbitrap Velos

The Orbitrap Velos has the similar principle design like the LTQ Orbitrap, the first mass spectrometer that included an Orbitrap mass analyzer, however, there were several improvements which made it even better mass spectrometer in terms of ions capturing, trapping and fragmentation. The front part was radically modified by introducing S–lens instead of the tube lens which provides better transmission of ions into the instrument and hence, the sensitivity is increased [123]. Furthermore, the linear ion trap in LTQ Orbitrap was replaced by a dual linear ion trap of the Orbitrap Velos. The first and second ion traps are operated in high (5.0 x 10^{-3} Torr) and low (3.5 x 10^{-3} Torr) pressure respectively and these allow very efficient trapping, isolation, fragmentation of ions and mass spectra recording at higher speed . On the other hand, other developments, including design (S-lens and C-trap HCD cell combination) and electronics provide higher numbers of iron accumulation due to efficient ion transfer, which allows five to ten times more ions per unit time into HCD cell and gives prominent HCD fragmentation for proteomics experiments .

All the advantages such as rapid fragmentation, scanning in the ion trap or efficient quadrupole like fragmentation in C-trap associated with high resolution mass analysis in the Orbitrap instrument allows this Orbitrap Velos instrument two analysis strategies. The high-low strategy allow high resolution and high mass accuracy of precursor masses recording in the Orbitrap and the low resolution with a low mass accuracy of fragmented ions in the linear ion trap. However, the high-high strategy uses the improved HCD set up and high resolution, high mass accuracy of fragmented spectra in the Orbitrap. Taken together, higher sensitivity and higher speed of the Orbitrap Velos offers efficient shotgun proteomics experiments.

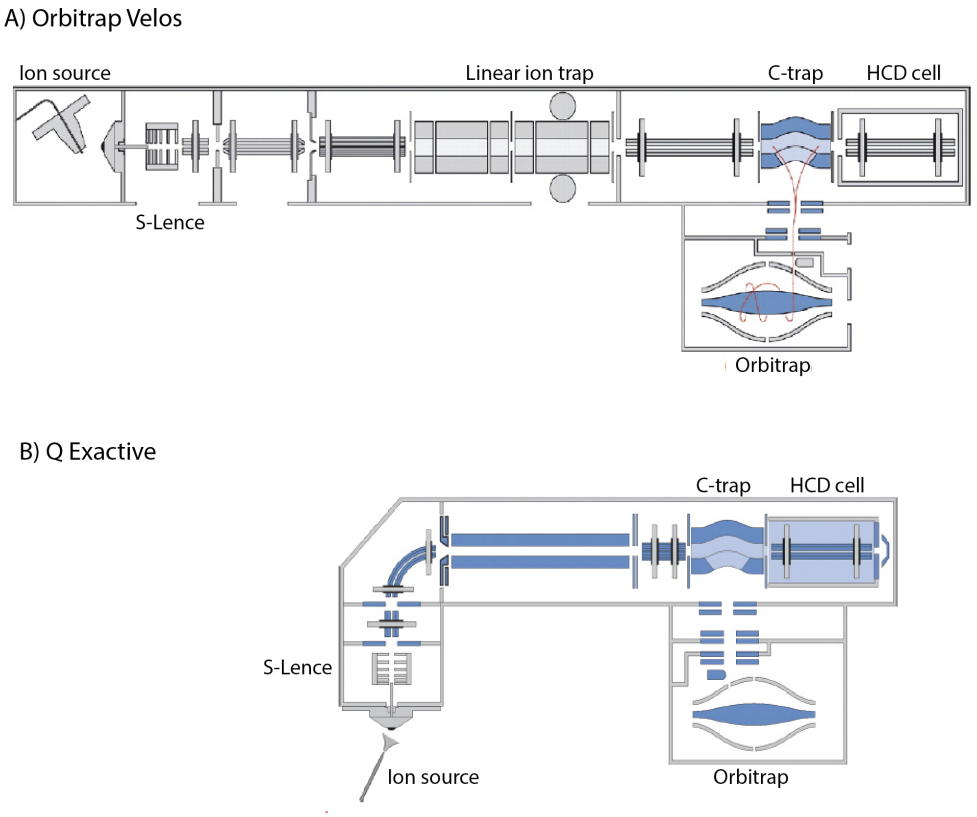

FIGURE 1.9: The schematic representation of two Orbitrap family members. A) The LTQ-Orbitrap Velos with its S-lens and dual ion trap with HCD. B) The Q Exactive, a benchtop instrument, with its Orbitrap mass analyzer (adopted from [131]).

1.12.2 Q-Exactive

The Q Exactive is a bench top instrument and one of the most latest members of the Orbitrap family. This bench top instrument allows to perform both precursor mass detection and all ions fragmentation with an Orbitrap mass analyzer [132]. The Q-Exactive has one of the most robust and mature mass filter which is capable of isolating selected ions on a faster time scale. Although it operates only HCD fragmentation mode, the speed and sensitivity of HCD are not limiting. The parallel filling of ions combined with simultaneous ion selection and fragmentation results the execution of top 10 method with 1^{-s} cycle time [131]. It provides the high-high data from proteomics measurements which resembles the HCD experiments with Orbitrap Velos. However, the shorter ion path, lack of a linear ion trap, improved electronics, software and the applied enhanced Fourier Transform (eFT) algorithm make the resolution of this instrument two times higher than any of its predecessor mass spectrometers. In summary, Q Exactive is one of the most robust and powerful mass spectrometer for shotgun proteomics, which provide high quality mass spectrometric data for the scientific community .

1.13 Aim of the thesis

As mentioned above, PD has been known for approximately two centuries, however the fundamental mechanisms underlying DA neuron degeneration remains poorly understood. So far about 20 LRRK2 mutations have been linked to PD and strikingly, gene mutations in the leucine-rich repeat kinase 2 (LRRK2) are the most common cause of autosomal dominant PD [52]. Recently, it has been shown that amino acid substitutions within the kinase and GTPase domain of LRRK2 are closely associated with the onset of PD [133]. However, direct targets of LRRK2 and its mutant forms are poorly described in living animals and it has not yet been explored how mutations in different LRRK2 domains initiate degeneration of DA neurons. Concurrent data are only available for the G2019S mutation which leads clearly to an increased kinase activity [134]. Likely, it has been shown that amino acid substitutions at amino acid position 1441 (R1441C/G) decreases the GTPase activity leading to an elevated GTP binding capacity and enhanced kinase activity [135]. However, other reports showed that the kinase activity of LRRK2 (R1441C/G) mutants is not affected [136].

Recent development in high-resolution MS-based proteomics has made it possible to identify thousands of proteins from complex biological samples within a couple of hours. In addition, MS-based phosphoproteomics is also enabled site-specific identification of hundreds of thousands of $in-vivo$ PTMs [90]. Therefore, high resolution mass spectrometry-based technologies become a powerful tool to study different diseases at the molecular level.

In the present study, we have chosen the fruitfly (*Drosophila*) as a model system to investigate the consequences of overexpressing human LRRK2 (R1441C) in DA neurons. We aimed to perform a global proteomics to study of PD progression in fly using SILAC fly based $in-vivo$ quantification at different disease stages. Since an important function of LRRK2 is its kinase activity under regular and mutated conditions, we also aimed performed a global phosphoproteome analysis to gain more insights into affected LRRK2-dependent signaling pathways and direct LRRK2 targets. Taken together, we intended to open a new window to address hLRRK2 (R1441C) mediated PD mechanisms that might shed light on fundamental ethiology of PD.

Chapter 2

Material and methods

2.1 *Drosophila* Stocks and Harvesting

Drosophila stocks- All *Drosophila* stocks were maintained on standard yeast-agar medium with 25^0C ± 1 and 12 h the light-dark cycle. The UAS/Gal4 system, a bipartite system, was used for tissue specific expression of transgenes in flies. This system conserves two components, namely, the UAS responder element and the Gal4 driver and it is only active when both UAS responder and Gal4 driver are present in the same lineage [79]. In this study, several driver lines such as *ddc*-gal4 (Dopamine decarboxylase), GMR-gal4 (Glass multiple receptor), and *elav*-gal4 (embryonic lethal abnormal vision) were used for tissue specific expression of UAS-hLRRK2 and R1441C mutant allele. The chromosomal location of transgenes was determined by using chromosome 2nd balancer (W^{1118}; Sco/Cyo; +/+) flies and 3rd balancer (W^{1118}; +/+; TM3/TM6B) flies.

2.1.1 Generation of Human LRRK2, mutant LRRK2 (R1441C) Transgenic flies

The LRRK2 and its mutant (R1441C) allele were cloned into N-terminal FLAG-tagged pPFW vector (Bloomington *Drosophila* Center) using Gateway technology from pDEST vector using PDNR (Invitrogen) as shuttle vector. pDONR vectors are Gateway adapted vectors designed to generate attL-flanked entry clones containing gene of interest following recombination with an attB expression clone. Once an entry was created, hLRRK2 gene was shuttled into pPFW expression vectors using the Gateway LR recombination reaction. The positive clones containing the insert were identified by restriction digestion and sequencing. The plasmids were sequenced by forward primer UASP

5 GGCAAGGGTCGAGTCGATAG 3 and reverse primer K10 5TGGTGCTATGTTTATGGCGC 3. Plasmids were then microinjected to w118 embryos (Venedis Injection Services, Oslo, Norway). Thus, we got two transgenic lines, namely, UAS-LRRK2 and UAS-LRRK2 (R1441C). To obtain the DA expression of transgenes, virgin females from *ddc*::GAL4 line was crossed with males from the UAS:LRRK2 and UAS-LRRK2 (R1441C) experimental flies. On the other hand, for pan neuronal expression, virgin females from *elav*:: GAL4 line was crossed with males from the UAS:LRRK2 and UAS-LRRK2 (R1441C) flies. Western blot analyses were performed to check LRRK2 expression level by using anti-FLAG. Transgenic flies (30 flies per vial) were transferred to new vial in every third day. We collected 2000 flies of each genotype at day 1, 10 and 30 post-eclosion. Flies were anesthetized with CO_2 and heads were collected on dry ice followed by storing them at-80^0C for further use.

2.1.2 *Drosophila* lines

Control and all transgenic flies used in this study are presented below. The list of constructs name and genotype are presented below,see table 2.1.

TABLE 2.1: The list of constructs name and genotypes

No	Construct name	Genotype
1	White eyes	W^{1118}; +; +
2	Canton S	+; +;+
3	*ddc*-Gal4	W^{1118}; p(w+,*ddc*-Gal4.L]; +
4	*elav*-Gal4	W^{1118}; p[w[+mc]=Gal4-*elav*.L]2/Cyo; +
5	UAS-hLRRK2 (Wt)	W^{1118}; p(w+,UAS-hLRRK2-wt]/Cyo; +
6	UAS-hRRL2 (R1441C)	W^{1118}; p(w+,UAS-hLRRK2-R1441C]/Cyo; +
7	UAS-HsapSNCA.F	W*; PUAS-Hsap\SNCA.F5B;+
8	UAS-HsapSNCA.A53T	W*; PUAS-Hsap\SNCA.A53T15.3;+
9	UAS-HsapSNCA.A30P	W*; PUAS-Hsap\SNCA.A30P40.1;+

2.1.3 Generation of SILAC flies

D.melanogaster, Strain W^{1118}, was cultured with standard method: 25^0C in 50-75% humidity. However, we used house made (Silantes GmbH) SILAC food (H20 700 ml, Agar 15 g, D(+)-Glucose anhydrous 50 g, Lys6 labeled Saccharomyces cerevisiae (S2886 TWY7) dry biomass 100 g, 30 ml 15% Nipagin solution) in a 12 h light-dark cycle to generate Lys-6 labeled heavy flies. Initially autoclaved sterile small tube (25 mm diameter) has been filled with 1-2 cm thick layer of medium. This corresponds to approximately 0.3 g of lysine (6)-yeast. The adult flies are transferred in to tubes when

the medium is being already cooled and hardened. The distribution of male and female flies will always be a ratio of 1 (male): 3 (female) since a male is able to mate with several females. In total, 20 flies were used for each vial to produce enough eggs on SILAC food. Parent flies were transferred to new vial after 3-4 day in order to avoid the mixing generation. After mating, the egg-laying begins on the yeast and within about 24 hours, the fertilized eggs develop into the first larval stage. The fully labeled adult flies from F1 generation were collected at day 1, 10 and 30 post-eclosion and few SILAC flies from F1 generation were taken for checking the labeling efficiency ($\geq 96\%$) of heavy Lysine-6 by Mass-spectrometry (MS).

2.2 Survival Curve

We chose 50 flies from each genotype in order to monitor the survival rates. Standardized media and standard temperature 25^0C were maintained to grow the flies. Flies were transferred to fresh food media in every 3 to 4 days. Dead flies were counted under the microscope and to achieve survival curves, mortality was scored daily and analyzed by using Kaplan-Meier survival curves. This experiment was repeated two times.

2.3 Climbing Assay

Locomotor ability of flies was tested by using a climbing assay (negative geoaxis assay) as previously described [137, 138]. Briefly, cohorts of 60 flies from each genotype were taken for the assay weekly from 1 week to 14 weeks. The age matched flies were selected randomly, anesthetized with CO_2 and followed by placing in a vertical plastic column (length, 30 cm; diameter, 1.5 cm) as described previously [47, 139]. After a 60 min recovery from anesthesia, flies were gently tapped to the bottom of the column. The number of flies that could climb above the median line of the cylinder in 10 seconds were counted and calculated in percentage. The climbing assay was repeated three times every week, with independently derived transgenic lines. We found similar results from each experiment.

2.4 Immunostaining and quantification of DA neurons

We executed Fluorescent immunostaining on whole-mount dissected adult brain at 1, 10, 30, and 45 days of age [140, 141]. Cohorts of six to eight flies per genotype were selected for immunostaining at each time point. All dissected brains were fixed and

TH positive neurons were stained as previously described [142]. Rabbit polyclonal anti-TH (Milipore), and anti-Flag-antibodies (Sigma) were used as the primary antibodies. For secondary antibodies, Alexa Fluor 488 goat anti-mouse IgG and Alexa Fluor 568 goat anti-mouse IgG (Invitrogen) were used for visualization. The stained brains were mounted in mounted media (MOWIOL). Each brain was scanned using optical section confocal microscopy (Zeiss LSM 510) and collected Z series images were projected into a 3D animation to quantify the number of TH positive neurons in *Drosophila* brain.

TABLE 2.2: Material and chemical used for immunocytochemistry

Chemical	**Specification**	**Company**
Paraformaldehyde		
Phosphate buffer	pH 7.5	
Sucrose		
Ringer solution		
Tissue-Tek		Sakura Fintek
TBST	1 % Tween 20	Sigma
	50 mM Tris	Roth
	150 mM NaCl	Roth
Goat serum		
MOWIOL		Sigma Aldrich
Rabbit polyclonal TH		Milipore
Rabbit anti Tan ap63	1:20000	RUB house made
Mouse anti-NC82 antibody	1:10	DSHB
Goat anti-rabbit antibody	1:400	Molecular Probes
Goat anti-rat	1:400	Molecular Probes
Dako Cytomation Glycergel		DakoCytoma-tion
Instrument		**Company**
Leica HM 5030 Cryostat		Leica
Leica TCS SP2 confocal		Leica
Zeiss LSM 510		Zeiss

2.5 Chemical and Material used for Proteomics Experiment

In this proteomics study, commercially available chemicals were purchased from the following companies: AppliChem, Applied Biosystems, Abcam, BioRad, BMG Labtech, Dako Cytoma-tion, Dr. Maisch GmbH, DSHB, Emsure, Eppendorf, Expedeon, GFL, GL Science, Invitrogen, Life Technologies, Leica, Molecular Probes, Merck, Microsoft, Milipore, Promega, Pierce, Proxeon, Roth, Roche, Sigma-Aldrich, Sigma, Sakura Fintek, Sigma Life Science, Thermo Scientific, Thermo Fischer, Ultra pure Roth, Waters,Wako, Zeiss and 3M. However, the detail list of chemicals is written below.

Table 2.3: Material and chemical used for Protein quantification

Chemical	**Company**
BSA	Sigma
SDS ultra pure	Roth
Assay DC	BioRad
Accessories	**Company**
96-Well Platte	ThermoFischer
Fluo32 Software	BMG Labtech
BMG Fluostar Galaxy	BMG Labtech

Table 2.4: Material and chemical used for Proteomics

Chemical	**Company**
Amoniumbycarbonate	Sigma Life Science
Ethanol	Emsure
Acetone	Roth
DTT	Sigma
iodoacetamide	Sigma
Lys-C	Wako
Acetonitrile	Sigma
Trifluoroacetic acid	Applied Biosystems
Methanol	Sigma
Acetic acid	AppliChem
C18-AQ RepoSil-Pur, 3 μm	Dr. Maisch GmbH
EMPORE C18 Extraction Disks	3M
Instrument	**Company**
Thermomixer	Eppendorf
Speed Vac	Eppendorf
Accessories	
C-18-Harz	Waters

2.5.1 In-solution digest

1 day, 10 days and 30 days old flies head were subjected for this experiment and 100 frozen flies head from each genotype and each time point were homogenized using a pestle. Samples were lysed with 4% SDS buffer followed by incubating the samples at 95^0C for 3 min. DNA shearing was performed by subjecting the samples to treatment with a sonicator (Branson Sonifier 250). Samples were then clarified by centrifugation at 16000g for 10 min and the supernatent was collected. Protein concentration was measured by using Bradford Assay Kit (Biored, USA) according to the manufacturers instructions. A pool of heavy samples was made by mixing identical amount proteins from 1,10 and 30 days old heavy flies head protein. For each sample, 5 μg proteins

from mixed Lysine-6 labeled fly head was spiked-in equally with protein samples from *ddc*-Gal4 line, transgenic flies head. Acetone precipitation was started by adding four times the sample volume of cold (-20^0C) 100 % acetone (Applichem GmbH, Germany) and 1 μl of GlycoBlue (Ambion, USA) to the samples. The samples were subjected to vortex and incubated for 60 min at -20^0C. After 10 min centrifugation (15000g) of samples at 40^0C, supernatent was carefully disposed without being dislodged the protein pellet. Proteins pellet was washed with 100 μl of 90 % cold (-20^0C) acetone followed by centrifuging (15000g) the samples for 10 min at 40^0C and supernatant was taken out to allow the complete evaporation of acetone. Proteins pellet was dissolved by adding 20μl of 6M urea/ 2M thiourea (Sigma Aldrich, Germany) and by vortexing thoroughly the samples. Next, we followed In-Solution digests protocol as described previously [143]. Briefly, disulphide bonds of protein mixture were reduced by adding dithiotreitol (100 mM) (DDT, Sigma Aldrich) for 30 min at room temperature. Alkylation of the samples was carried out by the addition of 550 mm iodoacetamide (Sigma Aldrich) for 20 min in the dark. The sample mixture was digested with LysC (enzyme:substrate ratio of 1:100) (Wako) at room temperature for 3 h and later on an overnight incubation with LysC was done at room temperature. The obtained peptides digestion was stopped by adding Buffer C (5% acetonitrile in 1% trifluroacetic acid). Stage Tips (Stop and Go Extraction Tips) preparation was done in two simple steps, first, two small discs of C18 Empore filter were punched out using an MPI house made puncher and second, ejection of these two discs into P200 pipette. These stage tips were conditioned by 20 μl methanol and buffer B (80% ACN, 0.1 % formic acid) followed by equilibrating in 0.1% formic acid. Peptide mixtures were then subjected to go through the C18 Empore column in order to bind the peptides with C18 material. Before MS analysis, peptides elusion from Stage tips was done by applying buffer C (80% ACN, 0.1% formic acid) into 96 well plates. Elluted Samples were dried in a SpeedVac to 2 μl and 15 μl final volume was made by adding 13 μl buffer A (0.1% formic acid (FA/H2O)). Finally 4 μl samples were applied for LC-MS/MS analysis.

2.5.2 In-gel digestion

Flie's heads were subjected for this experiment and 100 frozen flies head from each genotype were homogenized using a pestle. Samples were lysed with 4% SDS buffer and incubated at 95^0C for 3 min. DNA shearing was performed with a sonicator (Branson Sonifier 250) and samples were then clarified by centrifugation at 16000g for 10 min followed by the supernatent collection. Protein concentration was measured by using Bradford Assay Kit (Biored, USA). Next, We followed In-gel digestion protocol

as described previously [144]. Briefly, samples were loaded with 10 μl 4x LDS (Novex, Germany) loading buffer and 1 μl DDT followed by boiling the samples for 10 min at 95^0C .Afterwards samples were run on 4-12% SDS/NuPAGE Bis-Tris gels (Invitrogen, Germany), and were separated on an SDS-PAGE based on their molecular weight followed by the staining the proteins in gel.

TABLE 2.5: SDS-page materials

Chemical	**Company**
DTT	Sigma
InstantBlue	Expedeon
NuPAGE LDS Sample Buffer (4x)	Invitrogen
NuPAGE 4-12% Bis-Tris gels	Invitrogen
NuPAGE MOPS SDS Running Buffer (20x)	Invitrogen
Instrument	**Company**
Shaker	GFL
Thermomixer	Eppendorf

We cut each lane into 5 pieces and destaining of gel pieces was done by using 50mM ammonium bicarbonate and ethanol. Disulfide bonds of protein mixtures were reduced by addition of fresly prepared 10mM dithiothreitol (DTT) and subjected to vortex for allowing the reaction to proceed at 56^0C for 45 min. Iodoacetamide (55mM) was added to the samples to alkylate cysteines residues in the protein samples and vortexed briefly to continue the reaction in the dark for 30 min at room temperature. These two (reduction and alkylation of cysteines residues) steps improve the recovery of cystine-containing peptides from in-gel digests which minimizes the appearance of unknown masses in MS analysis due to disulfide bond formation and side chain modification. Since Trypsin is not stable when pure and non-acidic condition, we diluted down to 12 ng/μl from the stock solution. Therefore, digestion of the proteins in the gel pieces was carried out with 12 ng/μl Tripsin (Promega) and was kept for overnight digestion at 37^0C .Peptide digestion was stopped by acidification with trifluoroacetic acid (TFA) on the next day and peptides elution were made from the gel pieces with ascending concentrations of acetonitrile (ACN). The samples were then vacuum evaporated by using SpeedVac concentrator plus (Eppendorf) and mixtures were desalted using C18-based Stage Tips [91]. Briefly, Stage tip was prepared by ejecting two small discs of C18 Empore filter into P200 pipette and were conditioned by 20 μl methanol and buffer B (80 % ACN, 0.1 % formic acid) followed by equilibrating in 0.1 % formic acid. Peptide mixtures were then forced to bind with C18 material. Before MS analysis, peptides elusion was done by applying buffer C (80% ACN, 0.1% formic acid) and samples were concentrated to 2 μl . A final

volume of 10 μl was made by adding 8 μl buffer A (0.1% formic acid (FA/H2O)) and 4 μl samples were applied for LC-MS/MS analysis.

2.6 Immunoprecipitation

The *ddc*-Gal4 line was used to overexpress hLRRK2 and hLRRK2 (R1441C) in DA neurons of *Drosophila*. Thirty days old flies were choosen and 200 frozen flies head from each genotype were homogenized using a pestle. Samples were lysed by using 1X RIPA buffer at 4^0C. DNA shearing of the samples was performed with a sonicator (Branson Sonifier 250). Samples were subjected to centrifugation at 16000g for 10 min and the supernatent was collected. Protein concentration was measured by using Bradford Assay Kit (Biored, USA) and 1 mg protein was taken from each genotype. In total 30 μl anti-FLAG (Sigma) bead was added per 1 mg sample and incubated for 3 hours with rotation at 4^0 C. Samples were centrifuged (16000g) for 10 min at 4^0 C and supernatants was taken out. We washed the beads three times with 1X RIPA buffer with 1 min centrifugation at 1000 g between each washing step. The beads were collected and the samples were loaded with 10 μl 4x LDS (Novex, Germany) loading buffer and 1 μl DDT followed by boiling the samples for 10 min at 95^0C. Afterwards samples were run on 4 to 12 % SDS/NuPAGE Bis-Tris gels (Invitrogen, Germany) and in-gel digestion was performed for MS analysis in order to quantify the interaction partner.

Table 2.6: Material and chemical used for immuneprecipitation

Chemical	**Specification**	**Company**
RIPA-Buffer	50mM Tris-HCl pH 7.5	Ultra pure Roth
	150 mM NaCl	Roth
	1% NP-40	Sigma
	1 mM EDTA	Roth
	0,1% Natriumdeoxycholate	Sigma
PhosStop		Roche
Protease Complete		Roche
SDS ultra pure		Roth
ANTI-FLAGM2 Affinity Gel		Sigma
SeeBluePlus2Standard		Invitrogen
Trypsin		Promega
Instrument		**Company**
Centrifuge		Eppendorf

2.7 Western blot analysis

Adult fly heads were homogenized in 4 % SDS buffer and proteins were extracted followed by incubating the samples at 95^0C for 3 min. DNA shearing was performed by a sonicator (Branson Sonifier 250). Samples were then subjected to centrifugation at 16000g for 10 min and the supernatent was collected. Protein concentration was measured by using Bradford Assay Kit (Biorad, USA) to ensure equal protein loading. Thirty μg of lysate from control and transgenic flies head were mixed with 6 μl volumes of 4x NuPAGE LDS sample buffer, $2\mu l$ 40 mM DTT and heated at 95^0C for 5 min. Proteins were separated based on their molecular weight in SDS/NuPAGE Bis-Tris gels and transferred onto nitrocellulose membranes (Milipore). The membranes were blocked in TBST (pH 7.4, 10mM Tris-HCl/150mMNaCl/0.1 % Tween 20) containing 5% nonfat milk at room temperature and probed overnight at 4 ^0C with the respective primary antibody. Protein detection was done by using enhanced chemiluminescence reagents (Pierce) and visualized by an Image (VersaDoc).

Table 2.7: Instrument and chemical used for Western Blot

Chemical	**Specification**	**Company**
Transferpuffer	10 % Methanol	Sigma Aldrich
	25 mM Tris	Ultra pure Roth
	192 mM Glycin	Roth
TBS-T	1 % Tween 20	Sigma
	50 mM Tris	Roth
	150 mM NaCl	Roth
BSA	5%	Sigma
Milk powder	5%	Roth
AGO2 Antibody	1:1000	Abcam
Tan Antibody	1:2500	RUB house made
Goat anti-rabbit antibody	1:1000	Pierce
Instrument		**Company**
VersaDoc		BioRad
Accessories		
Gel		Life Technologies
Developing solution		Thermo Scientific
Whatman Paper		Roth
Nitro cellulose membrane		Roth

2.8 Immunocytochemistry

The proboscis was removed from 4 weeks old flies in ice-cold 4% paraformaldehyde in 0.1 M phostphate buffer pH 7.4. Tissues were allowed to fix for 3 h at 4^0C . The fixative was

replaced by 25 % sucrose in Ringers solution and flies were incubated overnight at 4 ^0C. Heads were embedded in Tissue-Tek (Sakura Fintek, Zoeterwoude, The Netherlands) and frozen in liquid nitrogen. Sections were made using a Leica HM 5030 Cryostat. Probes were washed twice for 10 minutes with TBST and blocked with 1 % normal goat serum (NGS) in TBST for 30 minutes (all at RT). First antibodies were applied at 4 ^0C over night at the following dilution: Rabbit anti Tan ap63 1:20.000 and mouse anti-NC82 1:10 (DSHB, Iowa, United States). Slides were incubated at RT for 30 minutes, washed twice 10 minutes with TBST and incubated with 2nd antibodies 1:400 in TBST 1 % NGS (Alexa488 conjugated goat anti rabbit, Alexa594 conjugated goat anti rat, Molecular Probes) overnight at 4 ^0C. After washing twice 10 minutes at RT using TBST slices were mounted in DakoCytomation Glycergel (DakoCytoma-tion, Hamburg, Germany) and probes were imaged using a a Leica TCS SP2 confocal microscope. In order to obtain comparable results, all procedure was done simultaneously using probes and control genotypes.

2.9 Sample preparation for phosphoproteome

Thirty days old control and transgenic flies were selected for phosphoproteomics experiment Flies heads were lysed with 4% SDS buffer and proteins were extracted by sonication, centrifugation at 16000g for 10 min followed by the supernatent collection. Bradford Assay Kit (Biorad, USA) was used to estimate the protein concentration. One mg proteins from each genotype were taken and spiked-in equally with proteins from SILAC fly's head. Acetone precipitation of the samples was executed by adding four times the sample volume of cold (-20^0C) 100 % actone (Applichem GmbH, Germany) and 1 μl of GlycoBlue (Ambion, USA). The samples were then vortex and incubated for 60 min at -20^0C. After centrifugation with 15000g at 40^0C, supernatent was discarded. Proteins pellet was washed with 90 % cold (-20^0C) acetone followed by centrifuging (15000g) the samples for 10 min at 40^0C and supernatant was taken out to allow the complete evaporation of acetone. Pellet was dissolved by adding 300 μl of 6M urea/ 2M thiourea (Sigma Aldrich, Germany). Disulphide bonds of protein mixture were reduced by adding 1 % DDT (100 mM) of total sample volume for 30 min at room temperature. Alkylation of the samples was carried out by the addition of 10 % 550 mM iodoacetamide of sample volume (Sigma Aldrich) for 20 min in the dark. The Proteins were digested with LysC (enzyme:substrate ratio of 1:100) (Wako) at room temperature for 3 h followed by an overnight incubation with LysC addition at room temperature. The digested peptide mixture was acidified (pH=2.67) by adding 0.5 % trifluoroacitic acid (TFA) of total sample volume. Strong Cation Exchange (SCX) method was employed to separate the phosphopeptides from non-phosphorylated peptides. Peptides samples

were loaded on ResourceS 1ml SCX column (ta Purifier, Ge Healthcare). A binary buffer system, consists of solvent A (7mM KH2PO4, 30 % ACN (pH=2.65) and solvent B (7mM KH2PO4, 350 mM KCI, 30 % ACN (pH=2.65), was used to apply a gradient run with increasing salt concentration.

Table 2.8: Material and chemical used for Phosphoroteomics

Chemical	**Specification**	**Company**
Amoniumbycarbonate		Sigma Life Science
Ethanol		Emsure
DTT		Sigma
iodoacetamide		Sigma
Lys-C		Wako
Acetonitrile		Sigma
Trifluoroacetic acid		Applied Biosystems
Methanol		Sigma
Acetic acid		AppliChem
AA buffer	7mM KH2PO4	Sigma
	30% ACN pH 2.65	Roth
AB buffer	7mM KH2PO4	Sigma
	350mM KCL,	Sigma
	30% ACN, pH 2.65	Roth
AC buffer	50 mM K2HPO4. 3H20	Sigma
	500mM NaCl, pH 7.5	Applichem
Binding Buffer	80% ACN	
	6% TFA	Applied Biosystems
Wash Buffer	80% ACN	
	3% TFA	Applied Biosystems
Elution Buffer	60% NH3, pH 11.6	
	40% ACN	
TitansphereTiO2 beads		GL Science
C8, 12 ?m		Sigma Aldrich
Instrument		**Company**
Thermomixer		Eppendorf
Speed Vac		Eppendorf
taPurifier		GE heathcare

The SCX fractions containing phosphopeptides were separated based on their charge and were collected in Eppendorf tubes. The FT and fractions were concentrated for several hours ($\sim$ 4 hours) by SpeedVac to a final volume of 100-250 μl so that they can be processed using eppendorf tubes during extraction. In total, 6 fractions were collected, including flow-troughs from each sample after pooling and were adjusted for binding conditions of Titan sphere (TiO_2) bead based phosphopeptides extraction. Appropriate amount of TiO_2 beads (SLSC) was adjusted based on phosphopeptides concentration and beads were washed consecutively with 60 % NH3 (pH 11.2) / 40% ACN, 70 % ACN

and washing buffer (80% ACN/3% TFA) followed by resuspended in binding buffer (80% ACN / 6% TFA). Extraction steps were performed by adding the right amount of beads to the samples and incubate on a rotating wheel for few times (three times for flow-troughs and two times for fractions) for 25 min followed by centrifuged at 2000g for 2 min for Eppendorf tubes or 5 min for falcon tubes. Beads were pooled and washed two times each with binding buffer (80% ACN/6% TFA), and washing buffer (80% ACN/3% TFA) to remove the remaining non-adsorbed material. These beads were loaded on C8 material tips and phosphopeptides elution was done with elution buffer (40 % Amonia/Acetonitrile (pH=11.6)). The eluted phosphopeptides were concentrated to 2 μl followed by reconstituted with 8 μl 0.1 % formic acid and finally, 4 μl samples were applied for MS analysis.

2.10 Liquid chromatography configuration

All nano scale liquid chromatographic seperation was done by using an online Easy nLC nanoflow HPLC system (Proxeon Biosystems, Odense, Denmark now Thermo Fisher Scientific). Briefly, reversed phase separation of peptides was done by using an Easy nLC nanoflow HPLC system with a column with 50 cm length and 75 μm inner diameters, packed in-house with RepoSil-Pur C18-AQ 1.9 μm resin (Dr. Maisch, Ammerbuch-Entringen, Germany). Peptides elusion was performed in fraction optimized linear gradient from 7 % to 35 % B over duration of 220 min followed by 95% buffer B for 10 min and then re- equilibration to 5% buffer B for 10 min. The column temperature was controlled by using a custom-made column oven at 40^0C.

2.11 Mass spectrometry configuration

The precursor ion accurate masses and associated fragment ion spectra of the lysine/tryptic peptides were measured by Q Exactive (Thermo Scientific, Bremen, Germany) as described previously [131]. We operated the mass spectrometer in positive ion mode and employed a data-dependent automatic switch between MS and MS/MS acquisition modes. The capillary temperature was 275^0C and the S-lens RF level was set to 64. MS1 spectra were acquired using a resolution of 70,000 (at 200 m/z), an Automatic Gain Control (AGC) target of 3e6, and a maximum injection time of 20 ms in a scan range of 300-1750 Th. In a data dependent mode, the 10 most intense peaks were selected for isolation and fragmentation in the HCD cell using a normalized collision energy of 25. Dynamic exclusion was enabled and set to 25 s. The MS/MS scan properties were: 17.500 resolution at 200 m/z, an isolation window of 2.1 Th an AGC target of

5e5 and a maximum injection time of 60 ms. The gradient and settings for MS/MS Scans properties were different for phosphoproteome experiments: Gradient time was 150 min and the MS/MS scan resolution was 35.000 (200 m/z), max. injection time was 120 ms aiming for an AGC target of 5e5, and an isolation window of 1.8 Th was used. $In-vitro$ kinase assay was measured with similar settings but a gradient time of 60 min was applied. Immunoprecipitation experiments were performed with a LTQ-Orbitrap Velos mass spectrometer (Thermo Fisher).

TABLE 2.9: Instrument and chemical used for Mass-spectrometry

Chemical	**Company**
Acetonitrile	Sigma-Aldrich
Acetic acid	Appli Chem
LTQ Velos ion ESI Positive Calibration Solution	Pierce
Q-Exactive ion ESI Positive Calibration Solution	Pierce
Methanol	Sigma-Aldrich
Formic acid	Merck
Instrument	**Company**
Q-Exactive	Thermo Scientific
LTQ Orbitrap Velos	Thermo Scientific
UHPLC	Proxeon
Electrospray ion source	Proxeon
Column oven	MPI House made

2.12 Proteomic Data Processing

2.12.1 Data Analysis

The MS raw datas were analyzed by MaxQuant software (developmental version 1.4.7.2) [104] to identify and quantify proteins. MaxQuant software analyzes the data by three main components, namely, feature detection and peptide quantitation (Quant.exe), Identification and validation (identify.exe) and Visualization (Viewer.exe). It processes an entire set of algorithms in detecting peaks, isotopes and quantify relative peak intensities of SILAC partners, as well as in performing statistics to large scale proteomic datasets. An eight folds improvement in mass accuracy has been achieved through its smart strategy where it uses different charged states of the same peptide for non-linear recalibration and those well identified peptides for global mass re-calibration. These identified peptides are rescued through this approach instead of falling out of the required mass accuracy window and therefore, it enhances the global identification statistics. Since SILAC approach is different from the conventional method, Maxquant allows SILAC

partners to be classified into groups which treats heavy amino acid labeling as a fixed modification and hence SILAC partners detection in MaxQuant is performed before the identification. This policy in Maxquant significantly shortens the time for database search, since too many variable modifications often make it too challenging to derive the data analysis in time. Moreover, the new strategy also restricts the possibility of mismatch.

TABLE 2.10: Used software

Software	Company
MaxQuant	MPI Martinsried
MaxQuant Viewer	MPI Martinsried
Perseus	MPI Martinsried
Excel	Microsoft
Andromeda Config	MPI Martinsried
Illustrator	Adobe
Photoshop	Adobe
MS File Reader	Thermo Scientific
Xcalibur	ThermoFisher
R	University of Auckland

2.12.2 Identification

The quant.exe processes the raw MS data and the pick list was searched using Andromeda search engine [145] against the database of *D.melanogaster* (flybase, release 5.13, Indiana University, IN, USA) with common contaminants. However, Human Parkinson's genes sequences were added in the *Drosophila* fasta files in order to identify those transgenes in our analysis. Carbamidomethylation of cysteine was taken as fixed modification and SILAC partners were classified with MaxQuant based on their labeling such as heavy, medium and light. Therefore, these were also set as fixed modification within each group. Oxidation of methionine and acetylation of the protein N-terminus were selected as variable modifications. However, Phospho (STY) was also included as variable modification for phosphoproteomics analysis. As a protease, LysC and trypsin was chosen with a maximum of 2 missed cleavages. Mass tolerances for selected fragment ions was set to 0.5 Da and initial mass deviation of precursor ion was kept 10 ppm. The identified peptides and their corresponding proteins were further processed with Identify.exe. The probability of having a random peptide match for each spectrum was estimated by the Posterior error probability (PEP) calculation. False discovery rate (FDR) represents the false identified hits percentage in the entire data set. However, we employed the following standard operating procedures in our study to achieve highly

reliable identifications. For Proteome dataset, peptide PEP <0.1, peptide FDR <0.1, protein FDR <0.1. A peptide with minimum six amino acids and at least two peptides per protein group were taken where one peptides should be unique to that protein. Although a single peptide can be utilized for the protein quantification , we required a minimum of two peptides for a protein to be considered for quantification in the present study. For Phosphoproteome dataset, peptide PEP <0.1, peptide FDR <0.1, protein FDR <0.1, peptide length >6 . The whole phosphorylation analysis was performed at the peptide level.

2.12.3 Quantification

Protein quantification in MaxQuant software was done by calculating peptide ratios based on the intensities of all 2D centroids from each of the SILAC forms and through linear line fitting of these intensities, a slope was given which denotes a ratio. SILAC labeling (element enrichment in 13C) were also included into account during this calculation. In addition, the median value was chosen to represent the peptide ratio if the peptide was quantified several times. However, protein ratios were the outcome from the median of all SILAC pair peptide ratios that belong to that protein and this certainly minimized the effect of outliers. A suitable threshold of 1.5 fold changes were considered a significant biological regulation. We reasoned that peptides from the same protein can result a decent standard deviation among the measured peptide ratios due to their individual drastic difference. Therefore, if a protein exhibits 1.5-fold change from multiple peptides in both duplicate experiments, it will be considered as a differentially expressed protein. Furthermore, proteins that exhibited 1.5-fold changes and identified in only one of the experiments were discarded to reduce suspicious protein candidates. Upregulated and downregulated expressions were presented with positive and negative ratio values, respectively in all the projects in this thesis.

2.13 Quantify the localization of phosphate group

Localization probability denotes the probability to detect specific phosphorylation site localization within different potential phosphorylated site locations when multiple serines, thereonines, or tyrosines are present in the sequence. MaxQuant calculated the localization probability score for each possible phosphorylation site by matching the observed b and y ions with the theoretical b and y ions [146] and displayed in MaxQuant output tables. Two simple processing steps were followed for the phosphoproteome analysis in order to assign a phosphorylation site accurately: first ignored the entries with post-translational modifications (PTM) scores that were lower than the maximum score

minus five and second, counted those modification where localization of PTM probabilities were at least 0.75.

2.14 Bioinformatic analysis

Most of the statistical analysis and graphical visualization were done by using the open PERSEUS environment (Part of MaxQuant). Significant differently expressed proteins were identified by using a two-sided t-test and a cutoff, if not stated differently, of log2 fold change >0.58 and p value <0.05 was used. However, R framework was also used for several calculations and plots. The category assignment and GO terms enrichment were done in the Perseus environment. The comparison between *Drosophila* and human databases were carried out as described previously [147]. Briefly, the software tool (BLAST 2.2.28+) was used for sequence comparison (BLAST search). All Uniprot identifiers of the *Drosophila* database with 18012 protein entries were searched against the human reference proteome. The results were extracted by the *Drosophila* ID importing the best blast hit. The Uniprot IDs of proteins was used to show the protein interaction network through STRING [148] and enrichment of functional GO [149] categories was performed using Gorilla tool [150] and PantherDB [151].

2.15 In vitro phosphorylation assay

In total, 0.31 μg/μl of purified synaptojanin (Origene) was incubated with 1 nM purified LRRK2 (Invitrogen) or LRRK2 (R1441C) or LRRK2 (D1994A) in 5 μl 10x kinase buffer (Cell Signalling Technology), 1 μl [γ- 32P] ATP (1 μCi) with a final vollume of 15 μl without incubation and 60 minute at 30^0C. In addition, increasing concentration (0.075, 0.3, 0.5 and 1 μm) of LRRK2 inhibitor LRRK2-in-1 was added in the mixtures and incubated for 60 minute at 30^0C. The reaction mixtures were terminated by adding 5 μl of 4x SDS sample buffer (Invitrogen) followed by denaturing the samples at 100^0C for 10 minutes. As a control, we used either Synaptojanin or LRRK2 kinase alone with rest of the ingredients. Each sample was loaded into 10 well 4-12 % Bis-tris polyacrylamide gel (Invitrogen) and run at 160 v for 2 hour. The gels were made dry and were subjected to autoradiography.

Table 2.11: Kinase assay

Chemical	**Company**
LRRK2	Invitrogen
LRRK2 (R1441C)	Invitrogen
LRRK2 (D1994A)	Invitrogen
LRRK2-In-1	Millipore
Synaptojanin	Origene
MBP	Sigma-Aldrich
Kinase buffer	Cell Signaling Technology
32 ATP	PerkinElmer, Inc
4 x LDS sample buffer	Invitrogen
Protein standards	Invitrogen
MOPS running buffer	Invitrogen
Bis-tris acrylamide gel	Invitrogen
Geiger counter	Mini Instriments
Heat blocks	Eppendorf
Phosphor screen	GE Heathcare
Phosphor imager	GE Heathcare
Exposure cassette	GE Heathcare
Centrifuge	Eppecdorf
Perspex shielding	
1.5 ml tubes	VWR international

Chapter 3

Results

3.1 Overexpression of Human LRRK2 (R1441C) induces Parkinsonism phenotypes in *Drosophila*

Mutations in LRRK2 lead to late onset autosomal dominant PD and previously, it was reported that the overexpression of hLRRK2 (G2019S) in the fly's brain caused PD phenotypes which includes climbing disability, shorter lifespan, retinal degeneration and the DA degeneration [72]. In this study, we also generated a novel hLRRK2 (R1441C) transgenic PD model flies by using Gal4/UAS system and overexpression of hLRRK2 (R1441C) induced severe PD phenotypes in flies which will be described in the following sections.

3.1.1 Transgenic human LRRK2 (R1441C) *Drosophila*

In collaboration with Prof. Dr. Bernhard Hovemann, molecular biochemistry, we generated human LRRK2 and human (R1441C) transgenic *Drosophila* as a PD model by using UAS/Gal4 system that ectopically express the hLRRK2 genes in *Drosophila* DA neurons and full brains. The successful overexpression of FLAG-tagged hLRRK2 in *Drosophila* brain was confirmed by immunoblotting, see fig. 3.1 B. A strong band at 265 kDa was observed in both hLRRK2 and hLRRK2 (R1441C) flies, however this band was not found in *ddc*-Gal4 flies.

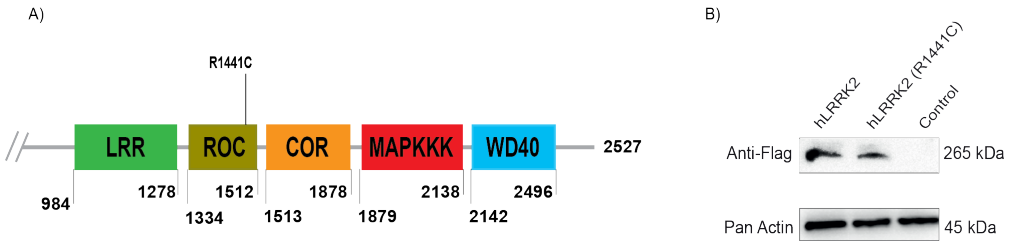

FIGURE 3.1: A)Schematic representation of the hLRRK2 domain structure. B) Expression of hLRRK2 and hLRRK2 (R1441C) in the *Drosophila* brain. Western blots from the heads of flies show *ddc*-driven hLRRK2 and hLRRK2 (R1441C) expression in the *Drosophila* brain.

3.1.2 Overexpression of hLRRK2 (R1441C) in the retina results in degeneration of photoreceptors

The Gal4/UAS expression system has been widely used in fly to ectopically overexpress transgenes in a tissue specific manner. To test whether the hLRRK2 and its substituted version have an impact on neuronal cell homeostasis in *Drosophila*, we first established a transgenic strain which overexpress hLRRK2 under the control of the glass multiple reporter (GMR) [152]. Degeneration of photoreceptor cells was used to assay neuronal degeneration previously [72], therefore we used the degeneration of photoreceptor cells to prove whether hLRRK2 and hLRRK2 (R1441C) causes neurodegeneration when overexpressed in flies. The *Drosophila* compound eyes are made of $\backsim$ 800 repeat units, called ommatidia, that includes seven photoreceptor cells (R1-R8) in given plane of section. Each photoreceptor cell has a rhabdomere, a microvillar structure, used for photoreception which resembles rod and cone outer segment from invertebrate. To examine the kinetics of retinal degeneration, we used an optical neutralization technique over seven weeks age at standard temperature and the data was generated by the examination of at least 90 ommatidia from six flies per genotype. We detected mild but progressive degeneration in the eyes of GMR control flies from fourth week until the end of the study at seventh week, see fig. 3.2 A. Figure 3.2 B shows that the overexpression of hLRRK2 (R1441C) caused a more severe and faster photoreceptor degeneration compared to hLRRK2 and control flies (p-value $<$ 0.05), respectively. This is consistent with previous findings that showed hLRRK2 causes retina degeneration in *Drosophila* [72]. Therefore, these results represent the toxic role of hLRRK2 (R1441C) overexpression in adult fly's eyes.

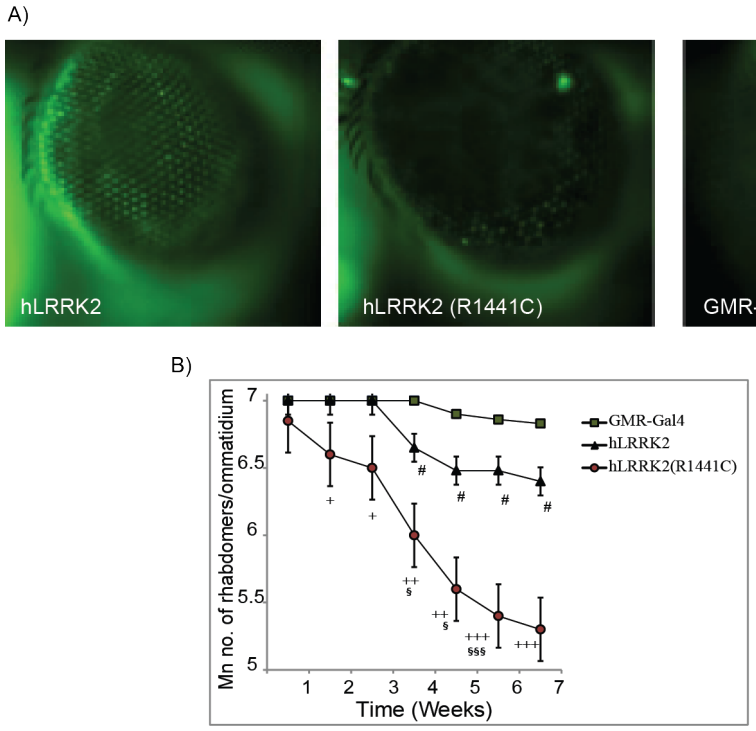

FIGURE 3.2: A) hLRRK2 (R1441C) induces retinal degeneration in *Drosophila* eye after 4 weeks. Representative images from the optical microscope for each indicated genotype were examined at their 4 weeks. B) The time course of photoreceptor degeneration determination by optical neutralization technique. Each data point was based on examination of $>$ 90 ommatidia from at least 6 flies. One way ANOVA, Bonferonni's post-hoc test. # $p <$ 0.05 GMR-Gal4 vs. hLRRK2, + $p <$ 0.05, ++ $p <$ 0.01, +++ $p <$ 0.005 GMR-Gal4 vs. hLRRK2 (R1441C), § $p <$ 0.05, §§§ $p <$ 0.01 hLRRK2 vs hLRRK2 (R1441C).

3.1.3 Early mortality and locomotion disability in *ddc*-Gal4 driven hLRRK2 and hLRRK2 (R1441C) strains

Since DA degeneration is tightly associated with movement disorder [153], next we explored whether the LRRK2 overexpression in DA neurons would induce an obvious locomotor phenotype in flies. We overexpressed hLRRK2 and hLRRK2 (R1441C) in DA neurons by combining the *UAS*-LRRK2 and *UAS*-LRRK2 (R1441C) transgenic strains with the *dopadecarboxylase* (*ddc*)-GAL4 driver [71]. Both hLRRK2 forms were tagged with a Flag at the n-terminus and fig. 3.1 B showed western blot analysis of both hLRRK2 proteins expression in brain tissue. In order to further test the phenotype of hLRRK2 expressing flies, we measured survival curves obtained from control (*ddc*-Gal4 and *UAS*-LRRK2), hLRRK2, and hLRRK2 (R1441C) flies. Our data indicated that hLRRK2 flies have a significant shorter life time compared to control flies. On average, we observed a negative effect (-17.5%) on the mean life span. Interestingly, significantly larger changes (-34%) to the median life span were observed for hLRRK2 (R1441C) flies

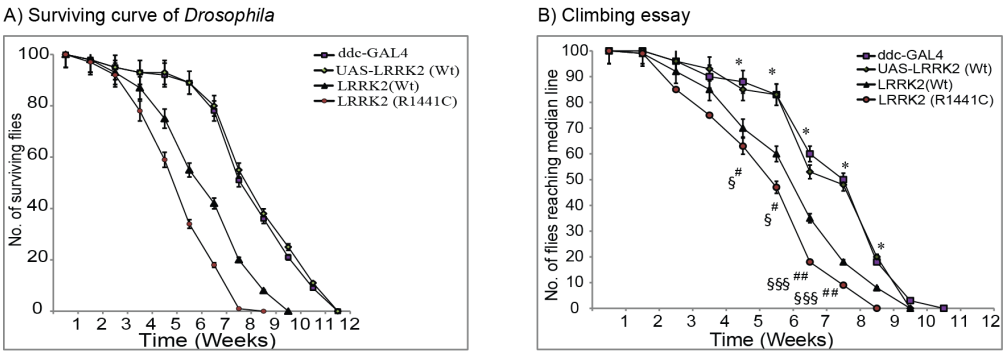

FIGURE 3.3: A) *ddc*-hLRRK2 (R1441C) causes short life span. Survival curves of flies (n=50) expressing either hLRRK2 or hLRRK2 (R1441C) under *ddc*-Gal4 driver. B) hLRRK2 (R1441C) expression by *ddc*-Gal4 causes locomotion disability. 50 flies were subjected to climbing essay. One way ANOVA, Bonferonni's post-hoc test. *p $<$ 0.05 UAS-LRRK2 vs *ddc*-Gal4, # p $<$ 0.05, # # p $<$ 0.01 *ddc*-Gal4 vs hLRRK2 (R1441C)). § p $<$ 0.05, §§ § p $<$ 0.01 hLRRK2 vs hLRRK2 (R1441C).

(fig. 3.3 A). Thus, our data indicate that a specific hLRRK2 expression in DA neurons reduces the average life span in adult flies significantly and in addition the hLRRK2 (R1441C) mutation apears to be more toxic to DA neurons compared to the regular hLRRK2 overexpression.

Since PD is a movement disorder, we next investigated whether the overexpression of hLRRK2 (R1441C) in DA neurons can cause Parkinsonism phenotype similar to other PD model. Therefore, we performed a climbing assay (negative geotaxis test). Initially flies from all genotypes rapidly climbed to the top of the vial when they were tapped. As they get older, hLRRK2 (R1441C) and hLRRK2 flies started to show climbing disability compared to their aged matched controls (fig. 3.3 B). First, we tested flies with an age of 2 weeks and observed no obvious changes between control and hLRRK2 overexpressing flies (n=60). However, during aging, we found a progressive loss of climbing ability in hLRRK2 and hLRRK2 (R1441C) flies. Notably, *Drosophila* expressing the LRRK2 (R1441C) showed a more severe effect, suggesting again enhanced biological toxicity of hLRRK2 (R1441C) in DA neurons.

3.1.4 hLRRK2 (R1441C) causes reduced tyrosine hydroxylase enzyme in a subpopulation of DA neurons

Degeneration of DA neurons is a pathological hallmark of PD and therefore, we investigated the consequences of DA neurons due to hLRRK2 (R1441C) overexpression in flies.

There are few neuronal DA clusters represents the adult brain hemisphere and these

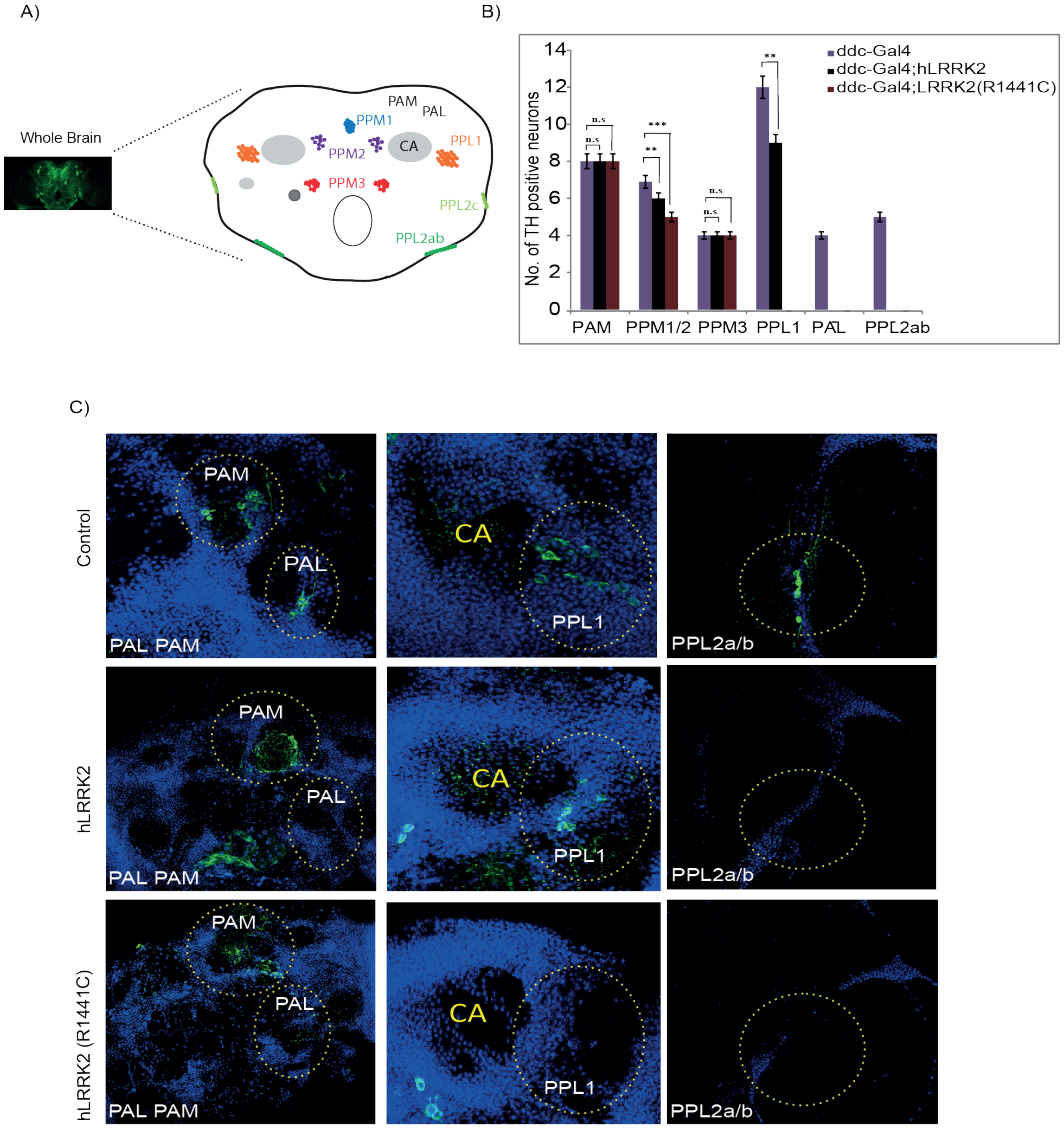

FIGURE 3.4: Overexpressed hLRRK2 (R1441C) degenerates DA neurons in *Drosophila*. A) Different DA clusters in flies brain and a representative image of TH staining in whole-mount 6 weeks old flies immunostained with primary mouse anti-TH antibody and secondary anti-mouse Alexa-Flour 568 antibody. B) Quantification of TH-positive neurons in control hLLRK2, hLRRK2 (R1441C) and *ddc*-gal4 6 weeks old flies. Dorsolateral posterior protocerebral (PPL1) and dorsomedial posterior protocerebral (PPM1/2) showed statistically significant differences between *ddc*-Gal4, control hLRRK2 and hLRRK2 (R1441C) that were indicated: ** $p < 0.01$, ***$p < 0.005$ one way ANOVA, Bonferonni post-hoc test. C) Degeneration of DA neurons in different DA clusters. Posterior prorocerebral (PPL1 and PPL2a/b) cluster and protocerebral anterior medial (PAM) showed complete DA neuronal degeneration in mutant flies.

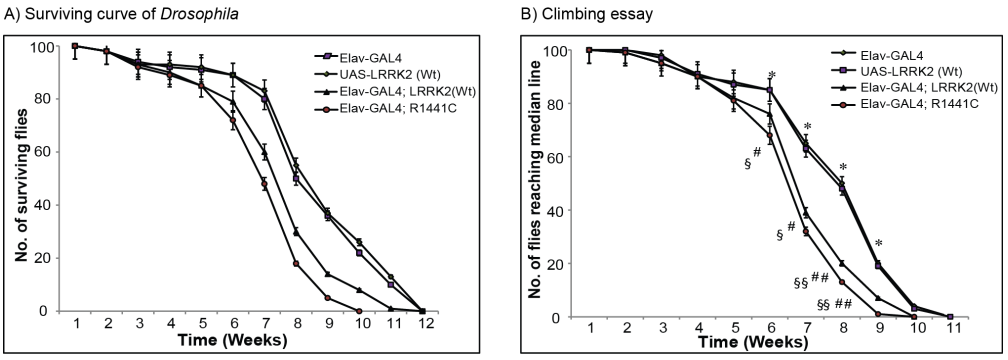

FIGURE 3.5: A) *elav*-hLRRK2 (R1441C) causes short life span. Survival curves of flies (n=50) expressing either hLRRK2 or hLRRK2 (R1441C) under *elav*-Gal4 driver. B) hLRRK2 (R1441C) expression by *elav*-Gal4 causes locomotion disability. 50 flies were subjected to climbing essay. One way ANOVA, Bonferonni's post-hoc test. * $p < 0.05$ UAS-LRRK2 vs *elav*-Gal4, # $p < 0.05$,## $p < 0.01$ *elav*-Gal4 vs hLRRK2 (R1441C)). § $p < 0.05$, §§§ $p < 0.01$ hLRRK2 vs hLRRK2 (R1441C).

neurons express tyrosine hydroxylase (TH) enzyme, an essential part for biosynthesis of dopamine. We analyzed posterior paired DA clusters in 6 weeks old *Drosophila* brain: dorsolateral posterior protocerebral (PPL1), lateral posterior protocerebral (PPL2a/b), two dorsomedial posterior protocerebral custers (PPM1/2 and PPM3), protocerebral anterior lateral (PAL) and protocerebral anterior medial (PAM)[154], see fig. 3.4 A. TH positive neurons in the DA clusters did not change significantly in number or morphology during aging in control Canton S and *ddc*-GAL4 flies. However, all 6 weeks old WT and mutant LRRK2 flies showed some significant or a trend of neuronal loss in PPM1/2 ($P < 0.01$) and ($P < 0.001$) compare with *ddc*-Gal4 line respectively. In addition, PPL1 clusters also indicated significant ($P < 0.01$) DA degeneration in LRRK2 flies compare with *ddc*-Gal4 flies. Remarkably, we found complete degeneration of DA neurons in PPL1, PAL and in PPLa/b clusters from mutant flies compare with control flies and *ddc*-Gal4 flies as shown in fig. 3.4 B. The effect in PAM and PPM3 did not reach the significant statistical significance [74] and thus, the overall prominent effect was observed in PPM1/2, PAL, PPL2a/b clusters in hLRRK2 (R1441C) flies when compared against control flies (fig. 3.4 C) .

3.1.5 Ectopic overexpression of hLRRK2 (R1441C) in all neurons induces late-onset mortality and late-onset locomotion impairment

To further examine the effect of hLRRK2 (R1441C) over all neurons in *Drosophila*, we overexpressed hLRRK2 (R1441C) under the control of the panneuronal driver *elav*-Gal4, the embryonic lethal abnormal visual system gene (*elav*)-Gal4.

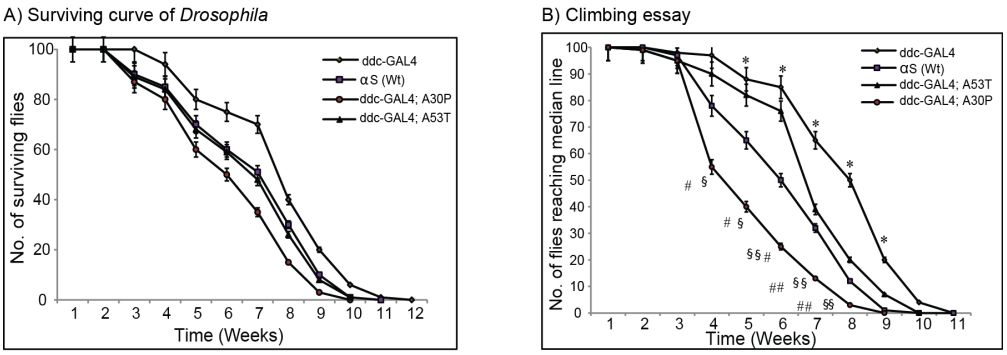

FIGURE 3.6: A) *ddc*-αS flies cause short life span. Survival curves of flies (n=50) expressing either αS or A30P-αS, A53T-αS under *ddc*-Gal4 driver. B) αS expression by *ddc*-Gal4 causes locomotion disability. 50 flies were subjected to climbing essay. One way ANOVA, Bonferonni's post-hoc test. * $p < 0.05$ α S vs *ddc*-Gal4,# $p < 0.05$, # # $p < 0.01$ αS vs A30P-αS, § $p < 0.05$, §§§ $p < 0.01$ αS vs A53T-αS.

The panneuronal expression of both hLRRK2 and hLRRK2 (R1441C) under the control of *elav*-Gal4 driver lead to shortened lifetime and significant motor impairment in hLRRK2 transgenic flies compared with control flies (fig. 3.5). These *elav* driven transgenic flies showed significant motor impairment after 6 weeks as shown in fig. 3.5 B and the climbing ability of hLRRK2 (R1441C) mutant flies showed rapid declination relative to hLRRK2 flies. Therefore, unlike our previous results these phenotypic variations in *elav* driven transgenic flies also represent the toxic role of both hLRRK2 and hLRRK2 (R1441C) over all neurons which might lead to common PD phenotypes in flies.

3.2 Alpha sy-nuclein (αS) A30P and A53T *Drosophila* model of PD

In order to screen the LRRK2 specific toxicity for PD phenotypes, we also included the αS *Drosophila* model of PD in our study. Hence, we overexpressed A30P-αS, A53T-αS and αS in flies under the control of the *ddc*-Gal4 driver and reexamined the early mortality and climbing disability as discussed previously [71]. The surviving essay demonstrated that A30P-αS overexpression lead to severe PD phenotype, such as shortened lifetime compared to αS transgenic and control flies (fig. 3.6 A).

Interestingly, αS flies and A53T-αS flies did not show any significant difference in lifetime as shown in fig. 3.6 A. Although both αS or mutant αS expressing flies exhibited normal locomotor activity at 1 week after eclosion (fig. 3.6 B), A30P-αS mutant flies showed

rapid declination of climbing ability at 3 weeks compared to both A53T-αS and αS flies. Nonetheless, significant locomotor impairment has been also observed for A53T-αS expressing flies relative to αS flies. Therefore, along with previous studies [71], our results also signifies αS toxicity in DA neurons that might cause severe locomotor impairment and shortened lifetime in flies.

3.3 Quantitative proteome analysis of transgenic flies with stable isotope labeling in living flies

Since we have analyzed the morphological changes and locomotor behavior of our transgenic LRRK2 and αS fly models, we next used an unbiased quantitative proteomics approach to analyze global proteome changes. For accurate protein quantification, we used the in-vivo stable isotope labeling of amino acids in cell culture (SILAC) method which is based on the metabolic incorporation of labeled amino acids into living organisms. The SILAC approach has been initially developed for cell culture systems and recently the method was extended to label also living flies [100]. In order to introduce the labeled amino acid into flies, we used the natural food source for flies the baker's yeast. After labeling the yeast with the stable isotope lysine-6 (13C6 Lysine) the flies were labeled with this SILAC amino acid by a simple feeding procedure with the labeled yeast. Fully labeled flies were obtained after one generation and we used the proteins derived from those SILAC flies as an internal spike-in standard to perform accurate and robust protein quantification.

3.3.1 Generation of SILAC fly and their labeling efficiency

First the auxotrophic yeast strain S. cerevisiae (S2886 TWY 7) was cultivated in the presence of stable isotope-labeled 13C6 lysine (from now on Lys6). After 5 days, the labeling efficiency was tested by in-solution digestion of extracted yeast proteins and LC-MS/MS analysis. We observed virtually no non-labeled peptides after the MS analysis and calculated an average labeling efficiency of >97%. Next, non-labeled wild type flies (strain W^{1118}) were fed with Lys6 labeled yeast until the F1 generation. Although both arginine and lysine can be used for SILAC labeling, we used only Lys6 to avoid arginine to proline conversion [155]. The labeling efficiency of adult flies from the F1 generation was again tested by MS measurements and on average the incorporation rate was above 97% (fig. 3.7 A). A representative MS spectrum of a fully labeled peptide is shown in fig. 3.7 B. Of note, the corresponding light isotope of this peptide has a much lower intensity compared to the 6 Da Lys6 containing peptide (heavy peak). Thus, our

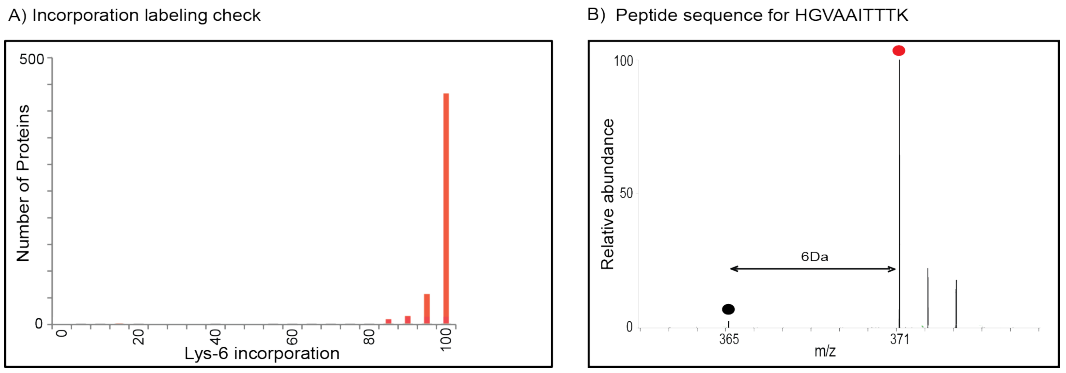

FIGURE 3.7: A) Approximately 82 % of total proteins are 100 % labeled and few proteins are 90-95 % labeled. B) Representative mass spectrum for peptide sequence (HGVAAITTTK) from heavy adult fly in the F1 generation. The mass difference between heavy peptide and light peptide is 6 Da due to one heavy lysine.

labeling tests indicate a complete labeling of the flies and we will use extracted proteins from SILAC labeled flies as a spike-in standard for all subsequent quantitative SILAC-based experiments.

3.3.2 Metabolic labeling does not change the proteome expression of *D.melanogaster*

Next, we examined whether metabolic labeling with lys 6 has any influence on the protein expression compared to non-labeled control flies. To do so, proteins from Lys6 labeled fly's head were extracted and after Bradford test, equal amounts of the non-labeled and labeled sample were subjected to in-solution digest followed by MS analysis with a 150 min gradient. The RAW data were calculated with the software tool MaxQuant (1.3.5.0) and Perseus [156]. In total, we quantified 1737 proteins between both conditions and after log transformation, the ratio differences were plotted against the ratio frequency (fig. 3.8 A). Notably, the spread of calculated ratios can be used to assess the proteomics difference between labeled (heavy) control flies and non-labeled (light) control flies. Here Log_2 fold changes ranged from -2 to 2 and more than 90 % of the protein ratios are between a log ratio of 0 and 0.25 reflecting a very similar expression profile between both populations. Since, we will use the SILAC fly as a spike-in sample, we also calculated ratio of the ratio of two independent experiments (between control flies) and observed most of the protein ratios (95%) are also distributed between -0.25 and 0.25 (Fig. 3.8B). This finding indicates that the both a direct comparison and the spike-in approach can be used to accurately quantify proteins from isolated fly brains.

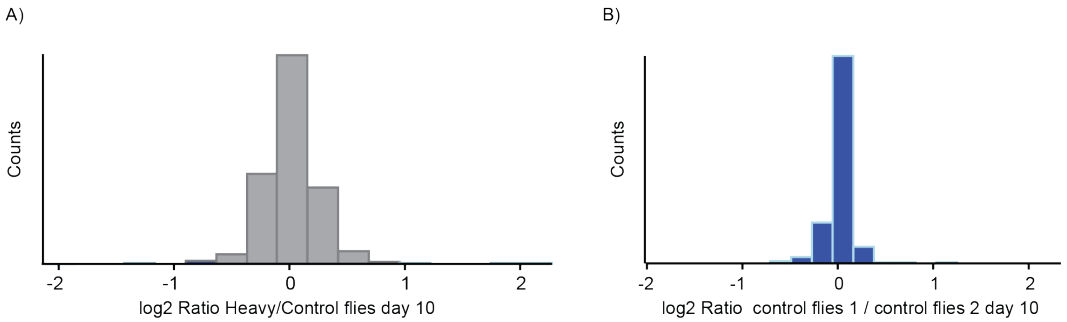

FIGURE 3.8: A) Proteins ratio distribution between Lys-6 labeled flies and unlabeled flies, where the majority of proteome ratios are close to 1 (Log_2 0 =1). Moreover, 97 % proteins ratio shows less than 1.5 fold change (Log_2 SILAC ratio between 0.5 to -0.5) in expression level for two biological replicate. B)The spike-in approach shows the ratio distribution for two independent experiments (control flies 1 / control flies 2).

3.4 SILAC protein quantification in flies overexpressing hLRRK2 and hLRRK2 (R1441C)

Similar to a previous report from Liu and Co-workers, our morphometric analysis clearly showed that hLRRK2 and hLRRK2 (R1441C) overexpression in *Drosophila* severely compromises DA neurons and causes a Parkinsonism phenotype [72]. To directly study how hLRRK2 affects DA neurons on the protein level, we used a SILAC-based quantitative proteomics approach to measure protein abundances in control, hLRRK2, and hLRRK2 (R1441C) overexpressing flies.

First, we performed an in-depth quantitative proteomics with biological duplicate on control, hLRRK2 and LRRK2-R1441C transgenic PD-like flies. Figure 3.9 shows the schematic representation of experimental steps for typical quantitative proteomics that are obtained from LC-MS/MS analysis of Lys-C digest mixtures. For the analysis, approximately 100 *Drosophila* heads were collected from each time point and protein isolation were performed with a buffer containing 4 % SDS to extract all proteins from the tissue sample. To monitor time dependent changes flies at day 1, 10 and 30 were collected. For the measurements, equal amounts of the SILAC spike-in (a pool of 1,10,30 days labeled flies) were mixed 1:1 at each time point according to their protein concentrations.

After in solution digestion with LysC, peptides were separated by 4h reversed phase gradients and analyzed with a quadrupole Orbitrap mass spectrometer, see 3.9. We

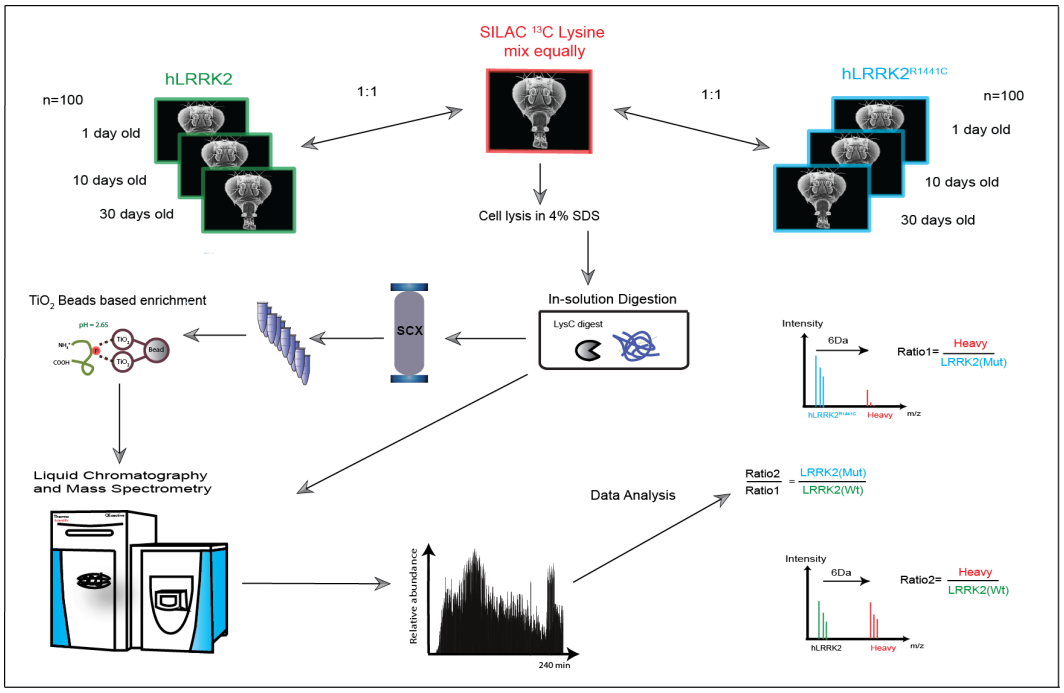

FIGURE 3.9: Experimental workflow for quantitative proteomics and phosphoproteomics analysis. SILAC mixtures, a pool of 1, 10, 30 days old Lys-6 labeled heavy fly's head, were spiked into 1,10, 30 days old control hLRRK2 (Wt) and hLRRK2 (R1441C) flies. The samples were then subjected to in-solution digestion and two independent experiments were performed using a nano UHPLC-QExactive mass spectrometer setup. The schematic spectra depicts typical SILAC pairs. For the enrichment of phosphopeptides, we used 30 days old flies and performed SCX fractionation and titanium dioxide beads (TiO_2).

measured three different time points day 1, day 10, and day 30 each in biological duplicates (n=2). Mass spectrometric data were further analyzed using the MaxQuant software package (Version 1.4.0.2) and overall we identified 2970 proteins. We found more than 2100 identified proteins overlap in three time points for both transgenic and control flies as shown in fig. 3.10 A.

To determine the global protein changes between control and transgenic flies, we applied principle component analysis (PCA). Our data showed a clear segregation between day 1 and later time points (day 10 and day 30) in the first two components. In addition, we observed a profound separation between the hLRRK2 and hLRRK2 (R1441C) at day10/30 (blue and green ellipse), indicating the different cellular function for the substituted hLRRK2 (R1441C) compared to overexpression of the regular hLRRK2 form (fig. 3.10 B).

Among the identified proteins, we were able to robustly quantify 1821 proteins (65 % of all proteins) over all three time points between biological duplicates of control, hLRRK2,

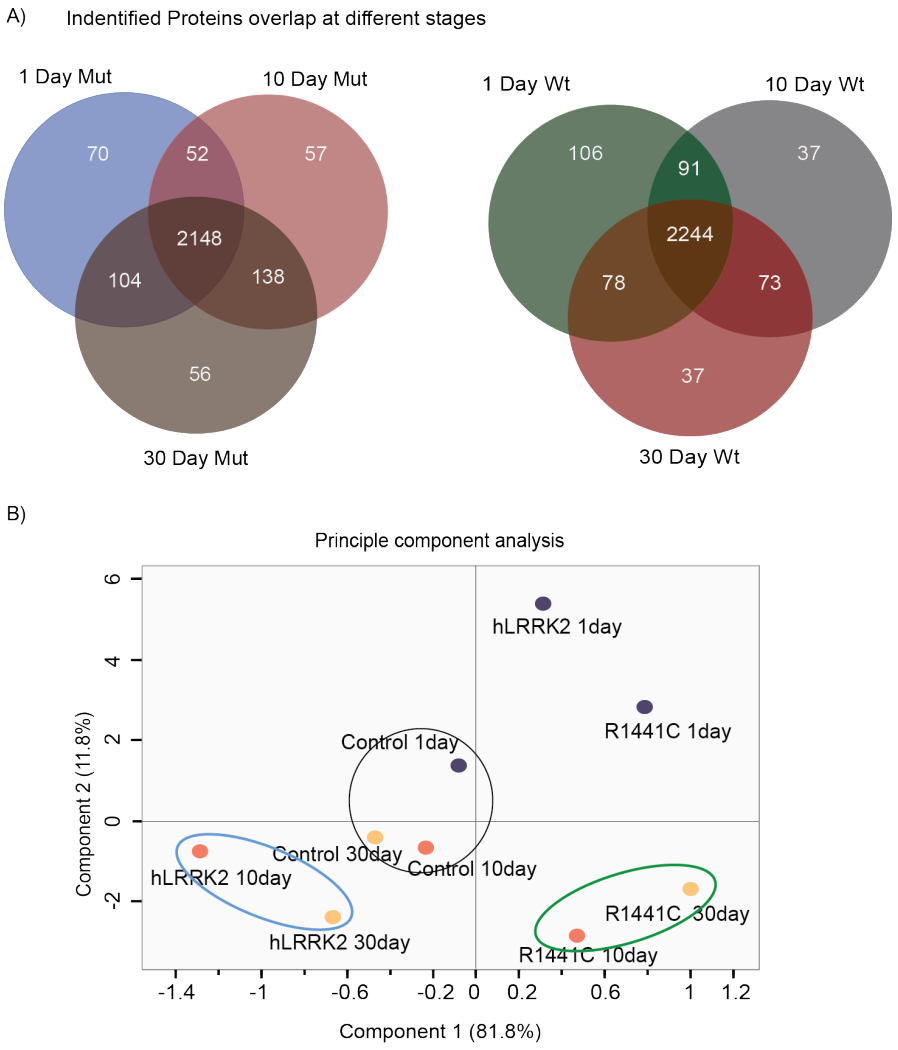

FIGURE 3.10: A) Venny diagram represents the number of identified protein overlap in Wt and Mut hLRRK2 at different disease stages. Both Wt and Mut preserves the maximum number of proteins at all stages. C) Principle component analysis of Wt and Mut LRRK2 at different time points. At day 1, it shows similar proteomic expression between Wt and Mut LRRK2. However, expressions are different from each other at day 10 and day 30.

and hLRRK2 (R1441C) transgenic flies (fig.3.11 A).

Next we considered how many proteins were significantly regulated in mutant transgenic flies compare with hLRRK2 transgenic flies at each time point. Table 3.11 B showed the summaries of quantified proteins numbers for mutant flies compared with hLRRK2 flies from duplicate analyses. Overall, 87 proteins were significantly (p value <0.5 % and fold changes >1.5) regulated in 1 day old mutant flies, however, these numbers considerably increased with the disease progression in transgenic lines (152 regulated genes in 10 days and 181 in 30 days). Therefore, this data may suggest a progressive perturbation due to hLRRK2 (R1441C) toxicity in Drosophia brains. To validate the reproducibility of the

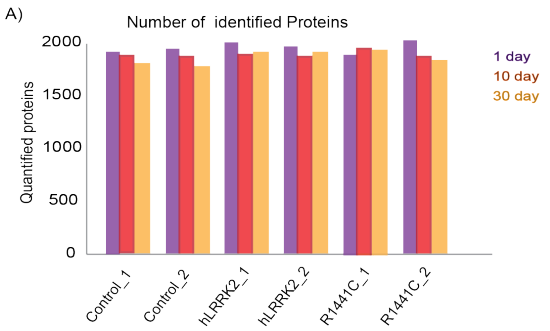

B)
Number of quantified Proteins

Day	1 day	10 day	30 day
Up regulated (Gene)	73	130	83
Not changed (Gene)	1469	1366	1241
Down regulated (Gene)	14	22	98
Total (Gene)	1556	1518	1422

FIGURE 3.11: A) Bar diagram represents the number of quantified proteins in hLRRK2, mutant and control flies at 1, 10 and 30 days. Approximately 1800 proteins were quantified in all measurements. B) The table indicates the number of significantly regulated candidates based on p values and fold changes (p value <0.5 % and fold changes >1.5) in hLRRK2 (R1441C) flies compared with hLRRK2 flies.

experiments, correlation clustering, based on Pearson's correlation, has been measured over protein expression levels of all 2970 expressed proteins across indicated *Drosophila* samples. We observed that Pearson's correlations for most of the biological duplicates were above 0.8, however the highest correlation (>0.91) was found between the proteins expression of 30 days old mutant flies. Hence, this correlation matrix among our *Drosophila* samples reflects the quantitative robustness of the measurement (fig.3.12).

In order to obtain protein changes over time, a k-means clustering were performed and protein profiles with similar regulations were grouped into different clusters (fig.3.13 A). Among 8 generated clusters, cluster 1 contains 25 proteins which were up-regulated over the entire time period and these genes could be directly associated with hLRRK2 (R1441C) toxicity since they are independent of disease or ageing. Interestingly, protein Pugilist (Pug) from cluster 1 had an enhanced expression at all time points in hLRRK2 (R1441C) flies. Pug is reported to be associated with interconvension of tetrahydrofolate pathways [157]. In addition, pug was also regulated in a study by Feany and co-workers which showed that pug has an increased abundance in tau and αS transgenic flies [158]. Furthermore, cluster 4 and cluster 8 also showed potentially interesting candidates with a positive or negative trend and late onset (after day 10). For example, the microtubule cytoskeleton associated protein Strn-mlck was found to be upregulated in mutant flies after 10 days [159]. Conversely, the protein purple showed a clear down regulation after 10 days.

To characterize differences of gene ontology terms between both hLRRK2 strains, we calculated enrichment values and plotted them against the respective p-values for annotation categories (GO-term and KEGG) by employing a fisher exact test implemented in the software tool Perseus (fig. 3.13 B). Fisher's exact test estimates the probability of

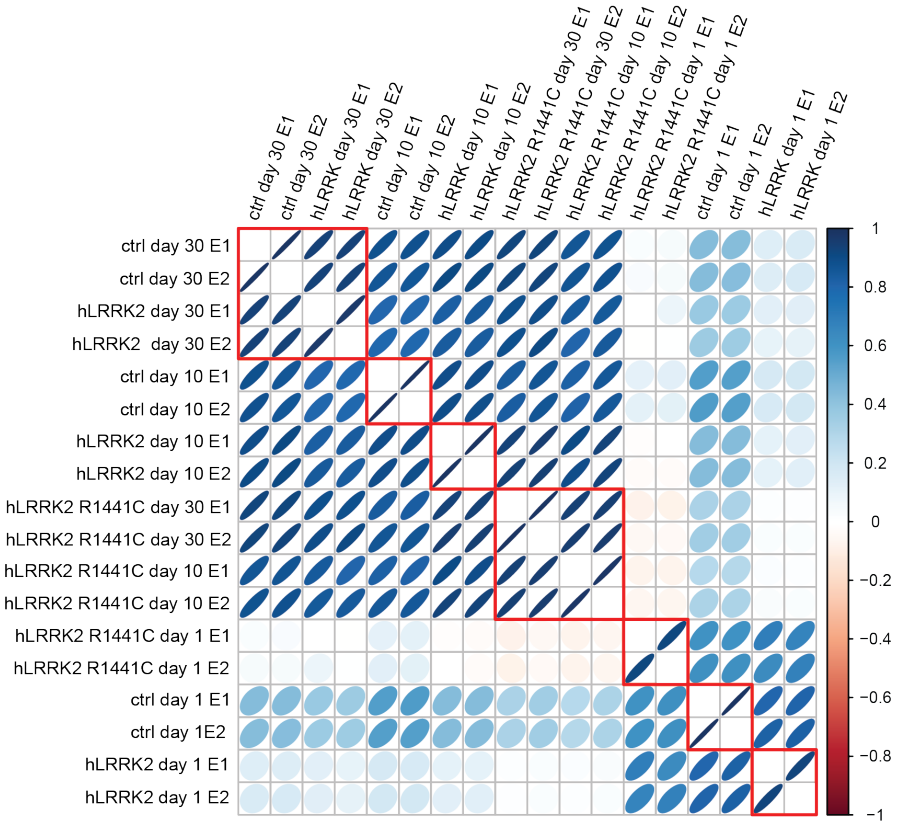

FIGURE 3.12: Pearson correlation clustering from all single-shot MS measurements. The replicate from all 30 days flies showed correlation over 0.85 from all measurements.

getting the observed data, and all data sets with more extreme deviations. Our enrichment analysis showed that both hLRRK2 and hLRRK2 (R1441C) flies are different from their wild type alleles in terms of neurological system process, synapse and phototransduction. For example, synapse linked annotations like GO biological process 'synaptic vesicle' and 'synapse part' were highly (2 times) enriched in hLRRK2 (R1441C) flies compared to hLRRK2 and control flies.

3.4.1 Transgenic hLRRK2 (R1441C) flies showed age-depending protein changes in brain tissue compared to the overexpression of hLRRK2

Since Parkinson's-associated neuronal degeneration is highly age dependent, we wished to follow protein abundances over time in our transgenic fly models. To identify potential targets for LRRK2 and its substituted version, we compared flies expressing hLRRK2 and LRRK2 (R1441C) over a time period of 30 days. We calculated the class of proteins based on p-values ($p < 0.05$) and protein ratios (fold change > 1.5) , which were significantly regulated between the control and both LRRK2 transgenic strains,

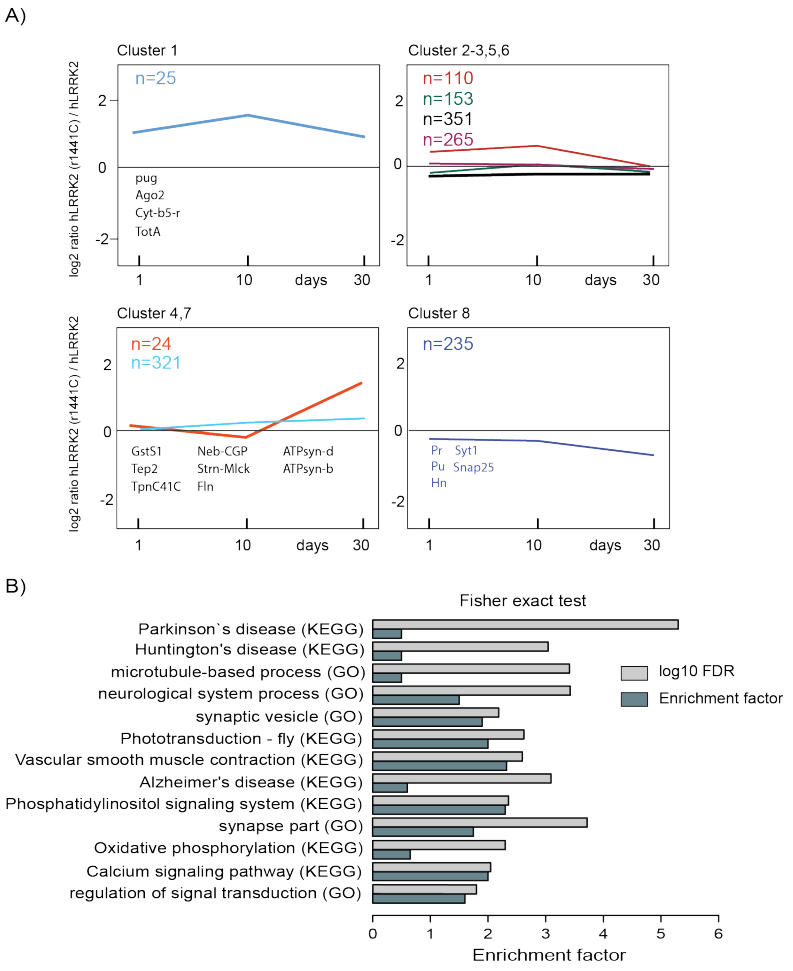

FIGURE 3.13: A) The cluster analysis of all time points illustrated the number of genes that were regulated over the PD progression. B) The enriched annotation by Fisher's exact test with FDR cutoff= 2 % and S0 fold-change cutoff = 4.

respectivly. The direct comparison of hLRRK2 and hLRRK2 (R1441C) flies revealed an age-dependent increase of regulated proteins indicated by red and green circles (fig. 3.14). In total, 1422 proteins were quantified at day 30 and 181 regulated proteins ($\sim$ 12%) were detected to be regulated. Among the regulated candidates, we found 98 of them to be down regulated and 83 of them upregulated in hLRRK2 (R1441C) compared to hLRRK2 transgenic flies.

In addition, 77 candidates out of 181 differentially expressed proteins ($\sim$ 42%) were quantified with a minimum of six peptides from each independent measurement. Next we selected some regulated genes based on statistical analysis and listed them in the table 3.15.

In total, 83 proteins showed a clear up regulation in hLRRK2 (R1441C) flies compared to control and hLRRK2 flies during aging, suggesting an accumulation of proteins due to increased hLRRK2 (R1441C) levels (Table. 3.11 B). For example, we observed several

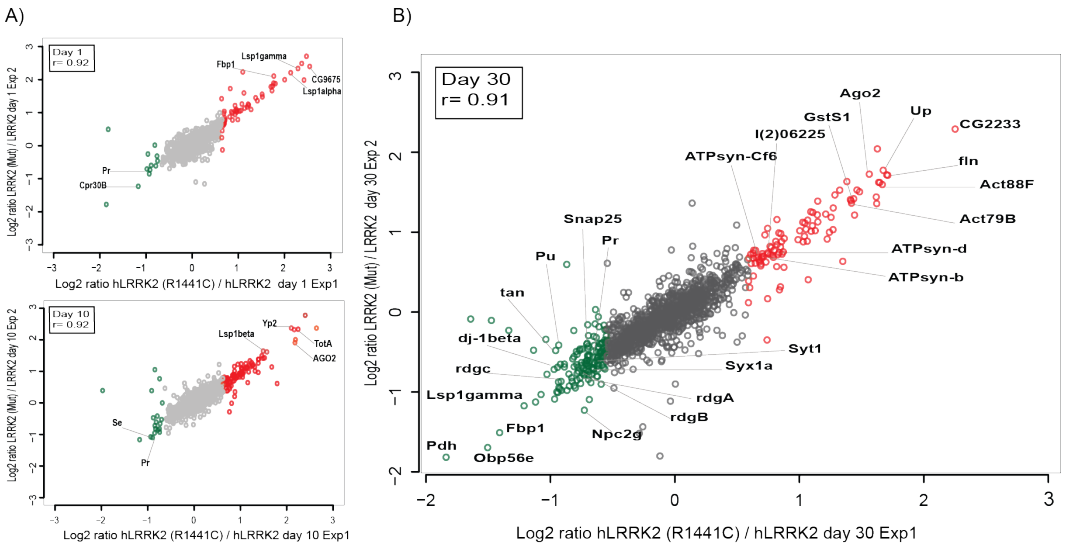

FIGURE 3.14: Reproducible quantification in protein groups within replicates. A,B) Logarithmic protein ratios (hLRRK2(R1441C)/hLRRK2 flies) were plotted for 1 day, 10 days, and 30 days old flies with two biological replicate. Up and down-regulated proteins are indicated by red and green respectively.

proteins that are associated with the actin cytoskeleton, mitochondria, and oxidative stress. The identification of three actins (Act88F, Act79B, and Act87E) with increased levels supports the association of LRRK2 to cytoskeletal actin filaments [160] and previously it was shown that LRRK2 has a physiological role in cytoskeletal dynamics [161]. Interestingly, Act88F and Act79B have a high sequence similarity with mouse Actb and Actg1 which were known as interacting partners of endogenous LRRK2 in mouse [161]. These actin cytoskeletal proteins disturbances are also in line with previous studies of *Drosophila* PD models [162, 163] and thus, it indicates that the actin cytoskeletal proteins are tightly associated with LRRK2 activity and may have a role in the onset of PD symptoms in flies.

Oxidative stress is a risk factor to develop PD and it has been shown that gluthatione-S-transferases S1 (GstS1) function as a cellular defense against toxic agents and radicals [164]. GstS1 was already documented for its predominant expression in flight muscles, however, it was also identified in other tissues including the nervous system [165]. This protein catalyzes the conjugation of reduced glutathione to the products of reactive oxygen species [166] and oxidative stress is a major contribution factor for sporadic PD [167]. Previous study on GstS1 function suggested that increased GstS1 rescues DA degeneration in a *Drosophila* model of PD [164]. Here, we also observed a clear up regulation of GstS1 in 30 days old hLRRK2 (R1441C) flies compared to hLRRK2 flies. Thus, increased expression of GSTs is most likely an adaptive mechanism to protect cells from oxidative stress in response to neurodegeneration.

	Uniprot id	Flybase ID	Protein names	Log2 ratio Mut/hLRRK2 day 30 E1	Log2 ratio Mut/hLRRK2 day 30 E2	Peptides	P-value
Actin cytoskeleton	P49455	FBgn0003721	Tropomyosin 1	1.73	1.56	26	0.0412
	Q7K860	FBgn0033027	Troponin C isoform 4	1.71	1.71	8	0.0001
	Q9VUQ5	FBgn0087035	Protein argonaute-2	1.60	1.67	9	0.0126
	P41043	FBgn0010226	Glutathione S-transferase S1	1.42	1.44	9	0.0014
	P10981	FBgn0000046	Actin-87E	1.23	1.21	17	0.0005
	Q8IPH5	FBgn0041182	Thioester-containing protein 2	1.39	1.37	24	0.0003
Mitochondial	Q24251	FBgn0016120	ATP synthase sub. d, mitochondrial	0.81	0.77	16	0.0009
	O77134	FBgn0038224	CG3321	0.74	0.75	3	0.0001
	Q9VKM3	FBgn0010612	lethal (2) 06225	0.73	0.75	3	0.0003
	P29843	FBgn0001216	Heat shock 70 kDa protein cognate 1	0.72	0.70	9	0.0004
	Q8IN44	FBgn0028396	Protein Turandot A	0.72	0.77	4	0.0020
	Q24407	FBgn0016119	ATP synth.-coupling factor 6, mito.	0.69	0.67	11	0.0002
Neuronal	E1JJK8	FBgn0003218	Protein retinal degeneration B	-0.50	-0.42	8	0.0059
	P25228	FBgn0005586	Ras-related protein Rab-3	-0.50	-0.51	7	0.0001
	P21521	FBgn0004242	Synaptotagmin 1	-0.51	-0.56	15	0.0040
	P17276	FBgn0001208	Protein Henna	-0.51	-0.51	11	0.0053
	P13607	FBgn0002921	Na/K-transporting ATPase α	-0.56	-0.62	47	0.0042
	P48611	FBgn0003141	6-pyruvoyl tetrahydrobiopterin synthase	-0.59	-0.52	5	0.0060
	Q9V427	FBgn0027108	Innexin inx2	-0.62	-0.69	6	0.0051
	Q24547	FBgn0013343	Syntaxin-1A	-0.63	-0.66	12	0.0021
	P62152	FBgn0000253	Calmodulin	-0.64	-0.64	8	0.0002
	P13677	FBgn0004784	Protein kinase C, eye isozyme	-0.65	-0.71	18	0.0051
	Q09103	FBgn0261549	Eye-specific diacylglycerol kinase	-0.67	-0.75	19	0.0075
	Q9VIU9	FBgn0032797	CG10186	-0.72	-0.62	3	0.0091
	Q9VFN7	FBgn0038198	Niemann-Pick type C-2b	-0.73	-0.65	3	0.0059
	P36975	FBgn0011288	Synaptosomal-associated protein 25	-0.73	-0.43	5	0.0418
	Q967D7	FBgn0010473	Protein turtle	-0.76	-0.85	4	0.0090
	Q9VA37	FBgn0039802	dj-1β	-0.89	-0.76	8	0.0152
	Q9W369	FBgn0030106	tan	-0.90	-0.59	7	0.0434
	P40421	FBgn0004366	Ser/Thr-protein phosphatase rdgC	-0.92	-0.81	9	0.0118
	P48596	FBgn0003162	punch	-0.95	-0.79	9	0.0326
	P23625	FBgn0004435	Guanine nucleotide-bdg. protein G(q) α	-0.98	-0.87	14	0.0124
	P29829	FBgn0004623	Guanine nucleotide-bdg. protein β2	-1.00	-0.95	13	0.0046
	Q04691	FBgn0000639	Fat-body protein 1	-1.51	-1.41	3	0.0120

FIGURE 3.15: List of significant candidates in mutant hLRRK2 flies compare with Wt flies at 30 days. Up-regulated candidates are mostly from cytoskeleton and mitochondrion whereas down-regulated proteins are from neuronal cell bodies and membranes.

Mitochondrial dysfunction is known as one of the biochemical hallmark of sporadic PD [168] and we found several upregulated mitochondrial proteins, including three members of the complex V (ATP synthase subunit d, b, f) and the ATP synthase-coupling factor 6. Proteome studies of human substantia nigra showed high abundant ATP synthase D chain in PD patients compared with age matched controls [169] and promisingly our result also showed upregulated ATP synthase subunit d in mutant flies. The consistency of upregulated ATPsyn-d in the human substantia nigra of PD patients and hLRRK2 (R1441C) *Drosophila* PD model further indicates similar mechanisms of the PD between human and flies. Therefore, the increased levels of these mitochondrial gene expression suggesting a dysregulation of the mitochondrial respiratory chain in hLRRK2 (R1441C) overexpressing flies. However, the association of the LRKK2 function and mitochondrial activity is still unclear.

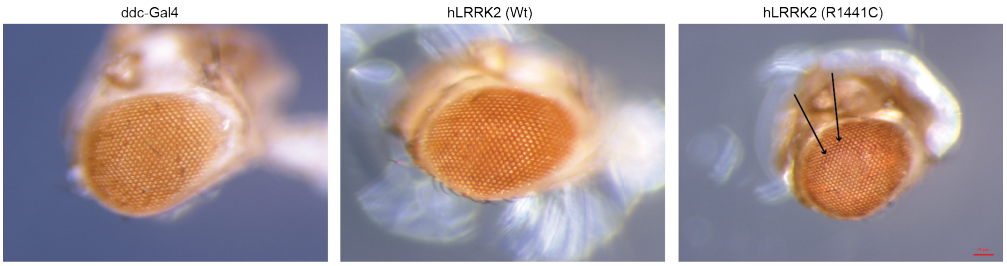

FIGURE 3.16: Retinal degeneration due to *ddc*-Gal4 driven hLRRK2 (R1441C) overexpression in DA neurons of *Drosophila*. 4 weeks old mutant flies show mild but visible retinal degeneration (black arrows) compare with others.

Another interesting candidate with a clear association to PD is the *Drosophila* Argonaute (Ago2) protein, a splicing regulator, in hLRRK2 (R1441C) expressing flies [170–172] . It has been reported that Ago2 is required to silence transposable elements in somatic tissue and moreover Ago2 mutations is leading to a reduced lifespan and progressive memory impairment [173–175].

Previously it was reported that membrane associated proteins were perturbed in PD model *Drosophila* [162, 163] and in line with that findings, we observed several differentially expressed membrane associated proteins such as Protein retinal degeneration B (rdgB), Serine/threonine-protein phosphatase (rdgC), Eye-specific diacylglycerol kinase (rdgA), Innexin (inx2) and Chaoptin (Chp). Drosphila rdgC is highly abundant not only in the compound eye but also in the photoreceptor-containing organ, optic lobes, ocelli and in the mushroom bodies of central brain [176]. However, it is also assumed to be involved in rhodopsin regeneration. The molecular function of rdgC gene is to inhibit light-induced retinal degeneration in *Drosophila* and rdgC mutants lead degeneration of photoreceptors cells [177]. Since we quantified few downregulated retina associated genes in mutant flies, next we examined the eyes of 30 days old hLRRK2, hLRRK2 (R1441C) and control flies. Interestingly we observed mild but obvious structural abnormalities in 30 days old mutant flies retina compared with control flies, see fig. 3.16.

Besides these regulated actin cytoskeleton, mitochondria and membrane associated proteins, we also detected several proteins connected to neuronal functions and plasticity with significant down regulation over the entire data set. Interestingly, cluster 8 revealed a class of proteins mainly involved in synaptic plasticity that were only down regulated in hLRRK2 (R1441C) flies compared to control flies as shown in fig. 3.13 A. Synaptic vesicles (SV) recycling process is an important step for the release of neurotransmitter and activation of postsynaptic receptor channels. Mainly three proteins, such as

Synaptobrevin, Syntaxin 1A, and SNAP-25 form the core of the SNARE complex (soluble attachment NSF protein receptor) mediates the vesicle formation and fusion [178]. Dysregulation of syntaxin and synaptobrevin in flies leads to defects in neurotransmission [179, 180] and deficiency in SNAP-25 (synapto-some-associated protein 25kDa) was associated with neuronal disorders in humans [181]. Here, we found two SNARE core proteins SNAP-25 and Syntaxin are down regulated in hLRRK2 (R1441C) compared to hLRRK2 flies. Similarly, the exocytosis related proteins synaptotagmin (Syt1) and the Ras-related protein (Rab-3) showed also exclusively decreased levels in hLRRK2 (R1441C) flies compared to control and hLRRK2 flies. Synaptotagamin (Syt1) is a presynaptic Ca2+ sensor for neuroendocrine cell function and an essential part for Ca^{2+} triggered exocytosis in neurons. It is also known as a molecular marker for adaptive changes in excessive neuronal activity during epileptic seizures comes from [182]. Of note, a loss of syt1 was discovered in human hippocampus of patients with Alzheimer's disease [183] and promisingly, our proteome data also showed the down regulation of syt1 in mutant flies compared with hLRRK2 flies. On the other hand, Rab3 is linked both in exo and endocytic trafficking of SV vesicles and thus, we reasoned that hLRKK2 (R1441C) dependent downregulation of several SV proteins could lead to a dysregulation vesicle formation and recycling leading most likely to an imbalance of synaptic plasticity in DA neurons.

It has been shown that hLRRK2 (R1441C) caused reduced dopamine and other catecholamines synthesis in cultured adrenal chromaffin cells isolated from hLRRK2 (R1441C) KI mice [184]. Strikingly, we detected three down regulated proteins, including punch (GTP cyclohydrolase), purple (6-pyruvoyl tetrahydrobiopterin synthase) and henna which are all involved in dopamine synthesis in *Drosophila*. Protein henna is a phenylalanine hydroxylase which catalyzes phenylalanine conversion to tyrosine and tyrosine is a major substrate for dopamine and other catecholamine synthesis. In humans, a mutation in GTP cyclohydrolase (GTPCH) and 6-pyruvoyl tetrahydrobiopterin synthase (PTS) causes childhood parkinsonism-dystonia characterized by decreased levels of dopamine and serotonin [185]. Moreover, a 50% reduction of tetrahydrobiopterin levels which is synthesized by the enzymes GTPCH levels, were also observed in sporadic PD patients [186]. Of note, punch seems to be more down regulated in the presence of αS compared to αS (A53T) overexpression [158]. Therefore, our results demonstrate a clear link between hLRRK2 (R1441C) and several enzymes involved in catecholamine biosynthesis.

3.4.2 Validation of selected candidates from proteome data

Western blot analysis was performed in order to validate protein expression changes observed in our mass spectrometric data. For example, *Drosophila* Protein argonaute-2

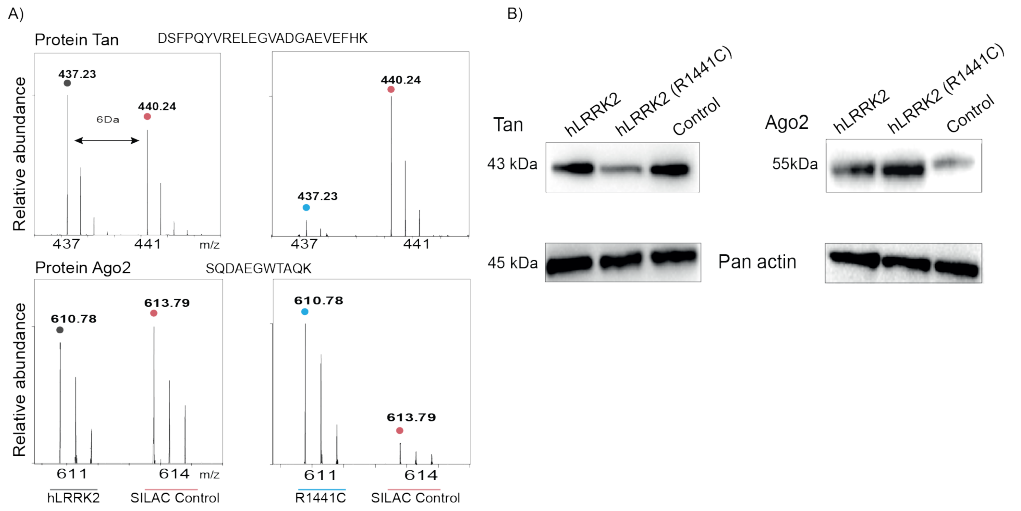

FIGURE 3.17: Validation of proteomics data. A) MS spectra of peptide sequences for Tan (Upper) and AGO2 (Lower). C) Western blots showed the upregulation of AGO2 protein and down regulation of Tan protein in mutant flies compare with hLRRK2 flies.

(encoded by AGO2) was selected and the mass spectra for Peptide sequence SQDAEGW-TAQK belonging to AGO2 showed up-regulation in hLRRK2 (R1441C) flies compared with heavy internal standard, whereas spectra remains unchanged in hLRRK2 flies based on the relative intensities of the peaks (3.17 A). In line with our proteomics data, Western blot analysis also showed up-regulation of the AGO2 in mutant flies compare with hLRRK2 flies, see fig. 3.17 B. For the second blot analysis, a differentially expressed candidate, protein Tan, was selected which showed down-regulation in the proteomics data. The blot analysis also detected down regulated band at 43 kDa as shown in fig. 3.17 B, in mutant flies as previously described [187]. Protein Panactin was used as a loading control since its expression did not change in mutant flies in comparison with hLRRK2 controls flies.

In addition, we performed immunocytochemistry to follow the cellular localization of the Tan protein. The hydrolsye Tan had shown 2-fold decrease in our MS data. Therefore, we have chosen this protein to validate our proteomics data by using an immunohistological approach. Tan has been shown previously to impact dopamine levels by hydrolysing N-beta-alanyl dopamine (NBAD) to beta-alanine and dopamine, respectively [188]. Flies lacking Tan have disturbed dark pigmentation due to reduced dopamine and melanin levels in the skin and Tan function is crucial for light detection by converting carcinine to histamine [188].

Tan expressing neurons were visualized on head-cryosections of adult flies using an affinity-purified anti-Tan antibody [187]. As an internal control, we have applied an

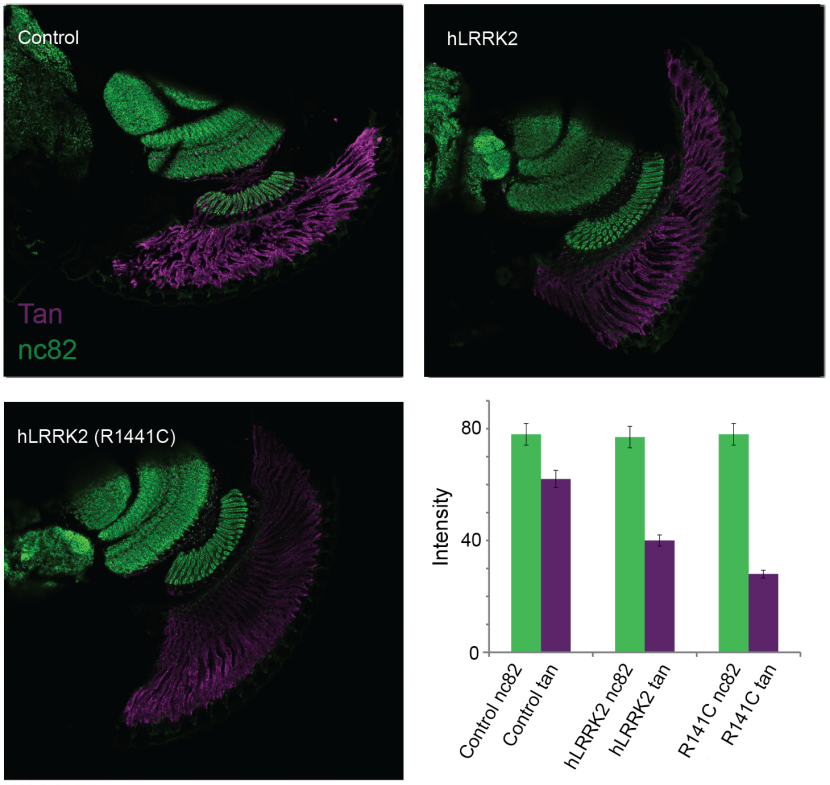

FIGURE 3.18: Immunocytochemical labeling of tan and nc82 in *Drosophila* head. When comparing 30 days old control, hLRRK2 with hLRRK2 (R1441C) flies, an overall decrease of tan protein (violet) is observed in mutant. Nc82 protein (green) is used as control which is unchanged in all genotypes.

anti-Bruchpilot (NC82) antibody, generated in a different species than anti-Tan. Bruchpilot is a pan-neuronal expressed synaptic protein [189]. Hence, we did not expect changes in its expression level due to heterologous expression of hLRRK2 or hLRRK2 (R1441C) in only DA neurons. Four-week-old *ddc*-Gal4 flies were used as control genotype. Both, Tan and Bruchpilot expression levels were quantified on confocal images. As compared to the control hLRRK2, flies expressing hLRRK2 (R1441C) showed about 25 % reduction of Tan expression and about 55 % reduction compare with *ddc*-gal4 flies as shown in fig. 3.18. As expected the anti-Bruchpilot labeling did not vary in between the three genotypes. The experiment was repeated 4 times yielding similar results.

3.4.3 Protein interaction of differiantilly expressed proteins of transgenic hLRRK2 (R1441C) flies map illustrates strong intermolecular connection

We next integrated the Search Tool for Retrieval of Interacting Genes (STRING) analysis of *Drosophila* protein interaction network in order to check the hypothesis that regulated

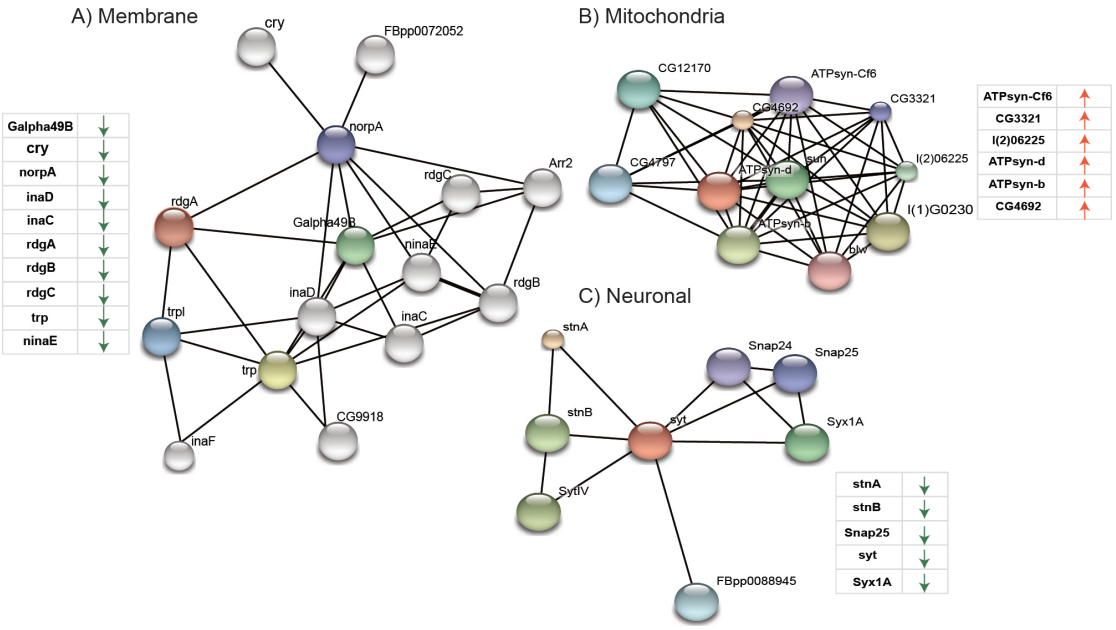

FIGURE 3.19: String subnetworks interaction maps of selected regulated proteins from different cellular compartment in mutant flies. Green and red arrows represent the upregulated and downregulated candidates respectively and these small lists show most of the connected candidates within this network were already regulated in mutant flies.

proteins may be connected by intermolecular interactions.

Therefore, we searched for regulated proteins from different compartments such as mitochondria, membrane etc. against a comprehensive *Drosophila* interaction network database. Fig. 3.19 shows a detailed network maps for rdgA, synaptotagmin and ATPsyn d proteins. We found that these three proteins have strong interaction subnetworks where most of the proteins within the networks were already found as regulated in our proteome data. For example, network analysis of membrane associated protein, rdgA, showed the high interconnection with other membrane linked proteins such as rdgC, norpA, rdgB, which were already found to be down regulated in hLRRK2 (R1441C) flies. Further, the neuronal protein synaptotagmin (Syt) is tightly associated with other neuronal proteins, including Snap25 and Syx1A, which were also down regulated in the hLRRK2 fly model. Taken together, the unbiased protein quantification approach confirmed several known PD related proteins and we found common molecular pathways which are equally affected in fly the human PD patients.

3.5 Proteome expression of αS *Drosophila* model of PD

In order to emphasize on hLRRK2 (R1441C) specific toxicity in PD flies, we next investigated the protein expression changes in the αS PD model and two fly strains with

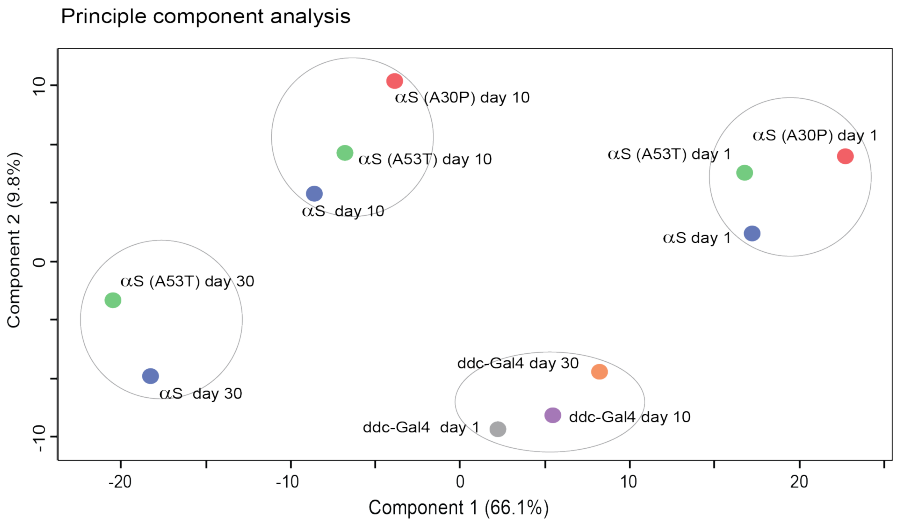

FIGURE 3.20: Principle component analysis of *ddc*-Gal4 driven control, αS, A30P-αS and A53T-αS flies show the global proteome difference at day 1 and day 10.

a point mutation in the Synuclein at position A53T and A30P [71]. All experiments were performed based on SILAC approach and biological duplicates on *ddc*-Gal4, αS, A30P-αS and A53T-αS transgenic PD-like flies between day 1, 10 and day 30. The experimental setup was kept similar as discussed previously. Quantitative proteomics were performed with two biological duplicate on *ddc*-Gal4, αS, A30P-αS and A53T-αS transgenic PD-like flies. In total, 4432 proteins were identified and 1980 proteins were quantified between control, two αS mutants and αS transgenic flies. Similar the hRLLK2 model a PCA analysis showed clear separations between control and mutant flies. We found four well separated clusters in PCA and *ddc*-Gal4 flies did not show significant proteome differences between 1, 10 and 30 days. Nevertheless, significant changes were observed in αS and mutants flies, specially A30P-αS flies showed a noticeable proteome changes compared with αS and A53T-αS flies in both in 1 day and 10 days as shown in fig. 3.20.

3.6 Transgenic hLRRK2 and αS flies show common and distinct age-dependent protein changes

To identify common and distinct protein changes of both PD models, hierarchical clustering was performed with the normalized expression profiles of transgenic hLRRK2, hLRRK2(R1441C), αS, A30P-αS, and A53T-αS overexpressing flies. In our study, the hierarchical clustering determined the biological relationship between individual genes in all transgenic and control flies. Notably, the analysis revealed a clear time-dependent separation between all hLRRK2 and αS strains, see fig. 3.21.

In addition, the analysis revealed several clusters with commonly regulated proteins. For example, General odorant-binding protein 99a (Obp99a) in cluster 1 was upregulated in both hLRRK2 and S transgenic flies. The Obp99a protein is expressed in olfactory sensory dendrites and it is thought to be associated with capturing and transporting hydrophobic odorants in flies [190]. On the other hand, cluster 2 represents the down-regulated proteins mostly associated with larval serum protein (LSP) in both hLRRK2 and αS transgenic flies compare with heavy flies although they showed unchanged expression between the transgenic flies. Next, we detected several proteins connected to neuronal functions and plasticity with significant down regulation over the entire dataset. Of particular interest is cluster 3 which revealed a class of proteins mainly involved in synaptic plasticity that were only down regulated in hLRRK2 (R1441C) flies compared to all αS transgenic and control flies.

To make hLRRK2 (R1441C) associated genes constitute a specific hLRRK2 (R1441C) signature, we compared the proteome changes of 30 days old hLRRK2(R1441C) flies and A53T-αS with respect to control flies and plotted against each other as shown in fig. 3.22.

A direct comparison of protein changes in hLRRK2 (R1441C) to A53T-αS showed a rather weak Pearson correlation of 0.3 (fig. 3.22). However, a group of actin cytoskeleton associated regulated proteins, including TpnC4, Act88f, up, GstS1 and Strn-Mlck were up regulated in both mutant strains at day 30. Similar, the elevated expression of glutathionine family member GstS1 in A53T-αS and hLRRK2 (R1441C) flies might reflects the defensive response against A53T-αS and hLRRK2 (R1441C) toxicity as discussed previously. Similarly, we also observed increased puglist protein levels in hLRRK2 and αS transgenic flies [158]. Interestingly, the downregulated candidates revealed a class of proteins mainly involved in synaptic plasticity which were only down regulated in hLRRK2 (R1441C) flies compared to αS transgenic and control flies as shown in fig. 3.22. For example, Synaptotagmin, Syntaxin 1A, SNAP-25, Rab3 and shi were down-regulated only in hLRRK2 (R1441C) flies which are linked with the vesicle formation and fusion, table. 3.23.

3.7 Quantitative proteomics of A30P-αS *Drosophila* model of PD at presymptomatic stage

Next we examined the proteome expression changes in αS and A30P-αS flies. We detected 163 proteins which were significantly regulated ($p < 0.05$) in A30P-αS flies relative to αS flies. Among these regulated candidates, 93 candidates were upregulated

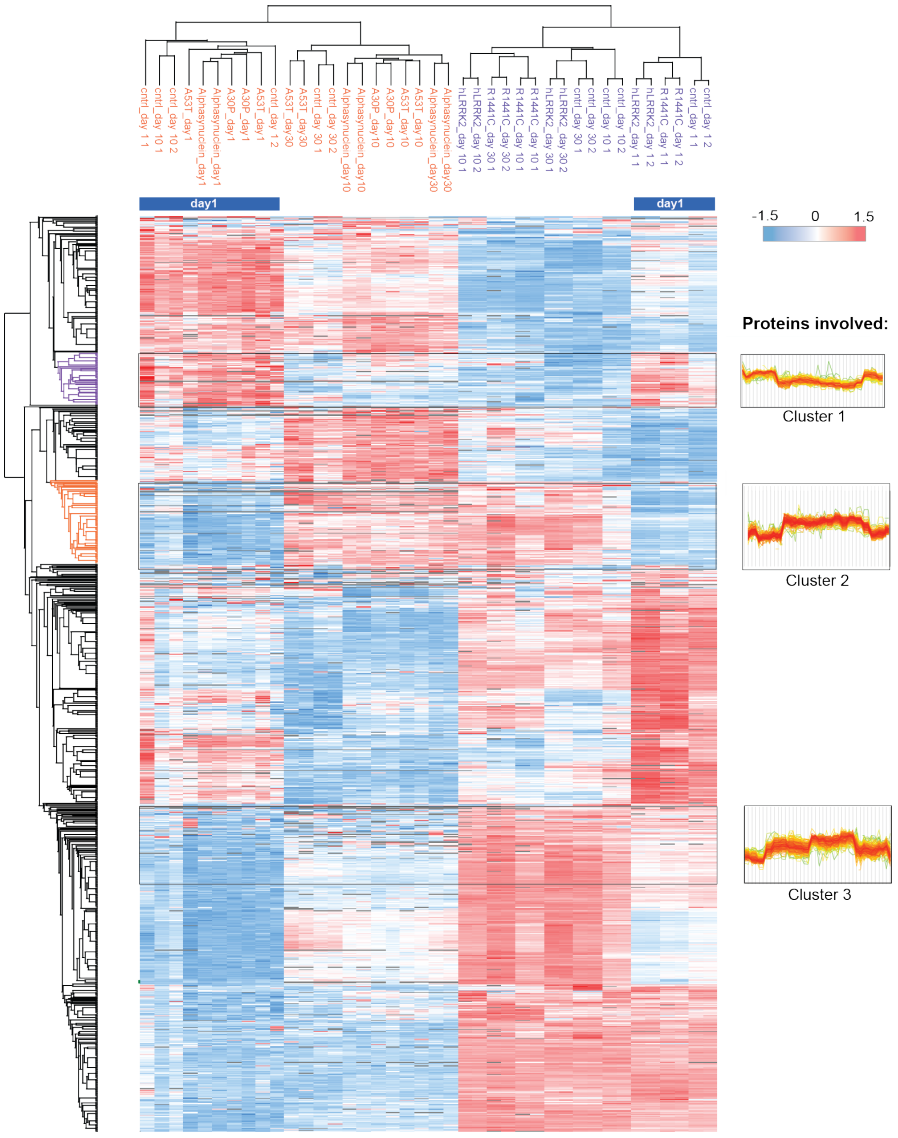

FIGURE 3.21: Hierarchical clustering of quantified proteins between hLRRK2, αS and control flies. Both αS and hLRRK2 transgenic flies demonstrated their distinct cluster compared with each other.

and 70 were downregulated. Table 3.1 denotes significant proteins that were differentially expressed in 10 days old A30P-αS flies compared with αS flies. A total of twelve upregulated proteins were associated with actin cytoskeleton related proteins including GstS1 and calpain. Calpain is a calcium dependent intracellular protease which acts as a leading candidate for the degradation of receptors and many cytoskeletal proteins were known to be degraded by calpain. *Drosophila* calpain has been reported as a organizer of cytoskeletal structure related to actin and similar to the hLRRK2 (R1441C) fly model actin cytoskeletal associated proteins such as, Troponin T and Act88f were also up regulated in the A30P-αS fly model [191, 192]. Connversely, several heat shock proteins, including Hsp27, Hsp26 and Hsc70-1. Hsp27 were quantified with increased

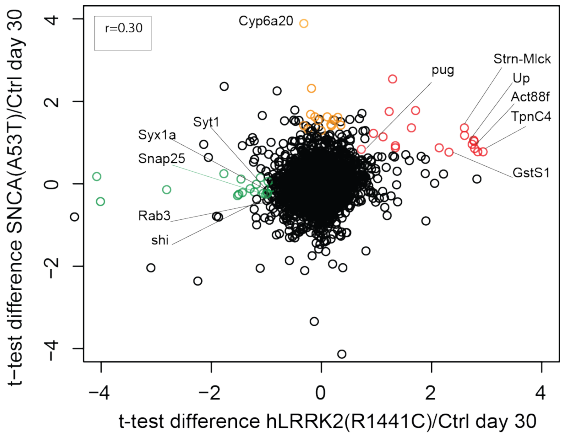

FIGURE 3.22: Scatter plotting with quantified proteins from A53T-αS and hLRRK2 (R1441C) flies compared with control flies.

	Uniprot id	Flybase ID	Protein names	Average Log2 ratio R1441C/hLRRK2	P-value	Average Log2 ratio A53T/ SNCA	P-value
Actin cytoskeleton	P49455	FBgn0003721	Tropomyosin 1	1.64	0.0412	0.67	0.0601
	Q7K860	FBgn0033027	Troponin C isoform 4	1.71	0.0001	0.77	0.0042
	Q9VUQ5	FBgn0087035	Protein argonaute-2	1.63	0.0126	0.20	0.1145
	P41043	FBgn0010226	Glutathione S-transferase S1	1.43	0.0014	0.76	0.0577
	P10981	FBgn0000046	Actin-87E	1.22	0.0005	0.24	0.0386
	Q8IPH5	FBgn0041182	Thioester-containing protein 2	1.39	0.0003	-0.32	0.0399
Mitochondrial	Q24251	FBgn0016120	ATP synthase sub. d, mitochondrial	0.79	0.0009	0.20	0.0401
	P19967	FBgn0000406	Cytochrome b5-related protein	1.22	0.0001	0.35	0.0433
	P29843	FBgn0001216	Heat shock 70 kDa protein cognate 1	0.71	0.0003	0.40	0.0573
	Q24407	FBgn0016119	ATP synth.-coupling factor 6, mito.	0.68	0.0004	0.14	0.1044
	O96553	FBgn0020385	pug	0.86	0.0020	0.77	0.0003
	Q8IN44	FBgn0028396	Protein Turandot A	0.74	0.0002	1.60	0.5478
	E1JJK8	FBgn0003218	Protein retinal degeneration B	-0.46	0.0059	0.20	0.0055
Neuronal	P25228	FBgn0005586	Ras-related protein Rab-3	-0.50	0.0001	-0.14	0.0632
	P21521	FBgn0004242	Synaptotagmin 1	-0.53	0.0040	-0.02	0.0726
	P17276	FBgn0001208	Protein Henna	-0.51	0.0053	-0.30	0.0744
	P13607	FBgn0002921	Na/K-transporting ATPase α	-0.59	0.0042	-0.03	0.0149
	P48611	FBgn0003141	6-pyruvoyl tetrahydrobiopterin synthase	-0.55	0.0051	0.08	0.0114
	Q9V427	FBgn0027108	Innexin inx2	-0.65	0.0021	0.16	0.0040
	Q24547	FBgn0013343	Syntaxin-1A	-0.64	0.0002	-0.39	0.0358
	P62152	FBgn0000253	Calmodulin	-0.64	0.0051	-0.30	0.1086
	P13677	FBgn0004784	Protein kinase C	-0.68	0.0075	-0.06	0.0074
	Q09103	FBgn0261549	Eye-specific diacylglycerol kinase	-0.71	0.0091	0.97	0.0431
	Q9VFN7	FBgn0038198	Niemann-Pick type C-2b	-0.69	0.0059	Not quantified	
	P36975	FBgn0011288	Synaptosomal-associated protein 25	-0.58	0.0418	0.05	0.0088
	Q967D7	FBgn0010473	Protein turtle	-0.81	0.0090	-0.47	0.1299
	Q9VA37	FBgn0039802	dj-1β	-0.83	0.0152	0.44	0.0268
	Q9W369	FBgn0030106	tan	-0.75	0.0434	-0.37	0.0448
	P40421	FBgn0004366	Ser/Thr-protein phosphatase rdgC	-0.87	0.0118	0.53	0.0218
	P48596	FBgn0003162	punch	-0.72	0.0326	0.54	0.0245
	P23625	FBgn0004435	Guanine nucleotide-bdg. protein G(q)	-0.92	0.0124	-0.27	0.0708
	P29829	FBgn0004623	Guanine nucleotide-bdg. protein β2	-0.97	0.0046	-0.15	0.0256
	Q04691	FBgn0000639	Fat-body protein 1	-1.46	0.0120	0.77	0.0116

FIGURE 3.23: List of significant candidates in hLRRK2 (R1441C) flies compare with LRRK2 flies and A53T-αS flies.

abundance in A30P-αS flies. Member of the small heat shock family have different functional relevance in autophagy, aging and neurodegeneration [193, 194].

For example, Hsp27 null mutant flies showed short life, however overexpression of Hsp27 increases the lifespan and prevents mosaic eyes from cellular toxicity [195–197]. Since, heat shock proteins act as a defense system in response to various stress conditions, elevated expression of Hsp proteins might be an adaption during the progression of the αS induced PD in flies.

TABLE 3.1: Significantly regulated proteins between 10 days old A3oP and αS flies

Gene names	Flybase	Protein IDs	A3oP/αS Log2 Ratio E1	A3oP/αS Log2 Ratio E2	Peptides	P-value
CtsB1	FBgn0030521	Q9VY87	2.13	2.03	5	0.02406
Vps13	FBgn0033194	A1Z713	2.10	2.11	55	0.00205
Obp99b	FBgn0039685	Q9VAI6	1.20	1.18	9	0.00125
Gbs-76A	FBgn0036862	Q9VVY3	1.11	1.08	6	0.00146
wupA	FBgn0004028	P36188	1.01	0.74	33	0.05350
Fbp1	FBgn0000639	Q04691	1.01	0.96	3	0.00259
AIF	FBgn0031392	Q9VQ79	1.00	1.15	11	0.02341
Hsp26	FBgn0001225	P02517	0.91	1.03	4	0.01301
TppII	FBgn0020370	Q9V6K1	0.91	0.77	41	0.01431
CalpA	FBgn0012051	Q11002	0.89	0.98	13	0.00707
Map205	FBgn0002645	P23226	0.89	0.68	25	0.03049
Hsp27	FBgn0001226	P02518	0.88	0.99	6	0.01126
Acp36DE	FBgn0011559	Q9V3R1	0.82	1.09	10	0.05799
GstS1	FBgn0010226	P41043	0.78	0.74	12	0.00184
Aats-gln	FBgn0027090	Q9Y105	0.78	0.85	19	0.00447
Act88F	FBgn0000047	P83967	0.78	0.67	20	0.00802
fln	FBgn0005633	P35554	0.77	0.75	13	0.00025
TotA	FBgn0028396	Q8IN44	0.75	0.90	4	0.01657
betaCop	FBgn0008635	P45437	0.73	0.59	14	0.01385
Strn-Mlck	FBgn0265045	A1ZA66	0.72	0.85	122	0.01259
Cyp313a1	FBgn0038236	Q9VFJ0	0.71	0.85	17	0.01339
TpnC73F	FBgn0010424	P47949	0.71	0.75	10	0.00152
Gpo-1	FBgn0022160	Q7K569	0.69	0.68	34	0.00008
Hsc70-1	FBgn0001216	P29843	0.68	0.59	13	0.00547
Tm1	FBgn0003721	P49455	0.68	0.95	24	0.04967
CG12400	FBgn0031505	Q9VQM2	0.66	0.65	5	0.00012
mt:ND3	FBgn0013681	P18930	0.66	0.66	2	0.00001
ND42	FBgn0019957	P91929	0.66	0.68	13	0.00021
sec3	FBgn0086475	Q9VVG4	0.61	0.59	12	0.00026
Pu	FBgn0003162	P48596-2	0.59	0.65	11	0.00184
ND75	FBgn0017566	Q94511	0.59	0.61	21	0.00011
pr	FBgn0003141	P48611	0.58	0.60	5	0.00049
Dms	FBgn0011581	P61849	-0.62	-0.85	2	0.02991
Esyt2	FBgn0039208	Q9VC62	-0.62	-0.43	20	0.02035
CG15117-RB	FBgn0034417	Q7K173	-0.62	-0.49	10	0.01211
smp-30	FBgn0038257	Q9VFG5	-0.63	-0.67	13	0.00316
Cyp12e1	FBgn0037817	Q9VGZ0	-0.63	-0.62	8	0.00064
CG3590-RA	FBgn0038467	Q9VEP6	-0.67	-0.41	13	0.03258
Cpr57A	FBgn0034517	Q7K5J8	-0.68	-0.85	4	0.02097
CG17549	FBgn0032774	Q0E8P1	-0.69	-1.09	2	0.05928
CG10688	FBgn0036300	Q9VTZ6	-0.71	-0.49	7	0.02705
Sac1	FBgn0035195	Q9W0I6	-0.72	-0.35	9	0.05392
Pbprp3	FBgn0011281	P54193	-0.73	-0.81	4	0.00762
ATPCL	FBgn0020236	E2QCF1	-0.73	-0.70	32	0.00169
GstE4	FBgn0063496	A1ZB69	-0.88	-0.57	7	0.04351
UGP	FBgn0035978	E1JI91	-0.89	-0.69	25	0.02481
Cyp6g1	FBgn0025454	Q9V674	-1.04	-0.67	10	0.05413
PIP5K59B	FBgn0034789	Q9W1Y3	-1.15	-1.35	7	0.02607
Cyp6a20	FBgn0033980	Q9V773	-2.48	-2.70	15	0.02411

Among the downregulated cluster, several transmembrane and neuron associated proteins were found to be down regulated in A30P-αS flies compared with αS flies. For instance, the transmembrane protein Dystroglycan (Dg) is linked with a distrophin complex, which relates extracellular matrix to cytoskeletal actin and it was documented as a possible reason for muscular dystrophy and brain defects in human [198–200]. *Drosophila* Dg mutants show a similar phenotype with a progressive muscular dystrophy and neuronal degeneration. The finding that Dg is reduced in A30P-αS flies may

reflect brain abnormalities and leading finally to the PD phenotype. Another interesting down regulated protein is the phosphatidylinositide phosphatase Sac1, which highly expressed in the Drosophila nervous system [201]. This protein is known to play an important role in various kinds of cellular process, including synaptic morphology and intercellular trafficking [202]. Drosophila Sac1 mutant showed defect in dorsal closure and axonal pathfinding which caused neurodegeneration in dosage dependent manner [203]. Thus, The inactivation of Sac1 in *Drosophila* showed a defect in dorsal closure and axonal path finding leading to neurodegeneration.
Taken together, although both A30P-αS and hLRRK2 (R1441C) flies models showed similar cytoskeletal actin remodeling phenotypes, reflecting a common and more general event during the progression of the PD in *Drosophila*, proteome expression in A30P-αS *Drosophila* model of human neurodegentive disease speculates that the overwhelming majority of mitochondrial proteins associated with A30P-αS were highly distinct.

3.8 Quantitative proteomics of A53T-αS Drosophila model of PD at presymptomatic stage

Next, we performed the quantitative proteome analysis of 10 days A53T-αS flies in comparison with αS flies. In total, we quantified 60 proteins which were differentially expressend in A53T-αS flies and have been shown in table 3.2. Although 45 % significant proteins are ovelapped with A30P-αS flies, a fraction of 27 proteins were exclusively regulated in A53T-αS flies.
Among the actin cytoskeleton related proteins, two upregulated Gst family members, namely GstE1 and GstE7 were identified in A53T-αS and it is worth noting that, increased GstE1, GstE7 expression was also found in hypoxia induced neurodegenerative Drosophila model [204].

Therefore, the high expression level of Gst family members in mutant flies might reflect that cells may encountering stress condition which may trigger Gst expression to protect DA neurons. However, it is completely unclear why only A53T-αS overexpressing flies showing this specific up regulation of two Gst family members.

In addition, six mitochondrial associated proteins, including Probable cytochrome P450 12c (Cyp12c1), Cytochrome P450 9b2 (Cyp9b2), Probable cytochrome P450 6a20 (Cyp6a20), CG5703, Gpo-1 and Sdhb were also up regulated in A53T-αS flies. Cytrochrome p450 isoenzymes were found in human PD patients [205] and Cytrochrome p450 is associated to molecular detoxification. Hence, regulated three Cytrochrome p450 family members might represent their functional significance in the pathogenesis of PD in mutant flies.

TABLE 3.2: Significantly regulated proteins between 10 days old A53T and αS flies

Gene names	Flybase	Protein IDs	A53T/αS Log2 Ratio E1	A53T/αS Log2 Ratio E2	Peptides	P-value
GstE1	FBgn0034335	Q7KK90	1.52	1.74	8	0.04972
CG1665-RA	FBgn0033451	A1Z803	1.35	1.25	6	0.00738
Cyp12c1	FBgn0036806	Q9VVR9	1.02	1.06	6	0.00965
lectin-28C	FBgn0040099	Q9VLW1	1.00	0.58	6	0.03407
Aats-ile	FBgn0027086	Q8MSW0	0.96	1.07	32	0.04936
RanGap	FBgn0003346	Q9VIW3	0.96	0.95	8	0.02140
prtp	FBgn0030329	Q9VYV3	0.86	0.86	20	0.00005
Obp99b	FBgn0039685	Q9VAI6	0.83	0.82	9	0.00141
msk	FBgn0026252	Q9VSD6	0.83	0.59	11	0.01843
GstE7	FBgn0063493	A1ZB72	0.78	0.82	6	0.01560
Strn-Mlck	FBgn0265045	A1ZA66	0.73	0.62	122	0.03925
mRpL12	FBgn0011787	Q9VSR5	0.70	0.37	9	0.04578
up	FBgn0004169	P19351	0.69	0.72	56	0.01363
Pu	FBgn0003162	P48596	0.67	0.71	11	0.01648
Tm1	FBgn0003721	P49455	0.65	0.81	24	0.01415
TotC	FBgn0044812	Q8IN43	0.63	0.63	2	0.00109
fln	FBgn0005633	P35554	0.62	0.66	13	0.01638
TotA	FBgn0028396	Q8IN44	0.61	0.95	4	0.05211
Jabba	FBgn0259682	Q7K1Q6	0.58	0.65	5	0.03852
GstS1	FBgn0010226	P41043	0.58	0.57	12	0.00130
tobi	FBgn0261575	Q9VBR6	-0.60	-0.64	11	0.03845
Yp1	FBgn0004045	P02843	-0.61	-0.41	13	0.03506
Cpr49Ab	FBgn0050042	A1Z8Y3	-0.64	-0.66	3	0.00864
CG17121	FBgn0039043	Q9VCR9	-0.66	-0.57	6	0.03540
CG12926	FBgn0033437	A1Z7X8	-0.68	-0.34	10	0.05396
GstE4	FBgn0063496	A1ZB69	-0.69	-0.67	7	0.01547
Cpr30F	FBgn0051876	Q8IPD8	-0.73	-0.44	4	0.03327
CG9675	FBgn0030773	Q9VXC9	-0.93	-1.16	5	0.00615
Cpr57A	FBgn0034517	Q7K5J8	-1.03	-1.02	4	0.00151
CG5706	FBgn0039175	Q9VCA5	-1.10	-1.21	12	0.02937
Obp83b	FBgn0010403	Q23970	-1.24	-1.82	6	0.01939
CG8329	FBgn0036022	Q9VT23	-1.37	-1.15	3	0.00555
Cyp6a20	FBgn0033980	Q9V773	-3.18	-3.23	15	0.00138

On the other hand , Glycerophosphate oxidase-1(Gpo-1), a mitochondrial inner membrane protein, regenerates the NAD+ for glycolysis continuation and Drosophila Gpo mutant is flightless [206]. Promisingly, our previous study of hLRRK2 (R1441C) flies also showed high expression of Gpo-1. Thus, elevated expresson of Gpo-1 in PD model transgenic flies might indicates its role in mitochondrial system that may lead to high oxidative stress in mutant flies.

Besides regulated mitochondrial proteins, synaptic vesicle linked protein Rab18 was also regulated in A53T-S expressing flies. In Drosophila, cellular expression of the Rab18 protein is neuron specific and colocalizes with Rab5. The significance of Rab18 function in the Drosophila synaptic system, trafficking have been already reported and Drosophila mutated Rab gene showed a wide range of neurological disease phenotypes [207–210]. We quantified a regulated Rab gene namely, Rab18 in mutant flies that exhibits neuron specific or neuron enriched expression and colocalizes with Rab5. Previously we found the synaptic vesicle trafficking linked proteins were significantly regulated due to hLRRK2 (R1441C) overexpression in flies and thus, regulated Rab18 in mutant A53T-αS flies may also reflect may also reflect the functional association of synaptic vesicle proteins in PD.

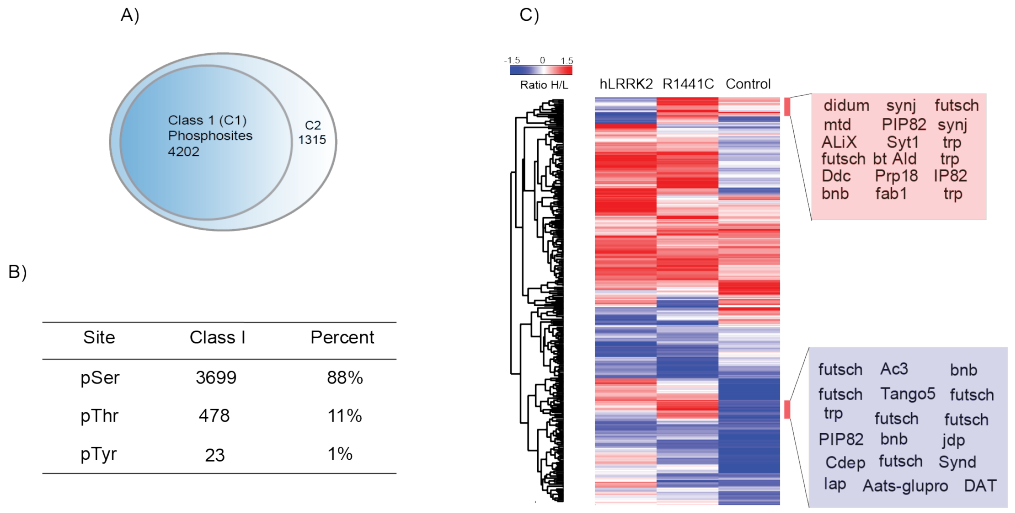

Site	Class I	Percent
pSer	3699	88%
pThr	478	11%
pTyr	23	1%

FIGURE 3.24: A) Class 1 and Class 2 Phosphorylation-sites analysis. B) The distribution of the pY/pS/pT phosphoproteome. C) Hierarchical clustering of quantified phosphoproteins. Some clusters are expressed at higher (red) or lower (blue) levels in mutant flies compared to control flies. Higher magnification of some cluster is shown in the heatmap. Red and blue colors indicating normalized and z-score ratios (n=3).

3.9 Phosphoproteome analysis of hLRRK2 (R1441C) transgenic flies

Reversible protein phosphorylation is an important regulatory element for cell signaling and rapid adaption to internal and external stimuli. Moreover, a global view on the protein phosphorylation status in living animal models will help to learn more about activated pathways. Thus, a comprehensive analysis of phosphorylation patterns in flies overexpressing different PD related proteins will give more insights into the pathobiology of the disease. The analysis of transgenic flies overexpressing hLRRK2 and its mutant forms might allow us to get a deeper understanding of the LRRK2 kinase function and activated signaling pathways during the disease progression.

3.9.1 Global phosphoproteome analysis of hLRRK2 (R1441C) mutant flies in PD

In order to identify potential hLRRK2 targets, we set out to analyze the phosphoproteome in control, hLRRK2, and hLRRK2 (R1441C) overexpressing 30 days old flies. Similar to the proteome analysis, we used the SILAC fly approach as an internal protein standard for accuarate phosphopeptide quantification and performed a biological triplicate for each fly strain (n=3). The experimental design for the phosphorylation analysis for hLRRK2 and hLRRK2 (R1441C) expressing 30 days old flies was shown

in fig. 3.9. Briefly, extracted proteins from head tissue ($\sim$ 1mg) were digested in solution. The phosphopeptides enrichment was done by separating the peptide mixtures with SCX chromatography followed by using titanium dioxide (TiO_2) extractions [211]. Each fraction was analyzed by 2.5h liquid chromatography gradients and measured with a quadrupole orbitrap mass spectrometer followed by analyzing the raw datas by MaxQuant software (1.5.0.0).

In total, 5518 phosphopeptides were identified and 2529 were quantified in at least two independent experiments. A fraction of 4202 phosphorylation sites (class I) were detected with localization probability > 0.75. In the case of multiple serines, thereonines, or tyrosines are present in the amino acid sequence, the probability to detect specific phosphorylation site localization is at least 75 % within different potential phosphorylated site locations (fig. 3.24 A). Localized phosphorylation sites with a probability > 75 % are termed class I sites and were considered for the further analysis. . The majority of detected class I phosphopeptides had one (61.47 %), two (23.18 %) and three (15.34 %) phosphorylated sites. Moreover, the detected phosphorylation sites are comprised of 88 % serine, 11 % threonine and 1 % tyrosine sites as shown in fig. 3.24 B. One likely reason for less identified tyrosine phosphorylated sites could be that tyrosine phosphorylation may occur on less abundant proteins compared to serine and threonine phosphorylation. Secondly, tyrosine is less stable in phosphoamino acid analysis than serine and threonine, which makes it more challenging to be identified.

Next, we clustered the SILAC ratios of enriched phosphopeptides from control, hLRRK2 and LRRK2 (R1441C) flies and observed for several GO-terms, including mitochondrial biogenesis and synaptic vesicle formation, clear differences. For example, microtubule related candidate, futsch is highly phosphorylated in hLRRK2 (R1441C) flies compared with control and hLRRK2 expressing flies, see 3.24 C.

The fig. 3.25 showed high reproducibility of our quantitative phosphoproteome data. The Pearson correlations for *ddc*-Gal4, hLRRK2 and hLRRK2 (R1441C) were between 0.88 , 0.81 and 0.87 respectively.Therefore, the experimental setup can be used to analyze accurately phosphopeptide and its changes between different conditions.

The comparison of control and hLRKK2 overexpressing flies revealed 23 regulated phosphosites (fig. 3.26 A) and 39 regulated sites for hLRRK2 (R1441C) flies . The direct comparison between both hLRRK2 and hLRRK2 (R1441C) mutant showed for 51 phosphopeptides an upregulation and 32 were quantified with a reduced phosphorylation. However, normalization according to the protein level and statistical calculation using a permutation based false discovery (FDR) rate < 5 % revealed for only 8 phosphosites a significant regulation as shown in fig. 3.26 B. As some of the significant regulated

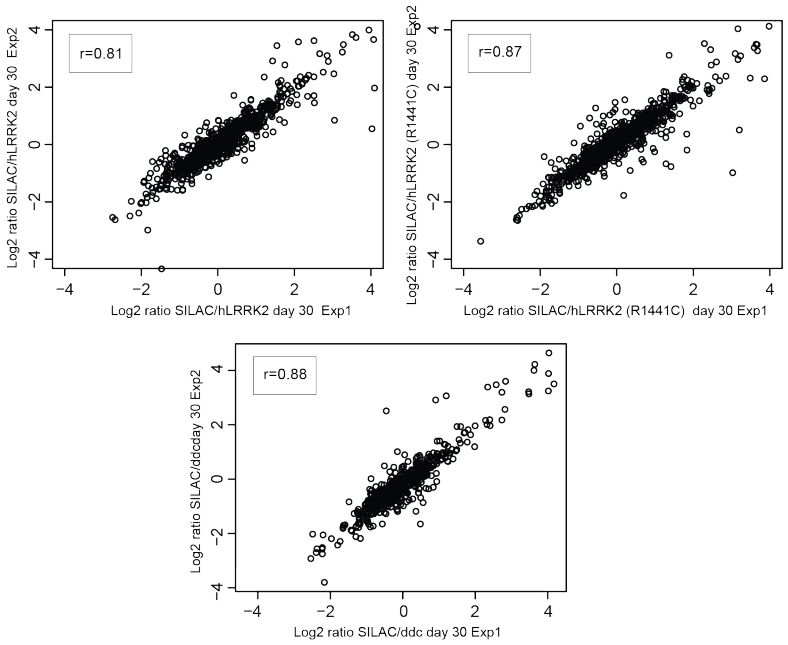

FIGURE 3.25: Reproducibility for phophoproteomics experiment between control, hLRRK2 and hLRRK2 (R1441C) flies.

phosphorylated sites were not quantified in the protein level, they were taken off, contributed for less quantified number after normalization. For example, Chro and Ptp61f were not considered as regulated candidates, since their corresponding SILAC protein ratio were not detectable. Table 3.26 C showed a list of significant candidates, including their amino acid sequence window, positions within the protein, log2 ratio, and p-value . Selected SILAC pairs of unmodified peptides and phosphopeptides from Synaptojanin, futsch and Ankyrin 2 are shown in fig. 3.27. Offnote, Futsch is already known to be phosphorylated by hLRRK2 [212] and therefore, it underscores our accurate quantitative phosphoproteomics approach. The Drosophila protein Futsch, is the orthologue of the mammalian microtubule associated protein (MAP1B), which plays a central role in synaptic morphogenesis. Our phosphoproteome data showed that futsch is highly phosphorylated (9.54 and 1.77 fold-change) at S4106 and S4909 by hLRRK2 (R1441C) compared to the hLRRK2 overexpressing condition, see 3.26 C.

In addition, we also detected enhanced phosphorylation levels of several proteins which are tightly associated to synaptic vesicle formation. For an example, Synaptojanin (Synj), a polyphosphoinositide phosphatase [213], is a presynaptic protein, localized presynaptically at the motor neuron synapse terminal and promotes synaptic vesicle (SV) uncoating [214]. Synj inactivation leads to endocytosis impairment and disrupted vesicle recycling process in Drosophila. Remarkably, the human SYNJ1 mutation was reported as a cause of early onset parkinsonism and defective recycling of the synaptic vesicle in the pathogenesis [215]. Notably, the sequence alignment of the fly, mouse/rat,

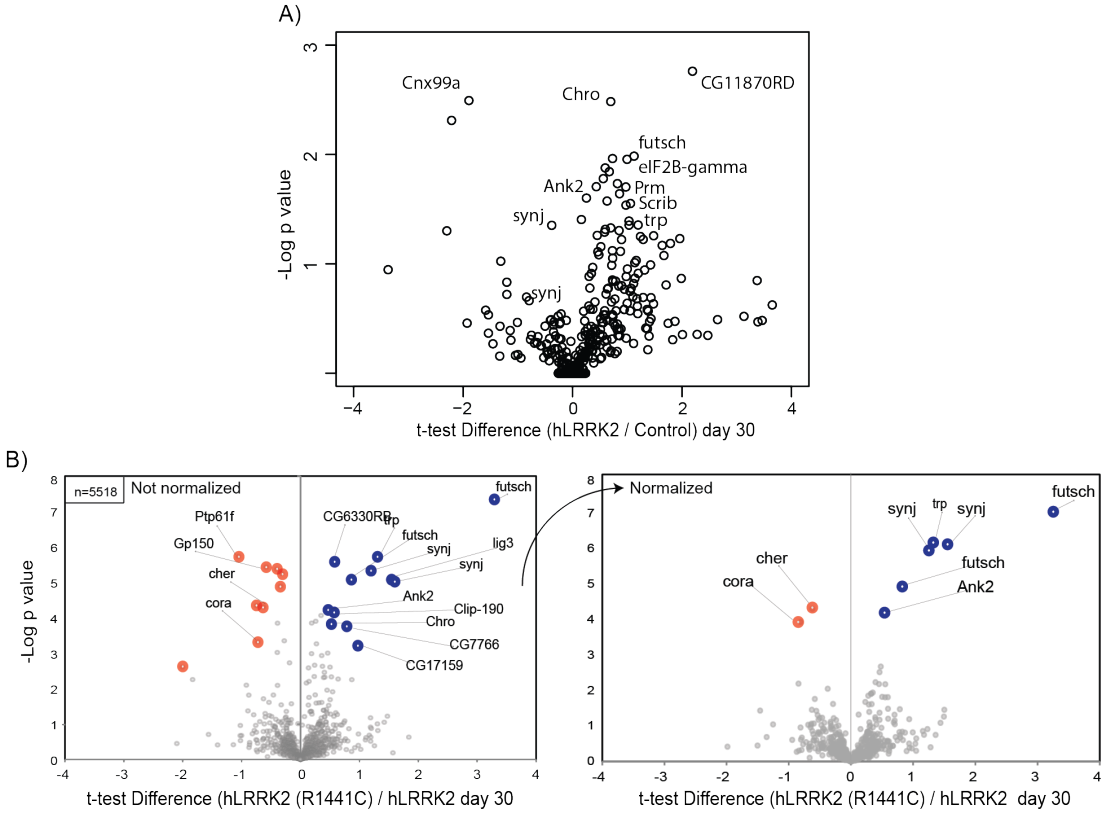

C)

Proteins ID	Proteins names	Phospho (STY) Probabilities	Position	Fold change (Mean)	P-value
Q9W596	Microtubule-associated protein futsch	SQVAS(1)RPESVAVSAK	4106	3.25	1.64E-07
Q9W596	Microtubule-associated protein futsch	CESSAASIVSSSGPMS(1)PK	4909	0.82	1.77E-05
Q5U0V7	Synaptojanin	QATPVSTPTRQVGS(1)PK	1142	1.57	1.34E-06
Q5U0V7	Synaptojanin	QAT(1)PVSTPT(0.81)RQVGSPK	1131	1.23	1.80E-06
X2JCM1	Ankyrin 2	SPAPPKS(0.97)PTPALTK	11169	0.60	9.95E-05
P19334	Transient receptor potential protein	SITS(0.99)GGTGGGASMLAAAALRASVK	964	1.32	9.28E-07
Q9VEN1	Filamin-A	IQTSGS(0.96)QSHLK	1240	-0.61	2.48E-03
Q9V8R9	Protein 4.1 homolog	SGADGQEQLS(1)PTSQQK	597	-0.81	7.49E-04

FIGURE 3.26: A) Volcano plot of phosphopeptide ratios between hLRRK2 and control flies with normalization. The y-axis and x-axis represents the -10log (adjusted p-value) and t-test difference (log2 ratio between hLRRK2 and control flies) respectively. B) Phosphopeptide ratios between mutant and hLRRK2 flies were plotted without and with normalization. Significant phosphoproteins changes are labeled with blue (up) and red (down) circle. C) List of significantly regulated phosphoproteins with their sequence and phosphorylated positions.

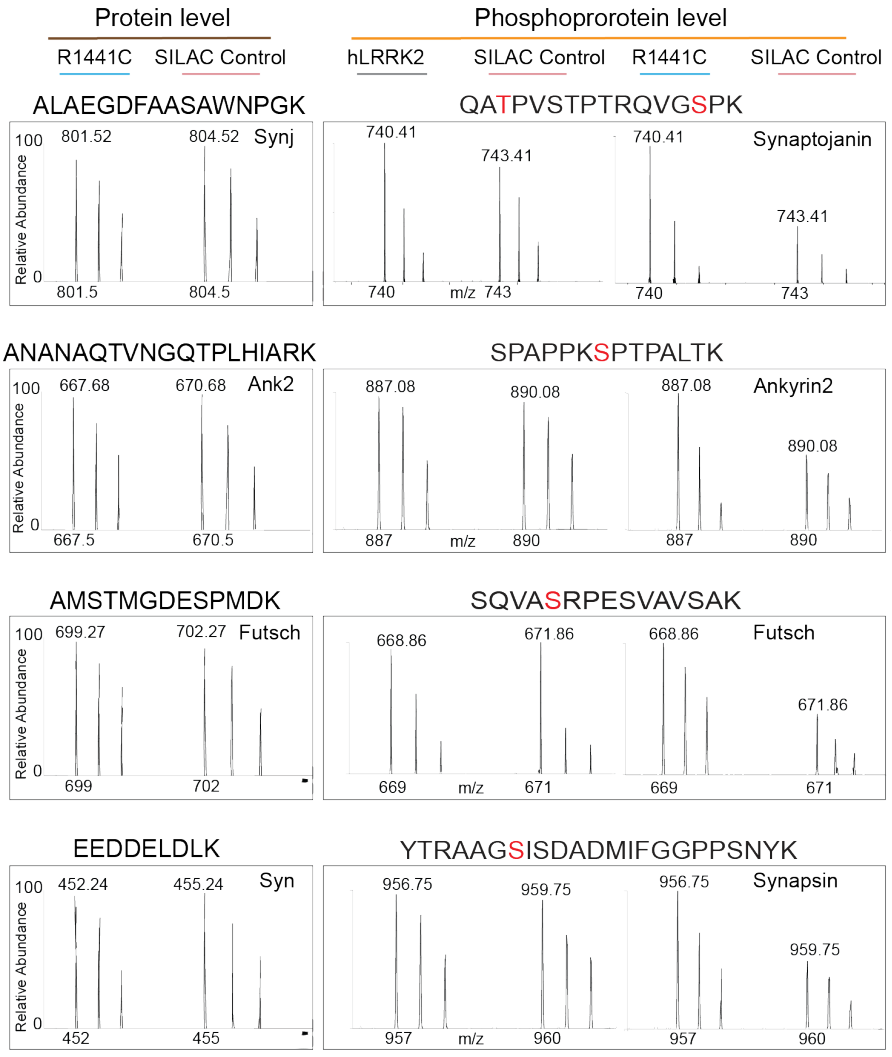

FIGURE 3.27: MS Spectra for Phosphorylated Synaptojanin, futsch and ank2.

and human synaptojanin protein sequence revealed a conservation of the T1131 site, see fig. 3.28 and recent global phosphorylation studies also showed that Synaptojanin is phosphorylated at a threonine (T1220) in humans [216] as well as in rats (pT1217)[217]. Taken together, the global phosphopeptide analysis revealed a hLRRK2 (R1441C) dependent regulation for 8 sites and the synaptic vesicle protein Synaptojanin showed an enhanced phosphorylation at position T1331.

3.9.2 *In – vitro* kinase assay revealed increased human Synj1 phosphorylation by hLRRK2 (R1441C) compared to hLRRK2

In order to validate the Synaptojanin phosphorylation mediated by hLRRK2 an *in – vitro* kinase assay were performed. The conservation of the T1131 site on synaptojanin and its phosphorylation in flies, mouse/rat, and humans point to a more general

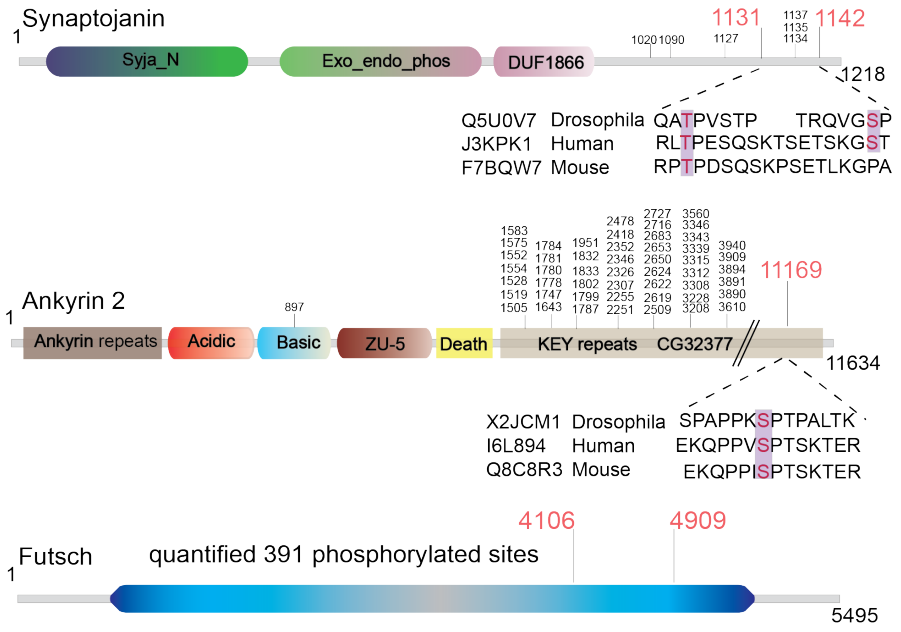

FIGURE 3.28: The sequence similarirties of regulated phosphorylated sites of significant candidates between human, fly and mouse.

mechanism to regulate the activity of Synaptojanin by LRRK2 under regular and diseased conditions. Here we performed an $in-vitro$ kinase assays, using three different hLRRK2 recombinant proteins, including hLRRK2, hLRRK2 (R1441C), and hLRRK2 (D1994A) in combination with the recombinant human Synj1 as a potential target for the LRRK2 kinase. Recombinant LRRK2 proteins were incubated with the recombinant human Synj1 for 1h at 30^0C to allow phosphorylation by the LRRK2 kinase in the presence of radioactive labeled ATP (γ- 32P). After 1 hour of incubation, the reaction was terminated by adding 4x SDS sample buffer followed by denaturation at 100^0C for 10 minutes. The samples were run on SDS-PAGE gel for 3 hour and the dry gel was subjected to autoradiograhy. Since the hLRRK2 (D1994A) protein has no kinase activity, we used this recombinant protein as a negative control for our kinase assay [218] and the assay revealed no phosphorylation of synaptojanin under this conditions. In contrast, the combination of hLRRK2 and Synaptojanin revealed a clear phosphorylation in a dose dependent manner and the incubation with the LRRK2 inhibitor LRRK2-IN-1 inhibited the phosphorylation of Synaptojanin about 60 % (fig. 3.29 A).

In correlation to our quantitative phosphoproteomics experiments, the hLRRK2 (R1441C) mutant form showed the strongest phosphorylation of Synaptojanin and we also observed an elevated autophosphorylation of the hLRRK2 (R1441C) recombinant protein. Similarly, the incubation with the hLRRK2 kinase inhibitor reduced the Synaptojanin and hLRRK2 (R1441C) phosphorylation at similar doses as shown in fig. 3.29 B. These results indicate that both recombinant proteins are able to phosphorylate Synaptojanin

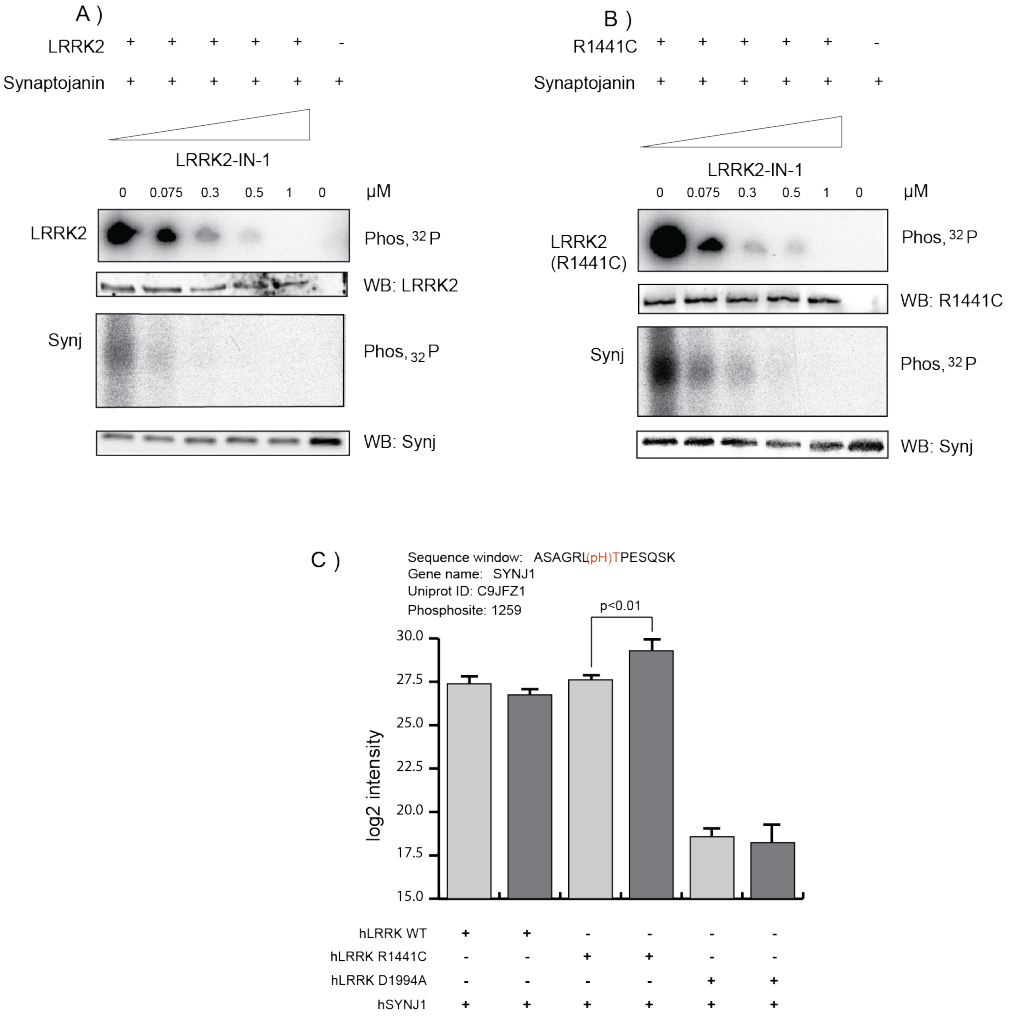

FIGURE 3.29: LRRK2 phosphorylates synaptojanin. A) Kinase assay with GST-LRRK2 was incubated with increasing amounts of LRRK2-IN-1. Kinase assay with recombinant hLRRK2 protein was subjected to Western blotting for detection of GST-tagged LRRK2 and Synaptojanin. B) As in (a) except GST-LRRK2 (R1441C) was utilized. C) LRRK2, R1441C and D1994A recombinant proteins were incubated separately with Synj for 0 and 60 minutes. Mixtures were subjected to MS analysis to find the phosphorylated sites and phosphorylation activity of Synj at T1259 was found to be regulated by LRRK2 (R1441C). Intensities were log2 transformed and signficiance was assesed by an unpaired t.test assuming equal variances.

and that the mutations within the GTPase domain results in enhanced kinase activity and Synaptojanin phosphorylation. Complementary, we used the same experimental conditions with non-radioactive ATP to measure the phosphorylation of Synaptojanin and hLRRK2 forms with our mass spectrometric workflow. As shown in fig. 3.29 C, we detected the pT1259 site to be phosphorylated and the incubation with the hLRRK2 (R1441C) clearly increased the Synaptojanin phosphorylation at T1259. Conversely, the hLRRK2 (D1994A) had no influence on the phosphorylation of Synaptojanin.Of note, we detected 6 phosphorylation sites on hLRRK2 and 4 of them (pT1343, pT1348, pT1452, pT1503) are localized within ROC domain confirming the autophosphorylation of LRRK2 [219]. Although both LRRK2 and LRRK2 (R1441C) showed similar autophosphorylation signal, synaptojanin did not show any autophosphorylation signal and the hLRRK2 (D1994A) kinase dead mutant together with Synaptojanin also did not show any phosphorylation signals (fig. 3.30 A-B). In addition, Synaptojanin phosphorylation was effectively competed with non-radioactive ATP in the presence of LRRK2 and LRRK2 (R1441C) (fig. 3.30 C-D). The MS/MS spectra for phosphorylated peptide of synaptojanin has been shown in fig 3.30 E. These results indicate that both recombinant proteins are able to phosphorylate Synaptojanin and that the mutations within the GTPase domain results in enhanced kinase activity and Synaptojanin phosphorylation.

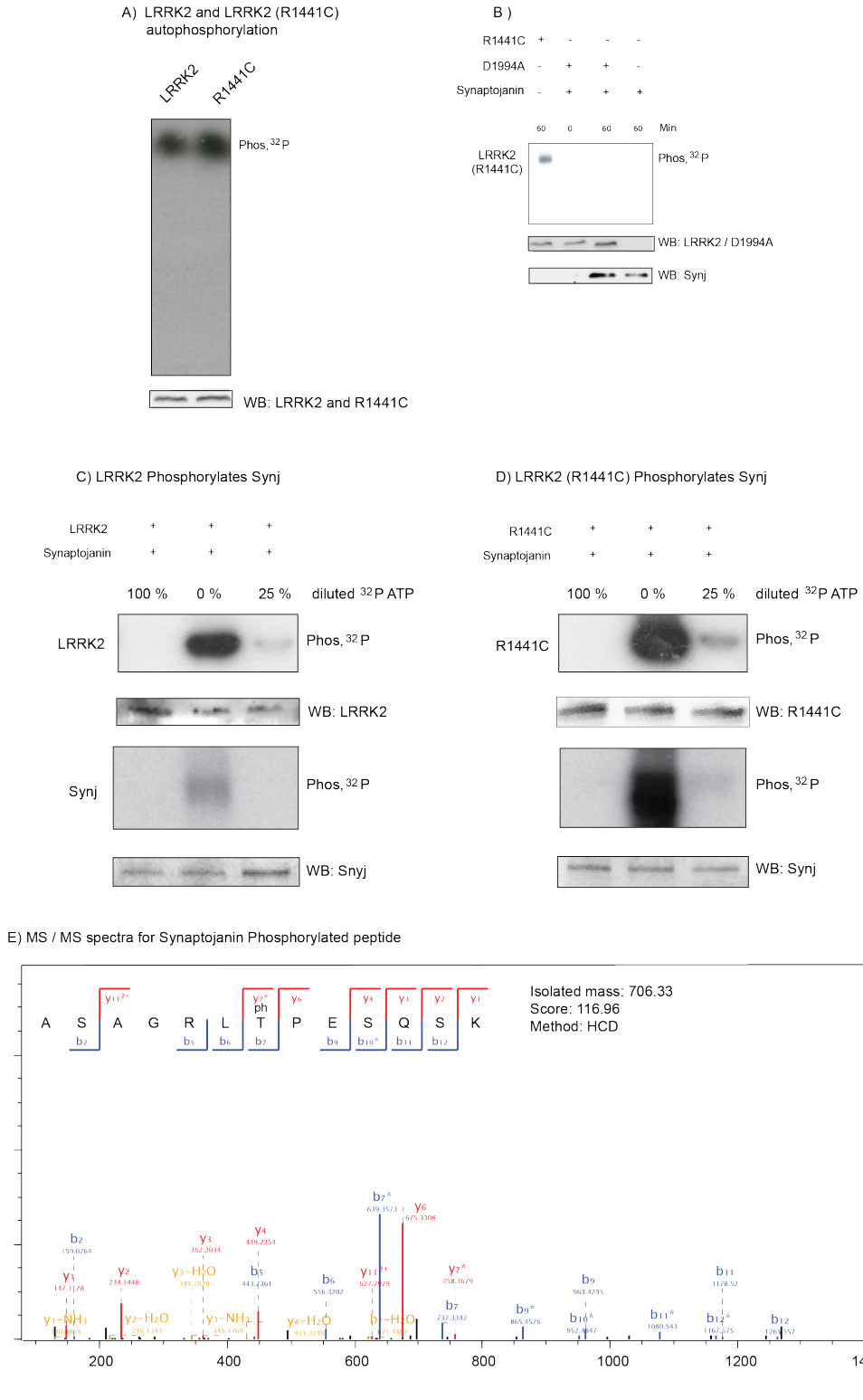

FIGURE 3.30: LRRK2 phosphorylates synaptojanin. A) Autophosphorylation of LRRK2, LRRK2 (R1441C) and synaptojanin. Recombinant proteins were subjected to Western blotting for detection of GST-tagged LRRK2 and R1441C in the presence of γ- 32P-ATP. B) Kinase dead LRRK2 (D1994A) mutant did not phosphorylates Synaptojanin. C) Phosphorylation of synaptojanin by hLRRK2 (R1441C) with different concentrations of LRRK2 ATP. D) As in (C) except LRRK2 was utilized. E) MS/MS spectra for phosphorylated peptide of synaptojanin.

3.10 Immunoprecipitaion of hLRRK2 in *Drosophila* brain revealed several synaptic proteins as potential interaction partners

To identify direct hLRRK2 interactors in our PD model, a protein-protein interaction screen based on Flag-Tag immunoprecipitation were used. For immunoprecipitation experiments, we used a mouse-monoclonal Flag antibody in order to enrich for potential binding partners of hLRRK2 in fly brains.

To distinguish between interactors and background binders, the extracts from *ddc*-Gal4 flies were used. MS analysis and label free protein quantification revealed 25 putative interactors with p-values < 0.05 and fold-change > 2 (n=2) as shown in table 3.31. However, 500 proteins were discarded as nonspecific binders since they were equally abundant in all genotypes. Among 25 interacting partners, 11 genes were associated with synaptic vesicle recycling process, 4 were membrane linked genes. A complete list of hLRRK2 interacting genes were shown in fig. 3.31. Strikingly, we quantified 8 known LRRK2 binding partners, including Endophilin, Rab7, futsch, Synapsin, the vesicle fusing protein (Nsf2) from our analysis [212, 214, 220, 221]. Those interactors reflecting the crucial function of LRRK2 during synaptic vesicle formation and highlighting the sensitivity of our immunoprecipitation experiments. Notably, we also found futsch as up regulated phosphorylation site in our phosphoproteomic study, suggesting that hLRRK2 (R1441C) might directly interacts and phosphorylates these proteins. Another known hLRRK2 interator is dynamin, a microtubule associated protein regulating the vesicular trafficking processes [222]. Here, we identified the *Drosophila* orthologe Shi with a fold-change > 2.06 (p-value < 0.005). Similarly, we found a 3.6 fold-change for ankyrin 2 a cytoskeleton protein responsible for the stabilization of microtubule associated neuromuscular junctions (NMJ). Of note, we observed an increased phosphorylation close to the c-terminus at position S11169 in LRRK2 (R1441C) overexpressing flies.

These potential interacting partners suggested the functional connection of LRRK2 with mitochondrial proteins, membrane proteins and synaptic vesicle associated proteins. The identification of LRRK2 interaction partners may therefore ensure the better understanding of the physiological function of LRRK2 and associated PD pathology.

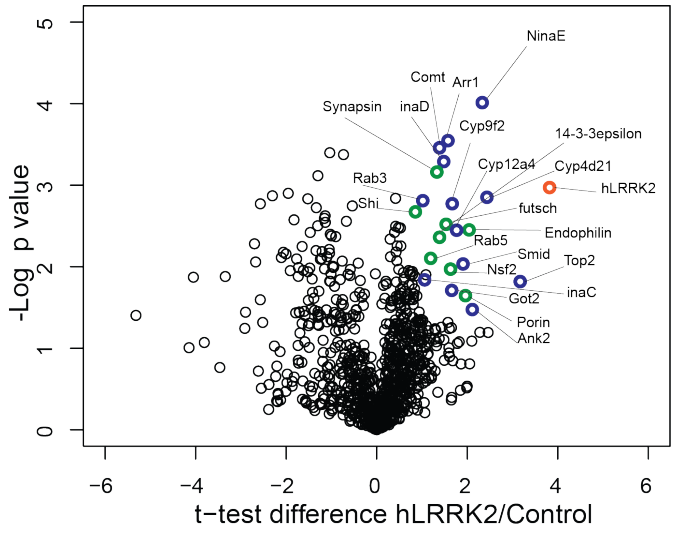

FIGURE 3.31: Interactome proteomics for hLRRK2 in *Drosophila*. A) Volcano plot of protein ratios between hLRRK2 and control flies. The y-axis and x-axis represents the log (adjusted p-value) and t-test difference (log2 ratio between hLRRK2 and control flies). All the known hLRRK2 interacting partners were colored by green (circle) and the provable interactors were colored by blue circles.

TABLE 3.3: Potential interacting partner of hLRRK2 in *Drosophila*

Protein Ids	GENE NAME	IP ratio LRRK2/Control	P value
Q5S008	lrrk2	14.11938039	0.0011
P15348	top2	8.997250174	0.0152
Q94920	porin	3.992056948	0.0196
Q9VLZ7	Cyp4d21	5.407541241	0.0014
Q9VG82	Cyp9f2	3.104322186	0.0018
Q9VE00	Cyp12a4	3.6359091	0.0043
Q8T0M9	Got2	3.84074511	0.0211
Q95U34	Galk	2.465127805	0.0138
P06002	ninaE	5.031092037	0.0001
P13677	inaC	2.709395708	0.0137
Q24008	inaD	3.130948481	0.0014
Q09103	rdgA	2.431195319	0.0008
P48159	RpL23	2.211324598	0.0000
Q9W596	futsch	2.892511878	0.0030
Q0E8H3	ank2	3.601410971	0.0354
P92177	14-3-3ep.	3.177910342	0.0017
Q7KU82	smid	3.750714699	0.0093
P54351	Nsf2	3.098467001	0.0107
Q24546	syn	2.981817378	0.0012
P15372	Arr1	2.980567968	0.0003
P46461	comt	2.792264823	0.0005
B5RIU6	endophilin	4.116709105	0.0035
O76742	rab7	2.039112968	0.0084
P25228	rab3	2.026335716	0.0015
E1JJA4	shi	2.055630435	0.0055

Chapter 4

Discussion

The molecular mechanisms leading to neuronal degeneration in PD or Amyotrophic lateral sclerosis (ALS) are poorly understood and disease modifying treatment is until now also not available. To gain a better understanding of the pathophysiology of these neurodegenerative diseases, several model organisms, including yeast, flies and rodents were established that overexpress a human gene and its disease associated gene variants. In this study, the fruit fly *D.melanogaster* has been used as a PD model system to understand the pathobiology of the PD associated gene hLRRK2. Furthermore, we generated another PD fly model by overexpressing αS to find common and gene specific mechanisms during the progression of PD. Though flies appear far away from human physiology, similar cellular process, including gene activities, and signaling pathways are conserved in the fly model, which are comparable to the human system [223]. Furthermore, the fly is one of the most striking model organisms for Parkinsonism research due to its complex DA system regulating motor activities such as climbing and flying. The DA system in *Drosophila* consists of mainly 5 distinct clusters within the protocerebrum of the fly brain. Each cluster contains several hundreds of dopamine producing neurons and similar to the human system, each cluster projects their axons into different functional areas of the brain. So far, the anatomy of DA neurons and their projections were mainly studied using reporter strains such as TH-specific GAL4 line and immunohistochemical approaches using anti-TH antibodies [71]. In addition, the short life span further emphasizes the fly model as a versatile tool to investigate the progression of the PD in a relative short time period. Thus, PD fly models recapitulate some features of the human disease and can be used to model human neurodegenerative diseases. In the present study, a hLRRK2 (R1441C) *Drosophila* strain was generated as a new PD model by overexpressing the human LRRK2 gene containing an amino acid exchange at position 1441 (R1441C) in *Drosophila*(DA) neurons under the control of *ddc*-Gal4 line. The study above showed that overexpression of the hLRRK2 and its

mutant form hLRRK2 (R1441C) in flies initiated severe degeneration of retinal and DA neurons, shorter life span and locomotor impairment compared to age matched control flies. Moreover, flies overexpressing the hLRRK2 (R1441C) mutant exhibited a more severe phenotype compared to hLRRK2 overexpressing flies. Since locomotor activity is tightly associated with viable DA neurons [224, 225], we used an immunohistochemistry approach to visualize TH positive neurons in fly brains and found significantly reduced levels of TH positive neurons in several DA clusters, including PPM1/2 PAL, PPL1, PPL2 a/b. Consistently, hLRRK2 (R1441C) flies showed a more severe phenotype compared to control flies, suggesting enhanced toxicity of the R1441C LRRK2 version which is also associated with enhanced kinase activity [57]. Although there is substantial evidence that LRRK2 (R1441C) does not increase in vitro kinase activity [219], however, when using the LRRK2 pS1292 antibody as a marker of autophosphorylation activity, R1441C does increase kinase activity [56]. Moreover, it is also possible that DA neurons are still present but do not express TH. Further marker proteins, including dopamine transporter (DAT) should be tested to trace DA neurons and their connections to other brain areas during disease progression [226]. The present results correlate with previous works from Liu and Karterina [72, 74] showing also the degeneration of DA neurons in hLRRK2 transgenic fly brains. Interestingly, the PPM1/2 and PPL1 cluster showed the most severe reduction of TH positive neurons in aged hLRRK2 (R1441C) flies compared to hLRRK2 and ddc-Gal4 control flies. DA neurons project long axons to distinct functional areas of the brain. It might be possible that DA neurons with longer projections are more affected by the overexpression of hLRRK2 and its mutant form. Conversely, some clusters such as the PPM3 and PAM cluster showed no significant change in TH positive neurons between control, hLRRK2 and hLRRK2 (R1441C) transgenic flies. However, this data is contradictory with a previous finding [72] where all DA clusters were equally affected. This might reflect different expression levels of the Gal4 activator protein between different fly strains and laboratory conditions. In addition, these differences might be due to the utilization of different methods monitoring DA neurons. For example, TH reporter strains such as TH-mCD8::GFP expression does not completely overlap with anti-TH antibody staining. Other reasons could be an unequal tissue preparation, causing differences in the detection of brain proteins, the transgene copy number or expression levels or differences between LRRK2 mutations. The apparent differences of DA clusters in the present work might be due to different sensitives between subclasses of DA neurons to the toxic effect of hLRRK2 overexpression. Notably, the ectopic overexpression of hLRRK2 (R1441C) under the control of the *elav*-Gal4 driver results in a milder phenotype compared to *ddc*-Gal4 driver system. It is tempting to speculate that the weaker *elav*-dependent expression due to lower Gal4 levels from the elav promoter might result in lower levels of hLRRK2 and thereby causing a milder PD phenotype.

Previous work from Sang and Wang [224, 225] reported that inhibition of Hsp90 chaperone function radically declines LRRK2 stability in primary neuronal cultures, suggesting Hsp90 as a useful target for suppressing the accumulation and pathogenic activity of PD related LRRK2 mutations in neurons. They also showed a clear correlation between locomotor impairment and DA neuron degeneration. Interestingly, Ng *et. al* [73] did not observe any significant locomotor dysregulation in hLRRK2 (G2385R) overexpression in flies. The mutations at amino acid position 2385 is in the WD40 domain and the missing phenotype may reflect reduced kinase activity for this LRRK2 mutation [227]. A report from Katerina *et. al* [74] using different LRRK2 *Drosophila* strains (WT, Y1699C and I2020T) presented the ectopic expression of WT or mutant LRRK2 in DA neurons caused severe neuronal loss accompanied by complex age-dependent changes in locomotor activity. Surprisingly, they showed an improved climbing ability after an initial locomotor impairment period and progressive DA degeneration in transgenic flies. They suggested that compensatory mechanisms between DA and non-DA neurons might rescue the phenotype. However, other reports excluded such a scenario and observed a clear proportional relation between reduced DA neurons and climbing disability [78]. Besides a reduced locomotor activity flies overexpressing hLRRK2 showed a reduced life span, and a significant retinal neurodegeneration in hLRRK2 and hLRRK2 transgenic flies compared to Canton S and GMR-Gal4 flies. These results are consistent with the results of Liu *et. al* and Katerina *et. al* [74], however Ng *et. al* did not observe any retinal degeneration in any LRRK2 expressing *Drosophila* lines (WT, Y1699C and G2019S). Ng *et. al* showed that the coexpression of human parkin in LRRK2 (G2019S) expressing flies protects against the DA degeneration that occurs with age. On the other hand, Elliot CJ *et. al* revealed that overexpressing LRRK2-G2019S in flies DA neurons leads to progressive loss of photoreceptor function. They also found elevated autophagy, apoptosis and mitochondrial disorganization in photoreceptor cells. The head sections demonstrated an extensive neurodegeneration throughout the visual system, including regions not directly innervated by DA neurons in these flies [228].

These variations between the present hLRRK2 (R1441C) transgenic flies and the previous work are probably due to different fly strains in combination with various expression constructs optimized for protein expression. It is also important to note that the same pathogenic LRRK2 mutation can also vary between different LRRK2 patients [229]. Taken together, the morphometric analysis and TH expression profile supports an important function of hLRRK2 and its mutant form hLRRK2 (R1441C) in DA neurons of flies. Although anatomical data concerning neuronal clusters are slightly incongruent in the literature, in many cases, LRRK2 overexpression results in a clear PD phenotype. However, the mechanistic details how the multi-enzymatic LRRK2 and its mutation variant influences DA neurons remains unclear.

4.1 Quantitative proteome analysis of hLRRK2 (R1441C) overexpressing flies revealed specific changes related to PD

In order to get more insight into the biochemical alterations induced by hLRRK2 and its mutant variant, a comprehensive quantitative MS analysis was performed. The unbiased screen of diseased flies revealed several hundreds of regulated proteins during early and late time points and the detection of several known PD related proteins and their related pathways are an excellent validation of our model system. Most interestingly, several regulated proteins were detected which have no obvious connection to the pathobiology of PD. Two independent biological replicates have been performed for day 1, day 10 and day 30 and proteins with 1.5 fold change ($p < 0.05$) were considered as significantly regulated candidates. A class of regulated proteins in hLRRK2 (R1441C) flies were only regulated during early time points (day 1 and day 10) and showed an equal distribution at later stages. We hypothesized that mutant flies might have encountered an unfavorable environment which was further compensated for later stages. Since, PD is an age dependent progressive neurological disorder, the analysis was therefore focused more on proteins which demonstrated late onset regulation. In total, 183 proteins have been quantified with an exclusive regulation at day 30. A Fisher's exact test showed for those late regulated proteins, an enrichment of Gene Ontology (GO) terms specific for microtubule based processes and synaptic vesicles. In addition, the KEGG pathway analysis also demonstrated the enrichment of pathways related to "oxidative phosphorylation", "Parkinson's and Alzheimer's disease". The term oxidative phosphorylation indicates mitochondrial energy production, mitochondrial function and has been reported to be tightly linked to different neurological disorder, including PD [230]. Another class of proteins known to be involved in cytoskeletal rearrangements during PD is microtubule and actin filament related proteins. Actin cytoskeletal proteins are widely known not only for their functional role in dynamic cellular processes, but also for their important function during neuronal development. Further, neuronal migration and neurite extension relies on actin-regulatory proteins such as moesin, ezrin, and radixin also known as ERM proteins. In addition, actin polymerization [231] and myosin heavy chain (MyHc) proteins are also important factors for the regulation of the actin based cytoskeleton [232]. A recent study showed that hLRRK2 (G2019S) overexpression in primary neurons from rat brains results in an inhibition of neurite outgrowth suggesting a direct function as a modulator for actin dynamics during neurite extension [161]. Conversely, LRRK2 knockout or silencing leads to increased neurite outgrowth suggesting that LRRK2 is a negative regulator of neurite outgrowth/complexity [233]. However, it is unclear whether LRRK2 functions as a scaffold protein or regulates actin

dynamics via its kinase and/or GTPase domain. A first indication for a direct link between the actin cytoskeleton and the LRRK2 kinase activity was shown by the phosphorylation of moesin at pT558 mediated by the hLRRK2 (G2019S) mutant variant in vitro kinase assays. However, this has never been confirmed in cells or tissues. What is more, moesin required heating to allow its phosphorylation by LRRK2 suggesting it only occurs when unfolded/denatured [234]. The phosphorylation of ERM proteins results in the activation of these proteins and induces the localization of F-actin to the plasma membrane and regulating thereby the formation of filopodia and neurite outgrowth. The overexpression of the hLRRK2 (G2019S) mutant also results in increased levels of F-actin and this upregulation inhibits the interplay between actin filaments and microtubule structures. Thus, elevated F-actin levels induced by hLRRK2 (G2019S) may act as an obstruction and thereby preventing neurite outgrowth. The quantitative proteome analysis revealed no changes for ERM proteins but a significant increase for two actin orthologs Act87E and Act88F in hLRRK2 (R1441C) flies at day 30. Feany *et al* previously raised the possibilities of actin cytoskeletal changes as important mediators of toxicity in *Drosophila* taupathies and reported the direct interaction between actin and tau [235]. Taken together, our study of hLRRK2 (R1441C) and hLRRK2 flies showed again that the regulation of the actin cytoskeleton is tightly associated with a correct LRRK2 function and abundance. However, the direct functional relationship of hLRRK2 with these two actin cytoskeleton proteins (Act87E and Act88F) needs to be addressed in future experiments.

4.2 LRRK2 overexpression affects several cellular compartments

Previous studies have shown that the expression of mutated hLRRK2 (G2019S) in DA neurons causes a functional and anatomical loss of a *Drosophila*'s visual system [72]. Here, we observed a mild but clear malformation in the eyes of hLRRK2 (R1441C) overexpressing flies along with several down regulated proteins associated with the photoreceptor cell membrane. There are three types of DA neurons innervating the visual system, the PPL neurons in the lobula, MC neurons in the medulla, and LA neurons which project from protocerebrum to lamina. PPL neurons only project to the lobula, well away from photoreceptor terminals and there is also no known direct synaptic connection between MC dendrites and photoreceptor axons [228]. Thus, LA DA neurons might be mostly responsible for neurotransmission to photoreceptor terminals. We observed that expression of hLRRK2 (R1441C) in DA neurons results in an anterograde degeneration of photoreceptors and most likely explains the eye phenotype.

4.2.1 Mitochondrial disruption in LRRK2 (R1441C) expressing flies

Mitochondrial dysfunction is a known biochemical hallmark of PD [168] and most likely one of the most important reasons for the sporadic appearance of PD in humans. LRRK2 plays a vital role in modulating mitochondrial activity and primary fibroblasts from PD patients carrying a LRRK2 mutation showing impaired mitochondrial function and morphology [236]. Recent studies reported a direct association of LRRK2 expression and mitochondria dynamics. For example, correct mitochondrial function is connected to fusion and fission processes of mitochondria and increased mitochondrial fragmentation was further exacerbated by LRRK2 (R1441C) [237]. Wang *et al* reported that LRRK2-induced mitochondrial fragmentation could be due to enhanced fission, reduced fusion or both. By using photo-convertible fluorescent labeling, they demonstrated that a reduced fusion is involved in the process. In total, 63 mitochondrial proteins (5 % of all proteins) were identified reflecting the abundance of mitochondria in neuronal tissue. The GO and KEGG pathway analysis revealed a fraction of 12 regulated mitochondrial proteins were also involved. The final step for energy production is the generation of ATP by several ATP synthase proteins within complex V of the respiratory chain. In total, 5 ATP synthases were up regulated in hLRRK2 (R1441C) expressing flies. One feature of DA neurons is the highly efficient transport of ions through the plasma membrane after each action potential. This is a highly energy demanding process and takes over 40% of the total energy requirement for cells of the nervous system [238]. One possible explanation for an increased level of ATP synthases could be that mutant flies might require more ATP synthase enzymes to provide enough energy to compensate for more inefficient ion transport and signaling in the presence of LRRK2 (R1441C).

4.2.2 Synaptic vesicle proteins are regulated by LRRK2 (R1441C)

The physiological relevance between increased levels of LRRK2 and synaptic vesicle trafficking has been shown by several reports [160, 239, 239]. In line with these observations, we also discovered several significantly down regulated proteins in LRRK2 (R1441C) flies which were associated with endocytosis and exocytosis. The question remains how LRRK2 (R1441C) overexpression disturbs the synaptic vesicle trafficking system, including endocytosis, exocytosis, and neurotransmitter release. The transportation of vesicles from the reserve pool relies on mitochondrial ATP. After docking and priming, the SNARE complex and accessory proteins (e.g., Synaptotagmin and CDCRel-1) facilitate SV fusion with the plasma membrane allowing for neurotransmitter release. Endophilin, Dynamin, and Rab5 participate in the retrieval and transport of SVs by

endocytosis. Although the clear scenario of LRRK2 (R1441C) molecular mechanism in association with synaptic vesicles still needs to be examined, our proteomics data outlined the possible function of LRRK2 mutant in endocytosis and exocytosis disruption in *Drosophila*. The quantitative proteomics data showed that synaptic transmission linked proteins such as Syntaxin and SNAP-25, proteins of the t-SNAREs complex, are significantly downregulated in hLRRK2 (R1441C) flies. In addition, another synaptic vesicle specific protein, Syanptotagmin (Syt), was also found to be downregulated in mutant flies. Syanptotagmin is a key player for neurotransmitter release and is known to interact with the carboxyl terminus of SNAP-25 and syntaxin. Hence, regulated Synaptotagmin can disrupt LRRK2's interaction with Syntaxin and SNAP-25 [240, 241] that might lead to perturbed exocytosis in mutant flies. However, other reports argued that binding between Synaptotagmin and Syntaxin may not be playing an important role for neurotransmitter release [242]. The observation of several proteins involved in synaptic vesicle formation confirmed that hLRRK2 is an important factor for these processes. It is important to mention that the overexpression of WT LRRK2 in primary mouse hippocampal neurons are associated with a decrease in SV endocytosis and results in a lower rate of SV trafficking [243]. More recently downregulated LRRK2 function in mouse cortical neurons was shown to affect SV recycling and redistribution supporting the assumption that LRRK2 controls the storage and mobilization of vesicle pools inside the presynaptic bouton [244]. Therefore, the significant down regulation effect of these proteins on the synaptic vesicle cycle might lead to an inefficient sequestration of dopamine into vesicles resulting in increased cytosolic DA levels and ensuing dopamine toxicity.

4.3 The proteome changes in αS PD model flies

In order to identify more specific hLRRK2 dependent mechanisms, further *Drosophila* PD models were generated overexpressing three different variants of αS (WT, A30P, A53T) under the control of the *ddc* promoter. Similar to hLRRK2 analysis, all experiments were performed in biological duplicates. In contrast, for the analysis of αS fly's strains only day 1 and day 10 were used for the analysis, since αS flies showing a severe PD phenotype after two weeks and most of the transgenic flies die around day 40. In total, 4400 proteins were identified from biological duplicates and 1707 candidates were quantified among all αS fly strains (Wt, A30P and A53T). The strongest effect in regard to protein changes was observed in A30P-αS flies compared to αS and A53T-αS flies. Though the proteome response of both A30P-αS and A53T-αS mutants showed a clear overlap of the regulated proteins (70%), each mutant strain conserves

a specific subset of regulated proteins. For example, A30P-αS expressing flies demonstrated increased protein levels of mitochondrial membrane respiratory chain proteins such as NADH dehydrogenase (Complex I). Interestingly, disturbed complex I formation was documented in human PD patient's brain tissue and it has been suggested that disturbed mitochondrial DNA might be one of this reasons for these biochemical dysfunction [24]. Several complex I inhibitors have been described to replicate some of the key motor features of PD and lead to death of DA neurons. For example, parkinsonism in humans has been reported to result from unintentional exposure to 1-methyl-4-phenyl-1,2,3,6-tetrahydropyridine (MPTP) [245]. Moreover, administration of rotenone to *D.melanogaster* results in levodopa-responsive locomotor deficits and loss of DA neurons [246]. Therefore, differentially expressed complex I associated proteins in hLRRK2 (R1441C) flies might reflect the disturbance in the mitochondria inner membrane, which may play a role in PD. On the other hand, A53T-αS expressing flies showed a new set of mitochondrial proteins which were significantly regulated relative to αS flies. For example, 3 Cytrochrome p450 proteins (Cyp9b2, Cyp12c1 and GstE1) were found to be regulated in A53T mutant flies. Interestingly, hLRRK2 (R1441C) expressing flies also exhibited the elevated expression of Cyp9b2 protein compared with hLRRK2 flies. *Drosophila*'s Cytochrome p450 genes were also involved in neuronal defense against oxidative imbalance under hypoxia treatment [204] and therefore, elevated expression of Cytochrome p450 genes might represent the neuroprotective role against neuronal degeneration in A53T mutant flies. Therefore, these data sets demonstrate the involvement of various mitochondrial genes in PD progression relating to the variation of αS mutant form in flies.

Although both LRRK2 and αS PD models showed a common set of regulated proteins and similar phenotypes, the integrative analysis showed that LRRK2 and αS mutant fly strains mediate their PD-induction and toxicity through different pathways. For example, we observed several proteins involved in synaptic vesicle exo-and endocytosis to be affected only in hLRRK2 (R1441C) flies, whereas αS overexpressing flies revealed no changes in those vesicle proteins, suggesting a specific hLRRK2 function for this pathway. Conversely, the down regulation of a few proteins such as Cyp6a20 showed a specific function for αS during the progression of PD. Thus, the pathological mechanisms in both models during the course of PD is clearly different and our analysis provides a quantitative dataset to investigate the consequences of increased levels of LRRK2 and αS disease associated protein changes in neuronal tissues of living flies.

4.4 Phosphoproteome dynamics and hLRRK2 interaction partners in a PD model

To gain a deeper insight into affected signaling pathways and to learn more about potential kinase substrates of LRRK2, a global phosphoproteome analysis of flies expressing hLRRK2 and the mutant (R1441C) variant were performed after 30 days. In total, 2529 phosphorylation sites were identified by the *in vivo* SILAC approach. The comparison of control and hLRRK2 overexpressing flies revealed a time-dependent increase of protein phosphorylation in the presence of hLRRK2. We quantified 27 and 39 phosphosites which were at least 1.5 fold regulated in hLRKK2 and hLRRK2 (R1441C) flies respectively compared to control flies. A permutation based false discovery (FDR) rate of < 0.05 was applied for statistical calculation and after the normalization to protein levels, 9 significant regulated phosphorylation sites were quantified between hLRRK2 and hLRRK2 (R1441C) overexpressing flies [247, 248]. Until now, the number of identified LRRK2 kinase substrates *in vitro* studies is very low and none has been convincingly proved *in vivo*, leaving the pathophysiological relevance of kinase activity unclear. For example, Xiong *et. al* reported ArfGAP1 as a LRRK2 kinase substrate *in vitro* and showed the phosphorylation of ArfGAP1 by LRRK2 inhibits its GAP activity and LRRK2 kinase activity is significantly reduced in the presence of ArfGAP1 [243]. However, Stafa *et. al* demonstrated that co-expression of ArfGAP1 and LRRK2 synergistically promotes neurite shortening in rat primary cortical neurons in a manner dependent upon LRRK2 GTPase activity and silencing of LRRK2 expression rescues Arfgap1-induced neurite shortening [222]. Therefore, the effectors associated in the regulation of cellular LRRK2 phosphorylation are still unknown. A consensus phosphorylation motif based on a peptide library screen *in vitro* exists only for the LRRK2 (G2019S) mutant variant [249]. Strikingly, two microtubule (MT) associated proteins futsch (in vertebrates: microtubule-associated proteins, MAPs) and Ankyrin2 were quantified with increased phosphorylation levels in hLRRK2 (R1441C) mutants compared to hLRRK2 flies. The MT cytoskeleton plays an important role for synaptic vesicle transportation and maintenance of synaptic transmission and hence disruption of MT dynamics in neuronal synapse often leads to neurological disease [250, 251]. Consistently, we also found these two proteins in our LRRK2 interactome study, suggesting that both MT associated proteins are direct LRRK2 interaction partners and most likely also targets of the LRRK2 kinase. Thus, enhanced kinase activity of the hLRRK2 (R1441C) may cause hyperphosphorylation of microtubule associated proteins and thereby altering the binding to cytoskeletal structures. In addition, Futsch and Ank2 are responsible for the formation of early endosomes, correct assembly of the reserve pool, and neurotransmitter release within active zones [252]. However, whether the increased phosphorylation

of futsch impedes intact microtubule structures and changes the dynamics of synaptic vesicles remains to be elucidated. Electric stimulation of synapses causes a rapid calcium influx and activates synaptic vesicle exo-endocytosis near the presynaptic plasma membrane. Synaptic vesicle docking is mediated by a complex consisting of synaptobrevin (VAMP), synaptotagmin, Rab3, and two components of the presynaptic plasma membrane SNAP25 and syntaxin. Our study revealed a clear down regulation on protein level for this complex, but no change in the corresponding phosphopeptides. In fact, the R1441C mutation within the ROC domain of LRRK2 causes not only reduced GTPase activity but has also an toxic effect on cells [243, 248]. In this context it is possible that increased hLRRK2 (R1441C) levels cause an impairment of synaptic vesicle proteins by suppressing synaptic vesicle trafficking. Recent studies also showed a direct association of LRRK2 to endosomal-autophagic processes and increased levels of hLRRK2 (R1441C) causes an accumulation of autophagic vesicles [258]. Another example for an endogenous LRRK2 target is endophilin A (EndoA), an important regulator of synaptic endocytosis. LRRK2 dependent phosphorylation of endophilin regulates its association to membranes and facilitates synaptic vesicle endocytosis at *Drosophila*'s neuromuscular junctions [220]. Although we did not find a regulation of endophilin at the protein or phosphopeptide level, we found increased phosphorylation of two highly conserved sites (pT1131, pS1142) on synaptojanin a known interaction partner of endophilin [259]. In *c. elegans* the interaction between endophilin and synaptojanin is mediated by the EndoA-SH3 and proline rich domain (PRD) at the c-terminus of synaptojanin. This interaction is crucial for vesicle recycling and the phosphorylation of pT1131 and pS1142 may facilitate the interaction between both proteins in the fly system.

Notably, our *in vitro* kinase assay with human synaptojanin confirmed a direct phosphorylation by the hLRRK2 and moreover, we found increased phosphorylation levels for pT1131 and pS1142 in the presence of the hLRRK2 (R1441C) variant. Thus, it is possible that dynamic phosphorylation of synaptojanin mediated by hLRRK2 might be a requisite for the interaction with EndoA. Alternatively, synaptojanin is a highly dynamic protein and a reversible phosphorylation might regulate the transient recruitment to synaptic vesicles. Our findings that hLRRK2 (R1441C) mutant variant enhances Synaptojanin phosphorylation might be an important aspect for endophilin-dependent synaptic vesicle formation under regular and diseased conditions. Clearly, perturbed neurotransmission caused by dysregulated synaptic vesicle formation have been implicated in PD.

4.5 The functional relevance between SV trafficking dysfunction and DA degeneration

Synaptic dysfunctions have been assumed as one of the early and major neurobiological events in several neurological diseases [260] and accumulating evidence has pointed out the regulation of presynaptic activity by PD related genes. For example, αS-KO (knockout) mice have lent support for a pivotal role of αS in the regulation of presynaptic neurotransmitter vesicle pools [214]. Intriguingly, presynaptic defects such as reduced dopamine overflow and impaired striatal synaptic plasticity have been also identified in PINK1- and parkin-KO mice [261]. In addition, LRRK2 (R1441C) homozygous knockin mice and the R1441G LRRK2 BAC (bacterial artificial chromosome) transgenic mice displayed severe neurotransmission defects, including impairments in nigrostriatal DA innervation and degeneration of the nigrostriatal projections [69, 184]. Finally, it has been suggested that the presence of LRRK2 as an integral part of the presynaptic protein complex might play a key role in electrophysiological properties as well as proper vesicular trafficking and spatial distribution in the presynaptic pool [244]. Our proteome, phosphoproteome and protein-protein interaction profile have outlined the potential role of hLRRK2 (R1441C) for several cellular pathways and compartments, including mitochondria and synaptic vesicle formation/trafficking. Nevertheless, how does LRRK2 regulate SV dysfunction and lead to neuronal loss in the fly PD model still need to be addressed. Although LRRK2 conserves functional domains such as the N-terminal leucine-rich repeat domain and the C-terminal WD40 domain for protein–protein interactions, it also contains an active kinase domain. Therefore, it is tempting to speculate that LRRK2 might affect SV trafficking at different levels according to the functions of its proposed presynaptic targets: mobilization and priming of SV, disassembling of SNARE complex and recycling of SV. Secondly LRRK2 may disrupt SV fusion to the presynaptic membrane by regulating synaptotagmin, a SV integral protein which acts as a Ca^{2+} sensor. Moreover, LRRK2 interacts with NSF, an AAA (ATPase associated with various cellular activities) protein responsible for the disassembling of the SNARE complex [184]. Therefore, LRRK2 may also modulate the assembly–disassembly equilibrium of SNARE complexes by the LRRK2-NSF interaction. Finally, Rab5, a key regulator of vesicle endocytosis, has been demonstrated as an interacting partner of LRRK2. Interestingly, it has been shown that overexpressed Rab5 rescued endocytosis defects caused by LRRK2 overexpression [263]. Our study showed that SV cycling associated proteins and their phosphorylation are significantly regulated by LRRK2 at different steps of this process starting from the reserved pool (RP) to the early endosome (fig. 4.1B). Thus SV trafficking dysregulation of specific proteins and phosphorylation sites induced by the LRRK2 kinase could interrupt dopamine homeostasis that may result in increased

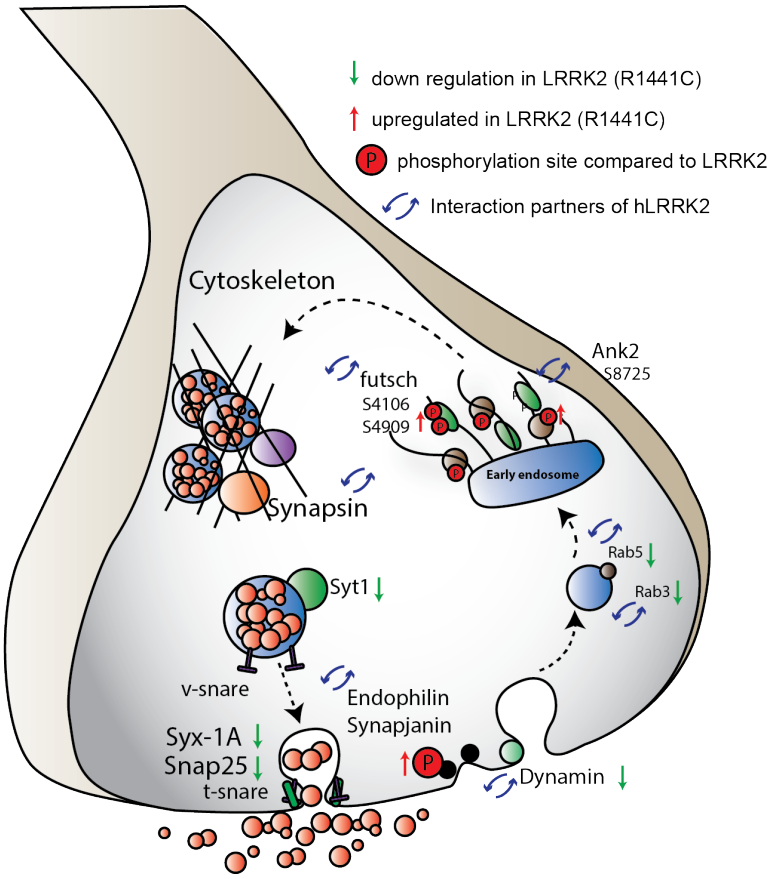

FIGURE 4.1: Synaptic vesicle trafficking system in *Drosophila*. Green arrow denotes down regulated proteins ratios in mutant flies, whereas red arrows represent the regulated phosphorylated site compared to hLRRK2 flies. The interaction partners were shown by circled arrow (Blue circled arrow).

pools of cytosolic DA, which is an oxidative stressor for the neuronal cells [264]. A previous report also suggested that DA can alter αS and induce toxic protofibrils [265]. Therefore, the neuronal degeneration in PD might be the result of extra cytocolic DA release.

Taken together, our MS study provides a comprehensive quantitative dataset of the human LRRK2 and human αS *Drosophila* Parkinson's models. In addition, our phosphoproteomics analysis of hLRRK2 (R1441C) overexpressing fly mutants revealed novel LRRK2 substrates, including several synaptic vesicle proteins, with increased phosphorylation. The identification of specific LRRK2 (R1441C) dependent phosphorylation sites will provide important clues to which pathways are activated in hLRRK2 (R1441C) overexpressing flies and we hope our analysis will help to discover new targets for therapeutic treatments PD.

Bibliography

[1] Joseph Jankovic. Parkinson's disease: clinical features and diagnosis. *Journal of Neurology, Neurosurgery & Psychiatry*, 79(4):368–376, 2008.

[2] Parkinson James. An essay on the shaking palsy. *The Journal of Nervous and Mental Disease*, 60(4):441, 1924.

[3] Arvid Carlsson, Margit Lindqvist, Tor Magnusson, and Bertil Waldeck. On the presence of 3-hydroxytyramine in brain. *Science*, 127:471, 1958.

[4] Charlotte A Haaxma, Bastiaan R Bloem, George F Borm, Wim JG Oyen, Klaus L Leenders, Silvia Eshuis, Jan Booij, Dean E Dluzen, and Martin WIM Horstink. Gender differences in parkinson's disease. *Journal of Neurology, Neurosurgery & Psychiatry*, 78(8):819–824, 2007.

[5] Sonja von Campenhausen, Bernhard Bornschein, Regina Wick, Kai Bötzel, Cristina Sampaio, Werner Poewe, Wolfgang Oertel, Uwe Siebert, Karin Berger, and Richard Dodel. Prevalence and incidence of parkinson's disease in europe. *European Neuropsychopharmacology*, 15(4):473–490, 2005.

[6] Manuela Neumann, Silke Adler, Oliver Schlüter, Elisabeth Kremmer, Reiner Benecke, and Hans A Kretzschmar. α-synuclein accumulation in a case of neurodegeneration with brain iron accumulation type 1 (nbia-1, formerly hallervorden-spatz syndrome) with widespread cortical and brainstem-type lewy bodies. *Acta neuropathologica*, 100(5):568–574, 2000.

[7] Benoit I Giasson, John E Duda, Ian VJ Murray, Qiping Chen, José M Souza, Howard I Hurtig, Harry Ischiropoulos, John Q Trojanowski, and Virginia M-Y Lee. Oxidative damage linked to neurodegeneration by selective α-synuclein nitration in synucleinopathy lesions. *Science*, 290(5493):985–989, 2000.

[8] Maria Grazia Spillantini, R Anthony Crowther, Ross Jakes, Masato Hasegawa, and Michel Goedert. α-synuclein in filamentous inclusions of lewy bodies from parkinson's disease and dementia with lewy bodies. *Proceedings of the National Academy of Sciences*, 95(11):6469–6473, 1998.

[9] William Dauer and Serge Przedborski. Parkinson's disease: mechanisms and models. *Neuron*, 39(6):889–909, 2003.

[10] CD Marsden. Neuromelanin and parkinson's disease. *Journal of neural transmission. Supplementum*, 19:121–141, 1982.

[11] KS Price, IJ Farley, and O Hornykiewicz. Neurochemistry of parkinson's disease: relation between striatal and limbic dopamine. *Advances in biochemical psychopharmacology*, 19:293, 1978.

[12] Heiko Braak, Kelly Del Tredici, Udo Rüb, Rob AI de Vos, Ernst NH Jansen Steur, and Eva Braak. Staging of brain pathology related to sporadic parkinson's disease. *Neurobiology of aging*, 24(2):197–211, 2003.

[13] Mariese A Hely, John GL Morris, Wayne GJ Reid, and Robert Trafficante. Sydney multicenter study of parkinson's disease: Non-l-dopa–responsive problems dominate at 15 years. *Movement Disorders*, 20(2):190–199, 2005.

[14] A Lieberman. Depression in parkinson's disease–a review. *Acta Neurologica Scandinavica*, 113(1):1–8, 2006.

[15] L Ishihara and C Brayne. A systematic review of depression and mental illness preceding parkinson's disease. *Acta neurologica scandinavica*, 113(4):211–220, 2006.

[16] M Frank. Dynamic dopamine modulation in the basal ganglia: a neurocomputational account of cognitive deficits in medicated and nonmedicated parkinsonism. *Cognitive Neuroscience, Journal of*, 17(1):51–72, 2005.

[17] Bonnie E Levin and H Katzen. Early cognitive changes and nondementing behavioral abnormalities in parkinson's disease. *ADVANCES IN NEUROLOGY-NEW YORK-RAVEN PRESS-*, 96:84, 2005.

[18] Donato A Di Monte. The environment and parkinson's disease: is the nigrostriatal system preferentially targeted by neurotoxins? *The Lancet Neurology*, 2(9):531–538, 2003.

[19] Christoph B Lücking, Alexandra Dürr, Vincenzo Bonifati, Jenny Vaughan, Giuseppe De Michele, Thomas Gasser, Biswadjiet S Harhangi, Giuseppe Meco, Patrice Denèfle, Nicholas W Wood, et al. Association between early-onset parkinson's disease and mutations in the parkin gene. *New England Journal of Medicine*, 342(21):1560–1567, 2000.

[20] Christine Klein and Michael G Schlossmacher. The genetics of parkinson disease: implications for neurological care. *Nature clinical practice Neurology*, 2(3):136–146, 2006.

[21] Suzanne Lesage, Pablo Ibanez, Ebba Lohmann, Pierre Pollak, François Tison, Myriem Tazir, Anne-Louise Leutenegger, Joao Guimaraes, Anne-Marie Bonnet, Yves Agid, et al. G2019s lrrk2 mutation in french and north african families with parkinson's disease. *Annals of neurology*, 58(5):784–787, 2005.

[22] Steven M Solano, David W Miller, Sarah J Augood, Anne B Young, and John B Penney. Expression of α-synuclein, parkin, and ubiquitin carboxy-terminal hydrolase l1 mrna in human brain: genes associated with familial parkinson's disease. *Annals of neurology*, 47(2):201–210, 2000.

[23] Makoto Sohmiya, Makoto Tanaka, Nyou Wei Tak, Makoto Yanagisawa, Yutaka Tanino, Yoko Suzuki, Koichi Okamoto, and Yorihiro Yamamoto. Redox status of plasma coenzyme q10 indicates elevated systemic oxidative stress in parkinson's disease. *Journal of the neurological sciences*, 223(2):161–166, 2004.

[24] Paula M Keeney, Jing Xie, Roderick A Capaldi, and James P Bennett. Parkinson's disease brain mitochondrial complex i has oxidatively damaged subunits and is functionally impaired and misassembled. *The Journal of neuroscience*, 26(19):5256–5264, 2006.

[25] Ted M Dawson and Valina L Dawson. Molecular pathways of neurodegeneration in parkinson's disease. *Science*, 302(5646):819–822, 2003.

[26] Matt Farrer, Wavrant-De Vrieze, Richard Crook, Lizzie Boles, Jordi Perez-Tur, John Hardy, William G Johnson, John Steele, Demetrius Maraganore, Katrina Gwinn, et al. Low frequency of α-synuclein mutations in familial parkinson's disease. *Annals of neurology*, 43(3):394–397, 1998.

[27] Mihael H Polymeropoulos, Christian Lavedan, Elisabeth Leroy, Susan E Ide, Anindya Dehejia, Amalia Dutra, Brian Pike, Holly Root, Jeffrey Rubenstein, Rebecca Boyer, et al. Mutation in the α-synuclein gene identified in families with parkinson's disease. *science*, 276(5321):2045–2047, 1997.

[28] Rejko Krüger, Wilfried Kuhn, Thomas Müller, Dirk Woitalla, Manuel Graeber, Sigfried Kösel, Horst Przuntek, Jörg T Epplen, Ludger Schols, and Olaf Riess. Alasopro mutation in the gene encoding α-synuclein in parkinson's disease. *Nature genetics*, 18(2):106–108, 1998.

[29] Maria Grazia Spillantini, Marie Luise Schmidt, Virginia M-Y Lee, John Q Trojanowski, Ross Jakes, and Michel Goedert. α-synuclein in lewy bodies. *Nature*, 388(6645):839–840, 1997.

[30] AB Singleton, M Farrer, J Johnson, A Singleton, S Hague, J Kachergus, M Hulihan, T Peuralinna, A Dutra, R Nussbaum, et al. α-synuclein locus triplication causes parkinson's disease. *science*, 302(5646):841–841, 2003.

[31] Juan J Zarranz, Javier Alegre, Juan C Gómez-Esteban, Elena Lezcano, Raquel Ros, Israel Ampuero, Lídice Vidal, Janet Hoenicka, Olga Rodriguez, Begona Atarés, et al. The new mutation, e46k, of α-synuclein causes parkinson and lewy body dementia. *Annals of neurology*, 55(2):164–173, 2004.

[32] Rainer von Coelln, Valina L Dawson, and Ted M Dawson. Parkin-associated parkinson's disease. *Cell and tissue research*, 318(1):175–184, 2004.

[33] Yasuko Hatano, Yuanzhe Li, Kenichi Sato, Shuichi Asakawa, Yasuhiro Yamamura, Hiroyuki Tomiyama, Hiroyo Yoshino, Masato Asahina, Susumu Kobayashi, Sharon Hassin-Baer, et al. Novel pink1 mutations in early-onset parkinsonism. *Annals of neurology*, 56(3):424–427, 2004.

[34] Enza Maria Valente, Patrick M Abou-Sleiman, Viviana Caputo, Miratul MK Muqit, Kirsten Harvey, Suzana Gispert, Zeeshan Ali, Domenico Del Turco, Anna Rita Bentivoglio, Daniel G Healy, et al. Hereditary early-onset parkinson's disease caused by mutations in pink1. *science*, 304(5674):1158–1160, 2004.

[35] S Gandhi, MMK Muqit, L Stanyer, DG Healy, PM Abou-Sleiman, I Hargreaves, S Heales, M Ganguly, L Parsons, AJ Lees, et al. Pink1 protein in normal human brain and parkinson's disease. *Brain*, 129(7):1720–1731, 2006.

[36] Laura Silvestri, Viviana Caputo, Emanuele Bellacchio, Luigia Atorino, Bruno Dallapiccola, Enza Maria Valente, and Giorgio Casari. Mitochondrial import and enzymatic activity of pink1 mutants associated to recessive parkinsonism. *Human molecular genetics*, 14(22):3477–3492, 2005.

[37] Alexandra Beilina, Marcel Van Der Brug, Rili Ahmad, Sashi Kesavapany, David W Miller, Gregory A Petsko, and Mark R Cookson. Mutations in pten-induced putative kinase 1 associated with recessive parkinsonism have differential effects on protein stability. *Proceedings of the National Academy of Sciences of the United States of America*, 102(16):5703–5708, 2005.

[38] Vincenzo Bonifati, Patrizia Rizzu, Marijke J van Baren, Onno Schaap, Guido J Breedveld, Elmar Krieger, Marieke CJ Dekker, Ferdinando Squitieri, Pablo Ibanez, Marijke Joosse, et al. Mutations in the dj-1 gene associated with autosomal recessive early-onset parkinsonism. *science*, 299(5604):256–259, 2003.

[39] Rina Bandopadhyay, Ann E Kingsbury, Mark R Cookson, Andrew R Reid, Ian M Evans, Andrew D Hope, Alan M Pittman, Tammaryn Lashley, Rosa Canet-Aviles,

David W Miller, et al. The expression of dj-1 (park7) in normal human cns and idiopathic parkinson's disease. *Brain*, 127(2):420–430, 2004.

[40] Takahiro Taira, Yoshiro Saito, Takeshi Niki, Sanae MM Iguchi-Ariga, Kazuhiko Takahashi, and Hiroyoshi Ariga. Dj-1 has a role in antioxidative stress to prevent cell death. *EMBO reports*, 5(2):213–218, 2004.

[41] Elisabeth Leroy, Rebecca Boyer, Georg Auburger, Barbara Leube, Gudrun Ulm, Eva Mezey, Gyongyi Harta, Michael J Brownstein, Sobhanadditya Jonnalagada, Tanya Chernova, et al. The ubiquitin pathway in parkinson's disease. *Nature*, 395(6701):451–452, 1998.

[42] B Sanjay Harhangi, Matthew J Farrer, Sarah Lincoln, Vincenzo Bonifati, Giuseppe Meco, Giuseppe De Michele, Alexis Brice, Alexandra Dürr, Maria Martinez, Thomas Gasser, et al. The ile93met mutation in the ubiquitin carboxy-terminal-hydrolase-l1 gene is not observed in european cases with familial parkinson's disease. *Neuroscience letters*, 270(1):1–4, 1999.

[43] Sarah Lincoln, Jenny Vaughan, Nick Wood, Matt Baker, Jennifer Adamson, Katrina Gwinn-Hardy, Tim Lynch, John Hardy, and Matt Farrer. Low frequency of pathogenic mutations in the ubiquitin carboxyterminal hydrolase gene in familial parkinson's disease. *Neuroreport*, 10(2):427–429, 1999.

[44] Keith D Wilkinson, KM Lee, Seema Deshpande, Penelope Duerksen-Hughes, Jeremy M Boss, and Jan Pohl. The neuron-specific protein pgp 9.5 is a ubiquitin carboxyl-terminal hydrolase. *Science*, 246(4930):670–673, 1989.

[45] Pablo Rodriguez-Viciana, Patricia H Warne, Asim Khwaja, Barbara M Marte, Darryl Pappin, Pamela Das, Michael D Waterfield, Anne Ridley, and Julian Downward. Role of phosphoinositide 3-oh kinase in cell transformation and control of the actin cytoskeleton by ras. *Cell*, 89(3):457–467, 1997.

[46] Manabu Funayama, Kazuko Hasegawa, Etsuro Ohta, Noriko Kawashima, Masaru Komiyama, Hisayuki Kowa, Shoji Tsuji, and Fumiya Obata. An lrrk2 mutation as a cause for the parkinsonism in the original park8 family. *Annals of neurology*, 57(6):918–921, 2005.

[47] Alexander Zimprich, Saskia Biskup, Petra Leitner, Peter Lichtner, Matthew Farrer, Sarah Lincoln, Jennifer Kachergus, Mary Hulihan, Ryan J Uitti, Donald B Calne, et al. Mutations in lrrk2 cause autosomal-dominant parkinsonism with pleomorphic pathology. *Neuron*, 44(4):601–607, 2004.

[48] Coro Paisàn-Ruìz, Amets Sàenz, Adolfo Lòpez de Munain, Itxaso Martì, Angel Martìnez Gil, Josè F Martì-Massò, and Jordi Pèrez-Tur. Familial parkinson's

disease: clinical and genetic analysis of four basque families. *Annals of neurology*, 57(3):365–372, 2005.

[49] Coro Paisán-Ruız, Shushant Jain, E Whitney Evans, William P Gilks, Javier Simón, Marcel van der Brug, Adolfo López de Munain, Silvia Aparicio, Angel Martınez Gil, Naheed Khan, et al. Cloning of the gene containing mutations that cause park8-linked parkinson's disease. *Neuron*, 44(4):595–600, 2004.

[50] Ignacio Marín. Ancient origin of the parkinson disease gene lrrk2. *Journal of molecular evolution*, 67(1):41–50, 2008.

[51] Leonard Bosgraaf and Peter JM Van Haastert. Roc, a ras/gtpase domain in complex proteins. *Biochimica et Biophysica Acta (BBA)-Molecular Cell Research*, 1643(1):5–10, 2003.

[52] Ignacio F Mata, William J Wedemeyer, Matthew J Farrer, Julie P Taylor, and Kathleen A Gallo. Lrrk2 in parkinson's disease: protein domains and functional insights. *Trends in neurosciences*, 29(5):286–293, 2006.

[53] Yoshimi Takai, Takuya Sasaki, and Takashi Matozaki. Small gtp-binding proteins. *Physiological reviews*, 81(1):153–208, 2001.

[54] Gerard Manning, David B Whyte, Ricardo Martinez, Tony Hunter, and Sucha Sudarsanam. The protein kinase complement of the human genome. *Science*, 298(5600):1912–1934, 2002.

[55] Gary L Johnson and Razvan Lapadat. Mitogen-activated protein kinase pathways mediated by erk, jnk, and p38 protein kinases. *Science*, 298(5600):1911–1912, 2002.

[56] Zejuan Sheng, Shuo Zhang, Daisy Bustos, Tracy Kleinheinz, Claire E Le Pichon, Sara L Dominguez, Hilda O Solanoy, Jason Drummond, Xiaolin Zhang, Xiao Ding, et al. Ser1292 autophosphorylation is an indicator of lrrk2 kinase activity and contributes to the cellular effects of pd mutations. *Science translational medicine*, 4(164):164ra161–164ra161, 2012.

[57] Andrew B West, Darren J Moore, Saskia Biskup, Artem Bugayenko, Wanli W Smith, Christopher A Ross, Valina L Dawson, and Ted M Dawson. Parkinson's disease-associated mutations in leucine-rich repeat kinase 2 augment kinase activity. *Proceedings of the National Academy of Sciences of the United States of America*, 102(46):16842–16847, 2005.

[58] Amardeep S Dhillon, Claire Pollock, Helge Steen, Peter E Shaw, Harald Mischak, and Walter Kolch. Cyclic amp-dependent kinase regulates raf-1 kinase mainly by

phosphorylation of serine 259. *Molecular and Cellular Biology*, 22(10):3237–3246, 2002.

[59] Paola Piccini, David J Burn, Roberto Ceravolo, Demetrius Maraganore, and David J Brooks. The role of inheritance in sporadic parkinson's disease: evidence from a longitudinal study of dopaminergic function in twins. *Annals of neurology*, 45(5):577–582, 1999.

[60] Darren J Moore, Andrew B West, Valina L Dawson, and Ted M Dawson. Molecular pathophysiology of parkinson's disease. *Annu. Rev. Neurosci.*, 28:57–87, 2005.

[61] Jie-Qiong Li, Lan Tan, and Jin-Tai Yu. The role of the lrrk2 gene in parkinsonism. *Molecular neurodegeneration*, 9(1):1–17, 2014.

[62] Vincenzo Bonifati. The lrrk2-g2019s mutation: opening a novel era in parkinson's disease genetics. *Eur J Hum Genet*, 14(10):1061–2, 2006.

[63] Udhaya Kumari and EK Tan. Lrrk2 in parkinson's disease: genetic and clinical studies from patients. *FEBS journal*, 276(22):6455–6463, 2009.

[64] Alessio Di Fonzo, Yah-Huei Wu-Chou, Chin-Song Lu, Marina van Doeselaar, Erik J Simons, Christan F Rohé, Hsiu-Chen Chang, Rou-Shayn Chen, Yi-Hsin Weng, Nicola Vanacore, et al. A common missense variant in the lrrk2 gene, gly2385arg, associated with parkinson's disease risk in taiwan. *Neurogenetics*, 7(3):133–138, 2006.

[65] Naheed L Khan, Shushant Jain, John M Lynch, Nicola Pavese, Patrick Abou-Sleiman, Janice L Holton, Daniel G Healy, William P Gilks, Mary G Sweeney, Milan Ganguly, et al. Mutations in the gene lrrk2 encoding dardarin (park8) cause familial parkinson's disease: clinical, pathological, olfactory and functional imaging and genetic data. *Brain*, 128(12):2786–2796, 2005.

[66] John R Adams, Hinke van Netten, Michael Schulzer, Edwin Mak, Jessamyn Mckenzie, Audrey Strongosky, Vesna Sossi, Thomas J Ruth, Chong S Lee, Matthew Farrer, et al. Pet in lrrk2 mutations: comparison to sporadic parkinson's disease and evidence for presymptomatic compensation. *Brain*, 128(12):2777–2785, 2005.

[67] Shamol Saha, Maria D Guillily, Andrew Ferree, Joel Lanceta, Diane Chan, Joy Ghosh, Cindy H Hsu, Lilach Segal, Kesav Raghavan, Kunihiro Matsumoto, et al. Lrrk2 modulates vulnerability to mitochondrial dysfunction in caenorhabditis elegans. *The Journal of Neuroscience*, 29(29):9210–9218, 2009.

[68] Benjamin Wolozin, Shamol Saha, Maria Guillily, Andrew Ferree, and Misha Riley. Investigating convergent actions of genes linked to familial parkinson's disease. *Neuro-degenerative diseases*, 5(3-4):182, 2008.

[69] Yanping Li, Wencheng Liu, Tinmarla F Oo, Lei Wang, Yi Tang, Vernice Jackson-Lewis, Chun Zhou, Kindiya Geghman, Mikhail Bogdanov, Serge Przedborski, et al. Mutant lrrk2r1441g bac transgenic mice recapitulate cardinal features of parkinson's disease. *Nature neuroscience*, 12(7):826–828, 2009.

[70] Xian Lin, Loukia Parisiadou, Xing-Long Gu, Lizhen Wang, Hoon Shim, Lixin Sun, Chengsong Xie, Cai-Xia Long, Wan-Jou Yang, Jinhui Ding, et al. Leucine-rich repeat kinase 2 regulates the progression of neuropathology induced by parkinson's-disease-related mutant α-synuclein. *Neuron*, 64(6):807–827, 2009.

[71] Mel B Feany and Welcome W Bender. A drosophila model of parkinson's disease. *Nature*, 404(6776):394–398, 2000.

[72] Zhaohui Liu, Xiaoyue Wang, YI Yu, Xueping Li, Tao Wang, Haibing Jiang, Qiuting Ren, Yuchen Jiao, Akira Sawa, Timothy Moran, et al. A drosophila model for lrrk2-linked parkinsonism. *Proceedings of the National Academy of Sciences*, 105(7):2693–2698, 2008.

[73] Chee-Hoe Ng, Shaun ZS Mok, Cherlyn Koh, Xuezhi Ouyang, Marc L Fivaz, Eng-King Tan, Valina L Dawson, Ted M Dawson, Fengwei Yu, and Kah-Leong Lim. Parkin protects against lrrk2 g2019s mutant-induced dopaminergic neurodegeneration in drosophila. *The Journal of Neuroscience*, 29(36):11257–11262, 2009.

[74] Katerina Venderova, Ghassan Kabbach, Elizabeth Abdel-Messih, Yi Zhang, Robin J Parks, Yuzuru Imai, Stephan Gehrke, Johnny Ngsee, Matthew J LaVoie, Ruth S Slack, et al. Leucine-rich repeat kinase 2 interacts with parkin, dj-1 and pink-1 in a drosophila melanogaster model of parkinson's disease. *Human Molecular Genetics*, 18(22):4390–4404, 2009.

[75] Andreas Mershin, Elias Pavlopoulos, Olivia Fitch, Brittany C Braden, Dimitri V Nanopoulos, and Efthimios MC Skoulakis. Learning and memory deficits upon tau accumulation in drosophila mushroom body neurons. *Learning & memory*, 11(3):277–287, 2004.

[76] Laura Torroja, Hsin Chu, Irina Kotovsky, and Kalpana White. Neuronal overexpression of appl, the drosophila homologue of the amyloid precursor protein (app), disrupts axonal transport. *Current Biology*, 9(9):489–493, 1999.

[77] Francisco A Perez and Richard D Palmiter. Parkin-deficient mice are not a robust model of parkinsonism. *Proceedings of the National Academy of Sciences of the United States of America*, 102(6):2174–2179, 2005.

[78] Sung Bae Lee, Wonho Kim, Sungkyu Lee, and Jongkyeong Chung. Loss of lrrk2/park8 induces degeneration of dopaminergic neurons in drosophila. *Biochemical and biophysical research communications*, 358(2):534–539, 2007.

[79] Andrea H Brand and Norbert Perrimon. Targeted gene expression as a means of altering cell fates and generating dominant phenotypes. *development*, 118(2):401–415, 1993.

[80] Donald G Gilbert. eugenes: a eukaryote genome information system. *Nucleic acids research*, 30(1):145–148, 2002.

[81] Julide Bilen and Nancy M Bonini. Drosophila as a model for human neurodegenerative disease. *Annu. Rev. Genet.*, 39:153–171, 2005.

[82] Bobby Thomas and M Flint Beal. Mitochondrial therapies for parkinson's disease. *Movement Disorders*, 25(S1):S155–S160, 2010.

[83] A Wood-Kaczmar, S Gandhi, and NW Wood. Understanding the molecular causes of parkinson's disease. *Trends in molecular medicine*, 12(11):521–528, 2006.

[84] Benjamin F Cravatt, Gabriel M Simon, and John R Yates Iii. The biological impact of mass-spectrometry-based proteomics. *Nature*, 450(7172):991–1000, 2007.

[85] Jürgen Cox and Matthias Mann. Is proteomics the new genomics? *Cell*, 130(3):395–398, 2007.

[86] Matthias Gstaiger and Ruedi Aebersold. Applying mass spectrometry-based proteomics to genetics, genomics and network biology. *Nature Reviews Genetics*, 10(9):617–627, 2009.

[87] Ruedi Aebersold and Matthias Mann. Mass spectrometry-based proteomics. *Nature*, 422(6928):198–207, 2003.

[88] Lyris MF de Godoy, Jesper V Olsen, Jürgen Cox, Michael L Nielsen, Nina C Hubner, Florian Fröhlich, Tobias C Walther, and Matthias Mann. Comprehensive mass-spectrometry-based proteome quantification of haploid versus diploid yeast. *Nature*, 455(7217):1251–1254, 2008.

[89] Nagarjuna Nagaraj, Jacek R Wisniewski, Tamar Geiger, Juergen Cox, Martin Kircher, Janet Kelso, Svante Pääbo, and Matthias Mann. Deep proteome and transcriptome mapping of a human cancer cell line. *Molecular systems biology*, 7(1):548, 2011.

[90] Chunaram Choudhary and Matthias Mann. Decoding signalling networks by mass spectrometry-based proteomics. *Nature reviews Molecular cell biology*, 11(6):427–439, 2010.

[91] Juri Rappsilber, Yasushi Ishihama, and Matthias Mann. Stop and go extraction tips for matrix-assisted laser desorption/ionization, nanoelectrospray, and lc/ms sample pretreatment in proteomics. *Analytical chemistry*, 75(3):663–670, 2003.

[92] Jesper V Olsen, Shao-En Ong, and Matthias Mann. Trypsin cleaves exclusively c-terminal to arginine and lysine residues. *Molecular & Cellular Proteomics*, 3(6):608–614, 2004.

[93] Jacek R Wiśniewski, Alexandre Zougman, Nagarjuna Nagaraj, and Matthias Mann. Universal sample preparation method for proteome analysis. *Nature methods*, 6(5):359–362, 2009.

[94] Suman S Thakur, Tamar Geiger, Bhaswati Chatterjee, Peter Bandilla, Florian Fröhlich, Juergen Cox, and Matthias Mann. Deep and highly sensitive proteome coverage by lc-ms/ms without prefractionation. *Molecular & Cellular Proteomics*, 10(8):M110–003699, 2011.

[95] James W Hager. A new linear ion trap mass spectrometer. *Rapid Communications in Mass Spectrometry*, 16(6):512–526, 2002.

[96] Y Oda, K Huang, FR Cross, D Cowburn, and BT Chait. Accurate quantitation of protein expression and site-specific phosphorylation. *Proceedings of the National Academy of Sciences*, 96(12):6591–6596, 1999.

[97] Shao-En Ong, Blagoy Blagoev, Irina Kratchmarova, Dan Bach Kristensen, Hanno Steen, Akhilesh Pandey, and Matthias Mann. Stable isotope labeling by amino acids in cell culture, silac, as a simple and accurate approach to expression proteomics. *Molecular & cellular proteomics*, 1(5):376–386, 2002.

[98] Kristoffer TG Rigbolt, Tatyana A Prokhorova, Vyacheslav Akimov, Jeanette Henningsen, Pia T Johansen, Irina Kratchmarova, Moustapha Kassem, Matthias Mann, Jesper V Olsen, and Blagoy Blagoev. System-wide temporal characterization of the proteome and phosphoproteome of human embryonic stem cell differentiation. *Science Signaling*, 4(164):rs3–rs3, 2011.

[99] Marcus Krüger, Markus Moser, Siegfried Ussar, Ingo Thievessen, Christian A Luber, Francesca Forner, Sarah Schmidt, Sara Zanivan, Reinhard Fässler, and Matthias Mann. Silac mouse for quantitative proteomics uncovers kindlin-3 as an essential factor for red blood cell function. *Cell*, 134(2):353–364, 2008.

[100] Matthias D Sury, Jia-Xuan X Chen, and Matthias Selbach. The silac fly allows for accurate protein quantification in vivo. *Molecular & Cellular Proteomics*, pages mcp–M110, 2010.

[101] Anne Konzer, Aaron Ruhs, Helene Braun, Benno Jungblut, Thomas Braun, and Marcus Krüger. Stable isotope labeling in zebrafish allows in vivo monitoring of cardiac morphogenesis. *Molecular & Cellular Proteomics*, 12(6):1502–1512, 2013.

[102] Shao-En Ong and Matthias Mann. Mass spectrometry–based proteomics turns quantitative. *Nature chemical biology*, 1(5):252–262, 2005.

[103] Christian A Luber, Jürgen Cox, Henning Lauterbach, Ben Fancke, Matthias Selbach, Jurg Tschopp, Shizuo Akira, Marian Wiegand, Hubertus Hochrein, Meredith O'Keeffe, et al. Quantitative proteomics reveals subset-specific viral recognition in dendritic cells. *Immunity*, 32(2):279–289, 2010.

[104] Jürgen Cox and Matthias Mann. Maxquant enables high peptide identification rates, individualized ppb-range mass accuracies and proteome-wide protein quantification. *Nature biotechnology*, 26(12):1367–1372, 2008.

[105] Joseph Schlessinger. Cell signaling by receptor tyrosine kinases. *Cell*, 103(2):211–225, 2000.

[106] Tony Hunter. Protein kinases and phosphatases: the yin and yang of protein phosphorylation and signaling. *Cell*, 80(2):225–236, 1995.

[107] Tony Pawson and John D Scott. Protein phosphorylation in signaling–50 years and counting. *Trends in biochemical sciences*, 30(6):286–290, 2005.

[108] Joerg Reinders and Albert Sickmann. State-of-the-art in phosphoproteomics. *Proteomics*, 5(16):4052–4061, 2005.

[109] Michelle T Barati, Madhavi J Rane, Jon B Klein, and Kenneth R McLeish. A proteomic screen identified stress-induced chaperone proteins as targets of akt phosphorylation in mesangial cells. *Journal of proteome research*, 5(7):1636–1646, 2006.

[110] Katrin Schmelzle, Susan Kane, Scott Gridley, Gustav E Lienhard, and Forest M White. Temporal dynamics of tyrosine phosphorylation in insulin signaling. *Diabetes*, 55(8):2171–2179, 2006.

[111] Scott B Ficarro, Mark L McCleland, P Todd Stukenberg, Daniel J Burke, Mark M Ross, Jeffrey Shabanowitz, Donald F Hunt, and Forest M White. Phosphoproteome analysis by mass spectrometry and its application to saccharomyces cerevisiae. *Nature biotechnology*, 20(3):301–305, 2002.

[112] Matthew C Posewitz and Paul Tempst. Immobilized gallium (iii) affinity chromatography of phosphopeptides. *Analytical Chemistry*, 71(14):2883–2892, 1999.

[113] Lennart Andersson and Jerker Porath. Isolation of phosphoproteins by immobilized metal (fe 3+) affinity chromatography. *Analytical biochemistry*, 154(1):250–254, 1986.

[114] Sean A Beausoleil, Mark Jedrychowski, Daniel Schwartz, Joshua E Elias, Judit Villén, Jiaxu Li, Martin A Cohn, Lewis C Cantley, and Steven P Gygi. Large-scale characterization of hela cell nuclear phosphoproteins. *Proceedings of the National Academy of Sciences of the United States of America*, 101(33):12130–12135, 2004.

[115] Masahiro Kawahara, Hiroshi Nakamura, and Terumi Nakajima. Titania and zirconia: possible new ceramic microparticulates for high-performance liquid chromatography. *Journal of Chromatography A*, 515:149–158, 1990.

[116] Martijn WH Pinkse, Pauliina M Uitto, Martijn J Hilhorst, Bert Ooms, and Albert JR Heck. Selective isolation at the femtomole level of phosphopeptides from proteolytic digests using 2d-nanolc-esi-ms/ms and titanium oxide precolumns. *Analytical chemistry*, 76(14):3935–3943, 2004.

[117] LI-RONG YU, THOMAS P CONRADS, and TIMOTHY D VEENSTRA. Mass spectrometry instrumentation. *Analytical Instrumentation Handbook*, page 429, 2004.

[118] John B Fenn, Matthias Mann, Chin Kai Meng, Shek Fu Wong, and Craig M Whitehouse. Electrospray ionization for mass spectrometry of large biomolecules. *Science*, 246(4926):64–71, 1989.

[119] Jürgen Cox and Matthias Mann. Computational principles of determining and improving mass precision and accuracy for proteome measurements in an orbitrap. *Journal of the American Society for Mass Spectrometry*, 20(8):1477–1485, 2009.

[120] Wolfgang Paul. Electromagnetic traps for charged and neutral particles (nobel lecture). *Angewandte Chemie International Edition in English*, 29(7):739–748, 1990.

[121] Ed Hoffmann and V Stroobant. Mass spectrometry: principles and applications 2007. *Ludwig Institute for Cancer Research, Brussels, Belgium*, 2007.

[122] Viveka Mayya, Karim Rezaul, Yu-Sheng Cong, and David Han. Systematic comparison of a two-dimensional ion trap and a three-dimensional ion trap mass spectrometer in proteomics. *Molecular & Cellular Proteomics*, 4(2):214–223, 2005.

[123] Jesper V Olsen, Jae C Schwartz, Jens Griep-Raming, Michael L Nielsen, Eugen Damoc, Eduard Denisov, Oliver Lange, Philip Remes, Dennis Taylor, Maurizio Splendore, et al. A dual pressure linear ion trap orbitrap instrument with very high sequencing speed. *Molecular & cellular proteomics*, 8(12):2759–2769, 2009.

[124] Tonya Pekar Second, Justin D Blethrow, Jae C Schwartz, Gennifer E Merrihew, Michael J MacCoss, Danielle L Swaney, Jason D Russell, Joshua J Coon, and Vlad Zabrouskov. Dual-pressure linear ion trap mass spectrometer improving the analysis of complex protein mixtures. *Analytical chemistry*, 81(18):7757–7765, 2009.

[125] Jae C Schwartz, Michael W Senko, and John EP Syka. A two-dimensional quadrupole ion trap mass spectrometer. *Journal of the American Society for Mass Spectrometry*, 13(6):659–669, 2002.

[126] Qizhi Hu, Robert J Noll, Hongyan Li, Alexander Makarov, Mark Hardman, and R Graham Cooks. The orbitrap: a new mass spectrometer. *Journal of mass spectrometry*, 40(4):430–443, 2005.

[127] Richard H Perry, R Graham Cooks, and Robert J Noll. Orbitrap mass spectrometry: instrumentation, ion motion and applications. *Mass spectrometry reviews*, 27(6):661–699, 2008.

[128] Alexander Makarov. Electrostatic axially harmonic orbital trapping: a high-performance technique of mass analysis. *Analytical chemistry*, 72(6):1156–1162, 2000.

[129] Michaela Scigelova and Alexander Makarov. Orbitrap mass analyzer–overview and applications in proteomics. *Proteomics*, 6(S2):16–21, 2006.

[130] Jesper V Olsen, Lyris MF de Godoy, Guoqing Li, Boris Macek, Peter Mortensen, Reinhold Pesch, Alexander Makarov, Oliver Lange, Stevan Horning, and Matthias Mann. Parts per million mass accuracy on an orbitrap mass spectrometer via lock mass injection into a c-trap. *Molecular & Cellular Proteomics*, 4(12):2010–2021, 2005.

[131] Annette Michalski, Eugen Damoc, Jan-Peter Hauschild, Oliver Lange, Andreas Wieghaus, Alexander Makarov, Nagarjuna Nagaraj, Juergen Cox, Matthias Mann, and Stevan Horning. Mass spectrometry-based proteomics using q exactive, a high-performance benchtop quadrupole orbitrap mass spectrometer. *Molecular & Cellular Proteomics*, 10(9):M111–011015, 2011.

[132] Tamar Geiger, Juergen Cox, and Matthias Mann. Proteomics on an orbitrap benchtop mass spectrometer using all-ion fragmentation. *Molecular & Cellular Proteomics*, 9(10):2252–2261, 2010.

[133] Cyrus P Zabetian, Mitsutoshi Yamamoto, Alexis N Lopez, Hiroshi Ujike, Ignacio F Mata, Yuishin Izumi, Ryuji Kaji, Hirofumi Maruyama, Hiroyuki Morino, Masaya Oda, et al. Lrrk2 mutations and risk variants in japanese patients with parkinson's disease. *Movement Disorders*, 24(7):1034–1041, 2009.

[134] Christian Johannes Gloeckner, Norbert Kinkl, Annette Schumacher, Ralf J Braun, Eric O'Neill, Thomas Meitinger, Walter Kolch, Holger Prokisch, and Marius Ueffing. The parkinson disease causing lrrk2 mutation i2020t is associated with increased kinase activity. *Human molecular genetics*, 15(2):223–232, 2006.

[135] Elisa Greggio, Shushant Jain, Ann Kingsbury, Rina Bandopadhyay, Patrick Lewis, Alice Kaganovich, Marcel P van der Brug, Alexandra Beilina, Jeff Blackinton, Kelly Jean Thomas, et al. Kinase activity is required for the toxic effects of mutant lrrk2/dardarin. *Neurobiology of disease*, 23(2):329–341, 2006.

[136] Danling Wang, Beisha Tang, Guohua Zhao, Qian Pan, Kun Xia, Rolf Bodmer, and Zhuohua Zhang. Dispensable role of drosophila ortholog of lrrk2 kinase activity in survival of dopaminergic neurons. *Mol Neurodegener*, 3(3):3, 2008.

[137] Barry Ganetzky and James R Flanagan. On the relationship between senescence and age-related changes in two wild-type strains of drosophila melanogaster. *Experimental gerontology*, 13(3):189–196, 1978.

[138] Eric Le Bourg and Frédéric A Lints. Hypergravity and aging in drosophila melanogaster. 4. climbing activity. *Gerontology*, 38(1-2):59–64, 1992.

[139] Owen A Ross, Mathias Toft, Andrew J Whittle, Joseph L Johnson, Spiridon Papapetropoulos, Deborah C Mash, Irene Litvan, Mark F Gordon, Zbigniew K Wszolek, Matthew J Farrer, et al. Lrrk2 and lewy body disease. *Annals of neurology*, 59(2):388–393, 2006.

[140] Florence Friggi-Grelin, Hélène Coulom, Margaret Meller, Delphine Gomez, Jay Hirsh, and Serge Birman. Targeted gene expression in drosophila dopaminergic cells using regulatory sequences from tyrosine hydroxylase. *Journal of neurobiology*, 54(4):618–627, 2003.

[141] Anathbandhu Chaudhuri, Kevin Bowling, Christopher Funderburk, Hakeem Lawal, Arati Inamdar, Zhe Wang, and Janis M O'Donnell. Interaction of genetic and environmental factors in a drosophila parkinsonism model. *The Journal of neuroscience*, 27(10):2457–2467, 2007.

[142] Joy S Wu and Liqun Luo. A protocol for dissecting drosophila melanogaster brains for live imaging or immunostaining. *Nature protocols*, 1(4):2110–2115, 2006.

[143] Earle Stone, Kent J Gillig, Brandon Ruotolo, Katrin Fuhrer, Marc Gonin, Albert Schultz, and David H Russell. Surface-induced dissociation on a maldi-ion mobility-orthogonal time-of-flight mass spectrometer: sequencing peptides from an "in-solution" protein digest. *Analytical chemistry*, 73(10):2233–2238, 2001.

[144] Andrej Shevchenko, Henrik Tomas, Jan Havli, Jesper V Olsen, and Matthias Mann. In-gel digestion for mass spectrometric characterization of proteins and proteomes. *Nature protocols*, 1(6):2856–2860, 2006.

[145] Jurgen Cox, Nadin Neuhauser, Annette Michalski, Richard A Scheltema, Jesper V Olsen, and Matthias Mann. Andromeda: a peptide search engine integrated into the maxquant environment. *Journal of proteome research*, 10(4):1794–1805, 2011.

[146] Jesper V Olsen, Blagoy Blagoev, Florian Gnad, Boris Macek, Chanchal Kumar, Peter Mortensen, and Matthias Mann. Global, in vivo, and site-specific phosphorylation dynamics in signaling networks. *Cell*, 127(3):635–648, 2006.

[147] Hendrik Nolte, Anne Konzer, Aaron Ruhs, Benno Jungblut, Thomas Braun, and Marcus Kruger. Global protein expression profiling of zebrafish organs based on in vivo incorporation of stable isotopes. *Journal of proteome research*, 13(4):2162–2174, 2014.

[148] Damian Szklarczyk, Andrea Franceschini, Michael Kuhn, Milan Simonovic, Alexander Roth, Pablo Minguez, Tobias Doerks, Manuel Stark, Jean Muller, Peer Bork, et al. The string database in 2011: functional interaction networks of proteins, globally integrated and scored. *Nucleic acids research*, 39(suppl 1):D561–D568, 2011.

[149] Michael Ashburner, Catherine A Ball, Judith A Blake, David Botstein, Heather Butler, J Michael Cherry, Allan P Davis, Kara Dolinski, Selina S Dwight, Janan T Eppig, et al. Gene ontology: tool for the unification of biology. *Nature genetics*, 25(1):25–29, 2000.

[150] Eran Eden, Roy Navon, Israel Steinfeld, Doron Lipson, and Zohar Yakhini. Gorilla: a tool for discovery and visualization of enriched go terms in ranked gene lists. *BMC bioinformatics*, 10(1):48, 2009.

[151] Huaiyu Mi, Anushya Muruganujan, John T Casagrande, and Paul D Thomas. Large-scale gene function analysis with the panther classification system. *Nature protocols*, 8(8):1551–1566, 2013.

[152] Corey Laverty, Fang Li, Esther J Belikoff, and Maxwell J Scott. Abnormal dosage compensation of reporter genes driven by the drosophila glass multiple reporter (gmr) enhancer-promoter. *PloS one*, 6(5):e20455, 2011.

[153] Stephen J Kish, Kathleen Shannak, and Oleh Hornykiewicz. Uneven pattern of dopamine loss in the striatum of patients with idiopathic parkinson's disease. *New England Journal of Medicine*, 318(14):876–880, 1988.

[154] Zhengmei Mao and Ronald L Davis. Eight different types of dopaminergic neurons innervate the drosophila mushroom body neuropil: anatomical and physiological heterogeneity. *Frontiers in neural circuits*, 3, 2009.

[155] Dennis Van Hoof, Martijn WH Pinkse, Dorien Ward-Van Oostwaard, Christine L Mummery, Albert JR Heck, and Jeroen Krijgsveld. An experimental correction for arginine-to-proline conversion artifacts in silac-based quantitative proteomics. *Nature methods*, 4(9):677–678, 2007.

[156] Juergen Cox and Matthias Mann. 1d and 2d annotation enrichment: a statistical method integrating quantitative proteomics with complementary high-throughput data. *BMC bioinformatics*, 13(Suppl 16):S12, 2012.

[157] Yikang S Rong and Kent G Golic. A targeted gene knockout in drosophila. *Genetics*, 157(3):1307–1312, 2001.

[158] Clemens R Scherzer, Roderick V Jensen, Steven R Gullans, and Mel B Feany. Gene expression changes presage neurodegeneration in a drosophila model of parkinson's disease. *Human molecular genetics*, 12(19):2457–2466, 2003.

[159] Julian R Hughes, Ana M Meireles, Katherine H Fisher, Angel Garcia, Philip R Antrobus, Alan Wainman, Nicole Zitzmann, Charlotte Deane, Hiroyuki Ohkura, and James G Wakefield. A microtubule interactome: complexes with roles in cell cycle and mitosis. *PLoS biology*, 6(4):e98, 2008.

[160] Loukia Parisiadou and Huaibin Cai. Lrrk2 function on actin and microtubule dynamics in parkinson's disease. *Communicative & integrative biology*, 3(5):396–400, 2010.

[161] Andrea Meixner, Karsten Boldt, Marleen Van Troys, Manor Askenazi, Christian J Gloeckner, Matthias Bauer, Jarrod A Marto, Christophe Ampe, Norbert Kinkl, and Marius Ueffing. A quick screen for lrrk2 interaction partners–leucine-rich repeat kinase 2 is involved in actin cytoskeleton dynamics. *Molecular & Cellular Proteomics*, 10(1):M110–001172, 2011.

[162] Zhiyin Xun, Renã A Sowell, Thomas C Kaufman, and David E Clemmer. Protein expression in a drosophila model of parkinson's disease. *Journal of proteome research*, 6(1):348–357, 2006.

[163] Zhiyin Xun, Rena A Sowell, Thomas C Kaufman, and David E Clemmer. Lifetime proteomic profiling of an a30p α-synuclein drosophila model of parkinson's disease. *Journal of proteome research*, 6(9):3729–3738, 2007.

[164] Alexander J Whitworth, Dorothy A Theodore, Jessica C Greene, Helen Beneš, Paul D Wes, and Leo J Pallanck. Increased glutathione s-transferase activity rescues dopaminergic neuron loss in a drosophila model of parkinson's disease. *Proceedings of the National Academy of Sciences*, 102(22):8024–8029, 2005.

[165] Houbo Jiang, Yong Ren, Jinghui Zhao, and Jian Feng. Parkin protects human dopaminergic neuroblastoma cells against dopamine-induced apoptosis. *Human molecular genetics*, 13(16):1745–1754, 2004.

[166] John D Hayes, Jack U Flanagan, and Ian R Jowsey. Glutathione transferases. *Annu. Rev. Pharmacol. Toxicol.*, 45:51–88, 2005.

[167] Srinivas Bharath, Michael Hsu, Deepinder Kaur, Subramanian Rajagopalan, and Julie K Andersen. Glutathione, iron and parkinson's disease. *Biochemical pharmacology*, 64(5):1037–1048, 2002.

[168] AHV Schapira, JM Cooper, D Dexter, JB Clark, P Jenner, and CD Marsden. Mitochondrial complex i deficiency in parkinson's disease. *Journal of neurochemistry*, 54(3):823–827, 1990.

[169] Manuela Basso, Sabrina Giraudo, Davide Corpillo, Bruno Bergamasco, Leonardo Lopiano, and Mauro Fasano. Proteome analysis of human substantia nigra in parkinson's disease. *Proteomics*, 4(12):3943–3952, 2004.

[170] Richard Lathe and Alyson Harris. Differential display detects host nucleic acid motifs altered in scrapie-infected brain. *Journal of molecular biology*, 392(3):813–822, 2009.

[171] Alysson R Muotri, Maria CN Marchetto, Nicole G Coufal, Ruth Oefner, Gene Yeo, Kinichi Nakashima, and Fred H Gage. L1 retrotransposition in neurons is modulated by mecp2. *Nature*, 468(7322):443–446, 2010.

[172] Renée Douville, Jiankai Liu, Jeffrey Rothstein, and Avindra Nath. Identification of active loci of a human endogenous retrovirus in neurons of patients with amyotrophic lateral sclerosis. *Annals of neurology*, 69(1):141–151, 2011.

[173] Alysson R Muotri, Vi T Chu, Maria CN Marchetto, Wei Deng, John V Moran, and Fred H Gage. Somatic mosaicism in neuronal precursor cells mediated by l1 retrotransposition. *nature*, 435(7044):903–910, 2005.

[174] Nicole G Coufal, José L Garcia-Perez, Grace E Peng, Gene W Yeo, Yangling Mu, Michael T Lovci, Maria Morell, K Sue O'Shea, John V Moran, and Fred H Gage. L1 retrotransposition in human neural progenitor cells. *Nature*, 460(7259):1127–1131, 2009.

[175] J Kenneth Baillie, Mark W Barnett, Kyle R Upton, Daniel J Gerhardt, Todd A Richmond, Fioravante De Sapio, Paul M Brennan, Patrizia Rizzu, Sarah Smith, Mark Fell, et al. Somatic retrotransposition alters the genetic landscape of the human brain. *Nature*, 479(7374):534–537, 2011.

[176] Fintan R Steele, Tracy Washburn, Rose Rieger, and JE O'tousa. Drosophila retinal degeneration c (rdgc) encodes a novel serine/threonine protein phosphatase. *Cell*, 69(4):669–676, 1992.

[177] Fintan Steele and Joseph E O'Tousa. Rhodopsin activation causes retinal degeneration in drosophila rdgc mutant. *Neuron*, 4(6):883–890, 1990.

[178] Jonathan Pevsner, Shu-Chan Hsu, Janice EA Braun, Nicole Calakos, Anthony E Ting, Mark K Bennett, and Richard H Scheller. Specificity and regulation of a synaptic vesicle docking complex. *Neuron*, 13(2):353–361, 1994.

[179] Kendal Broadie, Andreas Prokop, Hugo J Bellen, Cahir J O'Kane, Karen L Schulze, and Sean T Sweeney. Syntaxin and synaptobrevin function downstream of vesicle docking in drosophila. *Neuron*, 15(3):663–673, 1995.

[180] Yoshi Kidokoro. Roles of snare proteins and synaptotagmin i in synaptic transmission: studies at the drosophila neuromuscular synapse. *Neurosignals*, 12(1):13–30, 2003.

[181] William P Gilks, Patrick M Abou-Sleiman, Sonia Gandhi, Shushant Jain, Andrew Singleton, Andrew J Lees, Karen Shaw, Kailash P Bhatia, Vincenzo Bonifati, Niall P Quinn, et al. A common lrrk2 mutation in idiopathic parkinson's disease. *The Lancet*, 365(9457):415–416, 2005.

[182] Kebin Zeng, Xuefeng Wang, Yurong Wang, and Yong Yan. Enhanced synaptic vesicle traffic in hippocampus of phenytoin-resistant kindled rats. *Neurochemical research*, 34(5):899–904, 2009.

[183] Gordana Glavan, Reinhard Schliebs, and Marko Živin. Synaptotagmins in neurodegeneration. *The Anatomical Record*, 292(12):1849–1862, 2009.

[184] Youren Tong, Antonio Pisani, Giuseppina Martella, Maha Karouani, Hiroo Yamaguchi, Emmanuel N Pothos, and Jie Shen. R1441c mutation in lrrk2 impairs dopaminergic neurotransmission in mice. *Proceedings of the National Academy of Sciences*, 106(34):14622–14627, 2009.

[185] Nenad Blau, Luisa Bonafé, and Beat Thöny. Tetrahydrobiopterin deficiencies without hyperphenylalaninemia: diagnosis and genetics of dopa-responsive dystonia and sepiapterin reductase deficiency. *Molecular genetics and metabolism*, 74(1):172–185, 2001.

[186] W Lovenberg, RA Levine, DS Robinson, M Ebert, AC Williams, and DB Calne. Hydroxylase cofactor activity in cerebrospinal fluid of normal subjects and patients with parkinson's disease. *Science*, 204(4393):624–626, 1979.

[187] Stefanie Wagner, Christiane Heseding, Kamila Szlachta, John R True, Heino Prinz, and Bernhard T Hovemann. Drosophila photoreceptors express cysteine peptidase tan. *Journal of Comparative Neurology*, 500(4):601–611, 2007.

[188] John R True, Shu-Dan Yeh, Bernhard T Hovemann, Tobias Kemme, Ian A Meinertzhagen, Tara N Edwards, Shian-Ren Liou, Qian Han, and Jianyong Li. Drosophila tan encodes a novel hydrolase required in pigmentation and vision. *Plos Genet*, 2005.

[189] Robert J Kittel, Carolin Wichmann, Tobias M Rasse, Wernher Fouquet, Manuela Schmidt, Andreas Schmid, Dhananjay A Wagh, Christian Pawlu, Robert R Kellner, Katrin I Willig, et al. Bruchpilot promotes active zone assembly, ca2+ channel clustering, and vesicle release. *Science*, 312(5776):1051–1054, 2006.

[190] Daria S Hekmat-Scafe, Charles R Scafe, Aimee J McKinney, and Mark A Tanouye. Genome-wide analysis of the odorant-binding protein gene family in drosophila melanogaster. *Genome research*, 12(9):1357–1369, 2002.

[191] Mary C Beckerle, Keith Burridge, George N DeMartino, and Dorothy E Croall. Colocalization of calcium-dependent protease ii and one of its substrates at sites of cell adhesion. *Cell*, 51(4):569–577, 1987.

[192] AS Harris, DE Croall, and Jon S Morrow. Calmodulin regulates fodrin susceptibility to cleavage by calcium-dependent protease i. *Journal of Biological Chemistry*, 264(29):17401–17408, 1989.

[193] D Lanneau, M Brunet, E Frisan, E Solary, M Fontenay, and C Garrido. Heat shock proteins: essential proteins for apoptosis regulation. *Journal of cellular and molecular medicine*, 12(3):743–761, 2008.

[194] Cindy Voisine, Jesper Søndergaard Pedersen, and Richard I Morimoto. Chaperone networks: tipping the balance in protein folding diseases. *Neurobiology of disease*, 40(1):12–20, 2010.

[195] Pin-Chao Liao, Hung-Yu Lin, Chiou-Hwa Yuh, Lin-Kwei Yu, and Horng-Dar Wang. The effect of neuronal expression of heat shock proteins 26 and 27 on lifespan, neurodegeneration, and apoptosis in drosophila. *Biochemical and biophysical research communications*, 376(4):637–641, 2008.

[196] Horng-Dar Wang, Parsa Kazemi-Esfarjani, and Seymour Benzer. Multiple-stress analysis for isolation of drosophila longevity genes. *Proceedings of the National Academy of Sciences of the United States of America*, 101(34):12610–12615, 2004.

[197] Andreas Wyttenbach, Olivier Sauvageot, Jenny Carmichael, Chantal Diaz-Latoud, Andre-Patrik Arrigo, and David C Rubinsztein. Heat shock protein 27 prevents cellular polyglutamine toxicity and suppresses the increase of reactive oxygen species caused by huntingtin. *Human molecular genetics*, 11(9):1137–1151, 2002.

[198] Kevin P Campbell. Three muscular dystrophies: loss of cytoskeleton-extracellular matrix linkage. *Cell*, 80(5):675–679, 1995.

[199] Ronald D Cohn and Kevin P Campbell. Molecular basis of muscular dystrophies. *Muscle & nerve*, 23(10):1456–1471, 2000.

[200] Daniel E Michele, Rita Barresi, Motoi Kanagawa, Fumiaki Saito, Ronald D Cohn, Jakob S Satz, James Dollar, Ichizo Nishino, Richard I Kelley, Hannu Somer, et al. Post-translational disruption of dystroglycan–ligand interactions in congenital muscular dystrophies. *Nature*, 418(6896):417–421, 2002.

[201] Seongsoo Lee, Sungdae Kim, Minyeop Nahm, Euijae Kim, Tai-Il Kim, Jin Ho Yoon, and Seungbok Lee. The phosphoinositide phosphatase sac1 is required for midline axon guidance. *Molecules and cells*, 32(5):477–482, 2011.

[202] Gilbert Di Paolo and Pietro De Camilli. Phosphoinositides in cell regulation and membrane dynamics. *Nature*, 443(7112):651–657, 2006.

[203] Stuart Forrest, Andrea Chai, Mario Sanhueza, Manuela Marescotti, Katherine Parry, Atanas Georgiev, Virender Sahota, Raquel Mendez-Castro, and Giuseppa Pennetta. Increased levels of phosphoinositides cause neurodegeneration in a drosophila model of amyotrophic lateral sclerosis. *Human molecular genetics*, page ddt118, 2013.

[204] Christoph Gruenewald, Jose A Botella, Florian Bayersdorfer, Juan A Navarro, and Stephan Schneuwly. Hyperoxia-induced neurodegeneration as a tool to identify neuroprotective genes in drosophila melanogaster. *Free radical biology and medicine*, 46(12):1668–1676, 2009.

[205] MD Ferrari, EAJ Peeters, J Haan, RAC Roos, P Vermey, FA De Wolff, and OJS Buruma. Cytochrome p450 and parkinson's disease: Poor parahydroxylation of phenytoin. *Journal of the neurological sciences*, 96(2):153–157, 1990.

[206] Mary Beth Davis and Ross J MacIntyre. A genetic analysis of the alpha-glycerophosphate oxidase locus in drosophila melanogaster. *Genetics*, 120(3):755–766, 1988.

[207] Irene A Aligianis, Colin A Johnson, Paul Gissen, Dongrong Chen, Daniel Hampshire, Katrin Hoffmann, Esther N Maina, Neil V Morgan, Louise Tee, Jenny Morton, et al. Mutations of the catalytic subunit of rab3gap cause warburg micro syndrome. *Nature genetics*, 37(3):221–224, 2005.

[208] Kristien Verhoeven, Peter De Jonghe, Katrien Coen, Nathalie Verpoorten, Michaela Auer-Grumbach, Jennifer M Kwon, David FitzPatrick, Eric Schmedding, Els De Vriendt, An Jacobs, et al. Mutations in the small gtp-ase late endosomal protein rab7 cause charcot-marie-tooth type 2b neuropathy. *The American Journal of Human Genetics*, 72(3):722–727, 2003.

[209] Shreya Mitra, Kwai W Cheng, and Gordon B Mills. Rab gtpases implicated in inherited and acquired disorders. In *Seminars in cell & developmental biology*, volume 22, pages 57–68. Elsevier, 2011.

[210] Gaël Ménasché, Elodie Pastural, Jérôme Feldmann, Stéphanie Certain, Fügen Ersoy, Sophie Dupuis, Nico Wulffraat, Diana Bianchi, Alain Fischer, Françoise Le Deist, et al. Mutations in rab27a cause griscelli syndrome associated with haemophagocytic syndrome. *Nature genetics*, 25(2):173–176, 2000.

[211] Martin R Larsen, Tine E Thingholm, Ole N Jensen, Peter Roepstorff, and Thomas JD Jørgensen. Highly selective enrichment of phosphorylated peptides from peptide mixtures using titanium dioxide microcolumns. *Molecular & Cellular Proteomics*, 4(7):873–886, 2005.

[212] Seongsoo Lee, Hsin-Ping Liu, Wei-Yong Lin, Huifu Guo, and Bingwei Lu. Lrrk2 kinase regulates synaptic morphology through distinct substrates at the presynaptic and postsynaptic compartments of the drosophila neuromuscular junction. *The Journal of Neuroscience*, 30(50):16959–16969, 2010.

[213] Peter S McPherson, Elizabeth P Garcia, Vladimir I Slepnev, Carol David, Xiaomei Zhang, Detlev Grabs, Wayne S Sossini, Rudolf Bauerfeind, Yasuo Nemoto, and Pietro De Camilli. A presynaptic inositol-5-phosphatase. *Nature*, 1996.

[214] Giovanni Esposito, Fernandes Ana Clara, and Patrik Verstreken. Synaptic vesicle trafficking and parkinson's disease. *Developmental neurobiology*, 72(1):134–144, 2012.

[215] Marialuisa Quadri, Mingyan Fang, Marina Picillo, Simone Olgiati, Guido J Breedveld, Josja Graafland, Bin Wu, Fengping Xu, Roberto Erro, Marianna Amboni, et al. Mutation in the synj1 gene associated with autosomal recessive, early-onset parkinsonism. *Human mutation*, 34(9):1208–1215, 2013.

[216] Noah Dephoure, Chunshui Zhou, Judit Villén, Sean A Beausoleil, Corey E Bakalarski, Stephen J Elledge, and Steven P Gygi. A quantitative atlas of mitotic phosphorylation. *Proceedings of the National Academy of Sciences*, 105(31):10762–10767, 2008.

[217] Alicia Lundby, Anna Secher, Kasper Lage, Nikolai B Nordsborg, Anatoliy Dmytriyev, Carsten Lundby, and Jesper V Olsen. Quantitative maps of protein phosphorylation sites across 14 different rat organs and tissues. *Nature communications*, 3:876, 2012.

[218] Saurabh Sen, Philip J Webber, and Andrew B West. Dependence of leucine-rich repeat kinase 2 (lrrk2) kinase activity on dimerization. *Journal of Biological Chemistry*, 284(52):36346–36356, 2009.

[219] Elisa Greggio and Mark R Cookson. Leucine-rich repeat kinase 2 mutations and parkinson's disease: three questions. *ASN neuro*, 1(1):AN20090007, 2009.

[220] Samer Matta, Kristof Van Kolen, Raquel da Cunha, Geert van den Bogaart, Wim Mandemakers, Katarzyna Miskiewicz, Pieter-Jan De Bock, Vanessa A Morais, Sven Vilain, Dominik Haddad, et al. Lrrk2 controls an endoa phosphorylation cycle in synaptic endocytosis. *Neuron*, 75(6):1008–1021, 2012.

[221] Amaia M Arranz, Lore Delbroek, Kristof Van Kolen, Marco R Guimarães, Wim Mandemakers, Guy Daneels, Samer Matta, Sara Calafate, Hamdy Shaban, Pieter Baatsen, et al. Lrrk2 functions in synaptic vesicle endocytosis through a kinase-dependent mechanism. *Journal of cell science*, 128(3):541–552, 2015.

[222] Klodjan Stafa, Elpida Tsika, Roger Moser, Alessandra Musso, Liliane Glauser, Amy Jones, Saskia Biskup, Yulan Xiong, Rina Bandopadhyay, Valina L Dawson, et al. Functional interaction of parkinson's disease-associated lrrk2 with members of the dynamin gtpase superfamily. *Human molecular genetics*, page ddt600, 2013.

[223] Michael S Pollanen, Dennis W Dickson, and Catherine Bergeron. Pathology and biology of the lewy body. *Journal of Neuropathology & Experimental Neurology*, 52(3):183–191, 1993.

[224] Tzu-Kang Sang, Hui-Yun Chang, George M Lawless, Anuradha Ratnaparkhi, Lisa Mee, Larry C Ackerson, Nigel T Maidment, David E Krantz, and George R Jackson. A drosophila model of mutant human parkin-induced toxicity demonstrates selective loss of dopaminergic neurons and dependence on cellular dopamine. *The Journal of neuroscience*, 27(5):981–992, 2007.

[225] Lizhen Wang, Chengsong Xie, Elisa Greggio, Loukia Parisiadou, Hoon Shim, Lixin Sun, Jayanth Chandran, Xian Lin, Chen Lai, Wan-Jou Yang, et al. The chaperone activity of heat shock protein 90 is critical for maintaining the stability of leucine-rich repeat kinase 2. *The Journal of Neuroscience*, 28(13):3384–3391, 2008.

[226] Kazuhiko Kume, Shoen Kume, Sang Ki Park, Jay Hirsh, and F Rob Jackson. Dopamine is a regulator of arousal in the fruit fly. *The Journal of neuroscience*, 25(32):7377–7384, 2005.

[227] N Rudenko Iakov, Kaganovich Alice, N Hauser David, Beylina Aleksandra, Chia Ruth, Ding Jinhui, Maric Dragan, Jaffe Howard, and R Cookson Mark. The g2385r variant of leucine-rich repeat kinase 2 associated with parkinson's disease is a partial loss-of-function mutation. *Biochemical Journal*, 446(1):99–111, 2012.

[228] Samantha Hindle, Farinaz Afsari, Meg Stark, C Adam Middleton, Gareth JO Evans, Sean T Sweeney, and Christopher JH Elliott. Dopaminergic expression of the parkinsonian gene lrrk2-g2019s leads to non-autonomous visual neurodegeneration, accelerated by increased neural demands for energy. *Human molecular genetics*, 22(11):2129–2140, 2013.

[229] Benoit I Giasson, Jason P Covy, Nancy M Bonini, Howard I Hurtig, Matthew J Farrer, John Q Trojanowski, and Vivianna M Van Deerlin. Biochemical and pathological characterization of lrrk2. *Annals of neurology*, 59(2):315–322, 2006.

[230] DC Wallace, JM Shoffner, RL Watts, JL Juncos, and Antonio Torroni. Mitochondrial oxidative phosphorylation defects in parkinson's disease. *Annals of neurology*, 32(1):113–114, 1992.

[231] Gary Meyer and Eva L Feldman. Signaling mechanisms that regulate actin-based motility processes in the nervous system. *Journal of neurochemistry*, 83(3):490–503, 2002.

[232] Ryoki Ishikawa and Kazuhiro Kohama. Actin-binding proteins in nerve cell growth cones. *Journal of pharmacological sciences*, 105(1):6–11, 2007.

[233] David MacLeod, Julia Dowman, Rachel Hammond, Thomas Leete, Keiichi Inoue, and Asa Abeliovich. The familial parkinsonism gene lrrk2 regulates neurite process morphology. *neuron*, 52(4):587–593, 2006.

[234] Mahaboobi Jaleel, R Nichols, Maria Deak, D Campbell, Frank Gillardon, Axel Knebel, and D Alessi. Lrrk2 phosphorylates moesin at threonine-558: characterization of how parkinson's disease mutants affect kinase activity. *Biochem. J*, 405:307–317, 2007.

[235] Tudor A Fulga, Ilan Elson-Schwab, Vikram Khurana, Michelle L Steinhilb, Tara L Spires, Bradley T Hyman, and Mel B Feany. Abnormal bundling and accumulation of f-actin mediates tau-induced neuronal degeneration in vivo. *Nature Cell Biology*, 9(2):139–148, 2007.

[236] Heather Mortiboys, Krisztina K Johansen, Jan O Aasly, and Oliver Bandmann. Mitochondrial impairment in patients with parkinson disease with the g2019s mutation in lrrk2. *Neurology*, 75(22):2017–2020, 2010.

[237] Xinglong Wang, Michael H Yan, Hisashi Fujioka, Jun Liu, Amy Wilson-Delfosse, Shu G Chen, George Perry, Gemma Casadesus, and Xiongwei Zhu. Lrrk2 regulates mitochondrial dynamics and function through direct interaction with dlp1. *Human molecular genetics*, 21(9):1931–1944, 2012.

[238] David Attwell and Simon B Laughlin. An energy budget for signaling in the grey matter of the brain. *Journal of Cerebral Blood Flow & Metabolism*, 21(10):1133–1145, 2001.

[239] Rossana Migheli, Maria Grazia Del Giudice, Ylenia Spissu, Giovanna Sanna, Yulan Xiong, Ted M Dawson, Valina L Dawson, Manuela Galioto, Gaia Rocchitta, Alice Biosa, et al. Lrrk2 affects vesicle trafficking, neurotransmitter extracellular level and membrane receptor localization. *PloS one*, 8(10):e77198, 2013.

[240] Mark N Wu, Tim Fergestad, Thomas E Lloyd, Yuchun He, Kendal Broadie, and Hugo J Bellen. Syntaxin 1a interacts with multiple exocytic proteins to regulate neurotransmitter release in vivo. *Neuron*, 23(3):593–605, 1999.

[241] Roy RL Gerona, Eric C Larsen, Judith A Kowalchyk, and Thomas FJ Martin. The c terminus of snap25 is essential for ca2+-dependent binding of synaptotagmin to snare complexes. *Journal of Biological Chemistry*, 275(9):6328–6336, 2000.

[242] Shuzo Sugita and Thomas C Südhof. Specificity of ca2+-dependent protein interactions mediated by the c2a domains of synaptotagmins. *Biochemistry*, 39(11):2940–2949, 2000.

[243] Yulan Xiong, Candice E Coombes, Austin Kilaru, Xiaojie Li, Aaron D Gitler, William J Bowers, Valina L Dawson, Ted M Dawson, and Darren J Moore. Gtpase activity plays a key role in the pathobiology of lrrk2. 2010.

[244] Giovanni Piccoli, Steven B Condliffe, Matthias Bauer, Florian Giesert, Karsten Boldt, Silvia De Astis, Andrea Meixner, Hakan Sarioglu, Daniela M Vogt-Weisenhorn, Wolfgang Wurst, et al. Lrrk2 controls synaptic vesicle storage and mobilization within the recycling pool. *The Journal of Neuroscience*, 31(6):2225–2237, 2011.

[245] J William Langston, Philip Ballard, James W Tetrud, and Ian Irwin. Chronic parkinsonism in humans due to a product of meperidine-analog synthesis. *Science*, 219(4587):979–980, 1983.

[246] Hélène Coulom and Serge Birman. Chronic exposure to rotenone models sporadic parkinson's disease in drosophila melanogaster. *The Journal of neuroscience*, 24(48):10993–10998, 2004.

[247] Genta Ito, Takuro Okai, GO Fujino, Kohsuke Takeda, Hidenori Ichijo, Toshiaki Katada, and Takeshi Iwatsubo. Gtp binding is essential to the protein kinase activity of lrrk2, a causative gene product for familial parkinson's disease. *Biochemistry*, 46(5):1380–1388, 2007.

[248] Andrew B West, Darren J Moore, Catherine Choi, Shaida A Andrabi, Xiaojie Li, Dustin Dikeman, Saskia Biskup, Zhenshui Zhang, Kah-Leong Lim, Valina L Dawson, et al. Parkinson's disease-associated mutations in lrrk2 link enhanced gtp-binding and kinase activities to neuronal toxicity. *Human molecular genetics*, 16(2):223–232, 2007.

[249] Pooja P Pungaliya, Yuchen Bai, Kerri Lipinski, Vasanti S Anand, Saurabh Sen, Eugene L Brown, Brian Bates, Peter H Reinhart, Andrew B West, Warren D Hirst, et al. Identification and characterization of a leucine-rich repeat kinase 2 (lrrk2) consensus phosphorylation motif. *PLoS One*, 5(10):e13672–e13672, 2010.

[250] Yong Q Zhang, Adina M Bailey, Heinrich JG Matthies, Robert B Renden, Mark A Smith, Sean D Speese, Gerald M Rubin, and Kendal Broadie. Drosophila fragile x-related gene regulates the map1b homolog futsch to control synaptic structure and function. *Cell*, 107(5):591–603, 2001.

[251] Nick Trotta, Genny Orso, Maria Giovanna Rossetto, Andrea Daga, and Kendal Broadie. The hereditary spastic paraplegia gene, spastin, regulates microtubule stability to modulate synaptic structure and function. *Current biology*, 14(13):1135–1147, 2004.

[252] Simon Lepicard, Bénédicte Franco, Frédéric de Bock, and Marie-Laure Parmentier. A presynaptic role of microtubule-associated protein 1/futsch in drosophila: regulation of active zone number and neurotransmitter release. *The Journal of Neuroscience*, 34(20):6759–6771, 2014.

[253] Fabio Benfenati, Flavia Valtorta, James L Rubenstein, Fred S Gorelick, Paul Greengard, and Andrew J Czernik. Synaptic vesicle-associated ca2+/calmodulin-dependent protein kinase ii is a binding protein for synapsin i. *Nature*, 359(6394):417–420, 1992.

[254] Andrea Menegon, Dario Bonanomi, Chiara Albertinazzi, Francesco Lotti, Giuliana Ferrari, Hung-Teh Kao, Fabio Benfenati, Pietro Baldelli, and Flavia Valtorta. Protein kinase a-mediated synapsin i phosphorylation is a central modulator of ca2+-dependent synaptic activity. *The Journal of neuroscience*, 26(45):11670–11681, 2006.

[255] Yoko Yamagata, Jasmina N Jovanovic, Andrew J Czernik, Paul Greengard, and Kunihiko Obata. Bidirectional changes in synapsin i phosphorylation at map kinase-dependent sites by acute neuronal excitation in vivo. *Journal of neurochemistry*, 80(5):835–842, 2002.

[256] Mirko Messa, Sonia Congia, Enrico Defranchi, Flavia Valtorta, Anna Fassio, Franco Onofri, and Fabio Benfenati. Tyrosine phosphorylation of synapsin i by src regulates synaptic-vesicle trafficking. *Journal of cell science*, 123(13):2256–2265, 2010.

[257] Dayne A Beccano-Kelly, Naila Kuhlmann, Igor Tatarnikov, Mattia Volta, Lise N Munsie, Patrick Chou, Li-Ping Cao, Heather Han, Lucia Tapia, Matthew J Farrer, et al. Synaptic function is modulated by lrrk2 and glutamate release is increased in cortical neurons of g2019s lrrk2 knock-in mice. *Frontiers in cellular neuroscience*, 8, 2014.

[258] Javier Alegre-Abarrategui, Helen Christian, Michele MP Lufino, Ruxandra Mutihac, Lara Lourenço Venda, Olaf Ansorge, and Richard Wade-Martins. Lrrk2 regulates autophagic activity and localizes to specific membrane microdomains in a novel human genomic reporter cellular model. *Human molecular genetics*, 18(21):4022–4034, 2009.

[259] Helge Gad, Niels Ringstad, Peter Löw, Ole Kjaerulff, Jenny Gustafsson, Markus Wenk, Gilbert Di Paolo, Yasuo Nemoto, John Crum, Mark H Ellisman, et al. Fission and uncoating of synaptic clathrin-coated vesicles are perturbed by disruption of interactions with the sh3 domain of endophilin. *Neuron*, 27(2):301–312, 2000.

[260] Thomas M Wishart, Simon H Parson, and Thomas H Gillingwater. Synaptic vulnerability in neurodegenerative disease. *Journal of Neuropathology & Experimental Neurology*, 65(8):733–739, 2006.

[261] Matthew S Goldberg, Antonio Pisani, Marian Haburcak, Timothy A Vortherms, Tohru Kitada, Cinzia Costa, Youren Tong, Giuseppina Martella, Anne Tscherter, Andrea Martins, et al. Nigrostriatal dopaminergic deficits and hypokinesia caused by inactivation of the familial parkinsonism-linked gene dj-1. *Neuron*, 45(4):489–496, 2005.

[262] F Cesca, P Baldelli, F Valtorta, and F Benfenati. The synapsins: key actors of synapse function and plasticity. *Progress in neurobiology*, 91(4):313–348, 2010.

[263] Narae Shin, Hyerhan Jeong, Jungsun Kwon, Hye Young Heo, Jung June Kwon, Hye Jin Yun, Cy-Hyun Kim, Baek Soo Han, Youren Tong, Jie Shen, et al. Lrrk2 regulates synaptic vesicle endocytosis. *Experimental cell research*, 314(10):2055–2065, 2008.

[264] Fernando Antunes, Carla Nunes, Joao Laranjinha, and Enrique Cadenas. Redox interactions of nitric oxide with dopamine and its derivatives. *Toxicology*, 208(2):207–212, 2005.

[265] Kelly A Conway, Jean-Christophe Rochet, Robert M Bieganski, and Peter T Lansbury. Kinetic stabilization of the α-synuclein protofibril by a dopamine-α-synuclein adduct. *Science*, 294(5545):1346–1349, 2001.